



UNIVERSITÀ DI PARMA

UNIVERSITA' DEGLI STUDI DI PARMA

DOTTORATO DI RICERCA IN
"SCIENZE CHIMICHE"

CICLO XXXIV

Innovative miniaturized sample treatment techniques for the determination of Polycyclic Aromatic Hydrocarbons as organic tracers in snow and ice core samples

–

Coordinatore:
Chiar.ma Prof. Alessia Bacchi

Tutore:
Chiar.ma Prof. Maria Careri
Chiar.ma Prof. Federica Bianchi

Dottorando: Angela Arcoleo

CONTENTS

PREMISE	4
INTRODUCTION	6
1 Polycyclic aromatic hydrocarbons	7
1.1 PAHs in remote regions	9
2 Miniaturized sample treatment techniques	12
2.1 Solid-phase microextraction	12
2.2 Dispersive micro-solid-phase extraction	15
2.3 Microextraction by packed sorbent	15
3 Sorbent materials for the extraction of PAHs	18
3.1 Carbon nanotubes	18
3.2 Bonded silica phases	20
3.3 Cyclodextrins	20
MATERIALS AND METHODS	23
4 Chemicals and Materials	24
5 Instrumental equipment	25
5.1 Gas chromatography-mass spectrometry	25
5.2 Characterization of materials: instruments	26
6 Method Validation	28
7 Methods	29
7.1 SPME-GC-MS method using HMWCNTs as fiber coating	29
7.1.1 Analytical standards and reagents	29
7.1.2 Fiber preparation and characterization	29
7.1.3 SPME procedure	30
7.1.4 GC-MS conditions	30
7.1.5 Extraction optimization by experimental design	31
7.1.6 Validation	31
7.1.7 Enrichment factors	31
7.2 MEPS-GC-MS method	32
7.2.1 Analytical standards and reagents	32
7.2.2 Environmental snow sample collection	32
7.2.3 Semi-automated MEPS procedure	32
7.2.4 GC-MS conditions	33
7.2.5 Selection of the sorbent and elution solvent	34

7.2.6	Optimization of the MEPS procedure by experimental design	34
7.2.7	Validation	34
7.2.8	Enrichment factors	35
7.3	SPME-GC-MS method using MWCNT-CD nanocomposite as fiber coating	35
7.3.1	Preparation of SPME coatings	35
7.3.2	Characterization and fibers preparation	36
7.3.3	Optimization of the SPME procedure	36
7.3.4	SPME procedure	36
7.3.5	Validation	37
7.3.6	Enrichment factors	37
7.3.7	Solution for the preparation of co-crystals	37
RESULTS AND DISCUSSION		38
8	SPME-GC-MS method using HMWCNTs as fiber coating	39
8.1	Fiber coating selection	39
8.2	Carryover effect	41
8.3	SPME optimization	41
8.4	Method validation	42
8.5	Enrichment factors	46
8.6	Real snow samples analysis	47
9	MEPS-GC-MS method	49
9.1	Development of MEPS procedure	49
9.2	Performance of C2, C8 and C18 sorbents on PAHs microextraction	49
9.3	Effect of desorption solvents on PAHs microextraction	50
9.4	MEPS optimization	51
9.5	Method validation	53
9.6	Real snow sample analysis	56
10	SPME-GC-MS method using MWCNT-CD nanocomposite as fiber coating	59
10.1	Characterization of the MWCNT-CD nanocomposites	59
10.2	Performance study of different MWCNT-CD nanocomposites as fiber coatings	60
10.3	SPME optimization	62
10.4	Method validation	63
10.5	Enrichment factors	66
10.6	Solid state investigation	67
CONCLUSIONS		70
REFERENCES		73
APPENDIX		89

PREMISE

Since man's appearance on Earth, human activity has started to affect the environment. The progress of civilization and the consequent population growth have led to an alteration of the ecological balance due to deforestation, enhanced greenhouse effect, desertification, and contamination of the environment. In particular, starting from the industrial revolution, the atmosphere was highly influenced by human activities such as the combustion of biomass, vegetation and fossil fuels, industrial activities, transport, and alteration of land surface.

The human-related contribution to the global atmospheric composition over the centuries is permanently archived in the glacier ice of remote areas, i.e., regions characterized by a minimum contribution of anthropogenic emissions and a concentration of contaminants similar to natural background values [1].

During the atmospheric deposition, airborne particulates and air bubbles are trapped in the snow, so that the chemical content is preserved in the cryosphere including important tracers of transport processes and markers of human activity. Therefore, the analysis of pollutants trapped in snow pits and ice cores from polar regions such as Arctic and Antarctica, as well as high-altitude environments like Alps and Caucasus [1–3] provide chemical records on a temporal scale [4]. This information is fundamental for assessing pollution sources [5], long-range transport mechanisms of contaminants [4] and, more generally, the anthropogenic impact and climatic variations over time [1].

Paleoclimatic reconstruction is a great challenge for analytical chemistry as it requires the use of appropriate sample preparation methodologies and very sensitive analytical techniques to determine environmental proxies in snow and ice [4]. In particular, the organic markers trapped in ice samples are usually found at very low concentration, in the order of trace and ultra-trace levels. Moreover, the deeper layers of the ice cores, corresponding to the oldest ice, are expected to be highly compressed. Therefore, analysis of a small sample volume is required in order to improve the temporal resolution of the ice stratification and to obtain meaningful data.

Persistent organic pollutants (POPs) are a group of contaminants resistant to chemical and biological degradation in the environment so they accumulate in living organisms and ecosystems [6]. POPs are considered evident markers of human activity and include substances such as pesticides, polychlorinated biphenyls (PCBs), per- and polyfluoroalkyl substances (PFASs), and polycyclic aromatic hydrocarbons (PAHs) [1]. An investigation of these compounds provides information on sources, occurrence, and pathways of contaminants [7]

since they may volatilize and be transported over long distance [8]. The latitudinal temperature gradient is considered one of the main drivers of the long-range atmospheric transport (LRAT) of contaminants, since the low temperatures of remote areas reduce or block the evaporation of POPs, thus producing an accumulation of pollutants as a result of a “cold-trapping” process [8–11]. Among POPs, PAHs have been widely studied in remote environments as tracers of anthropogenic emission sources [3,10,12–15]. Nevertheless, a general lack of data on their occurrence and concentrations in Antarctica compared to the Arctic was described [16].

In this context, the present Thesis work is part of the project “Innovative Analytical Methods to study biogenic and anthropogenic proxies in Ice COres” (Progetti di Ricerca di Rilevante Interesse Nazionale - PRIN - grant 2017EZNJWN) which aimed to develop innovative analytical methods for the chemical characterization of ice and snow to support paleoclimatic reconstruction. The novel aspect of the herein described Thesis was the development of methods based on the use of miniaturized sample treatment techniques for the determination of PAHs as organic tracers in Antarctic snow and ice. The use of pre-concentration steps and low-volume miniaturized procedures has resulted in improved performance and selectivity of analytical methods providing promising tools capable of determining analytes at trace and ultra-trace levels and detecting even small differences of atmospheric proxy indicators in the ice sheets.

INTRODUCTION

1 POLYCYCLIC AROMATIC HYDROCARBONS

Polycyclic aromatic hydrocarbons (PAHs) include a broad class of ubiquitous organic compounds that consist of two or more fused benzene rings having linear, angular or cluster molecular arrangements [17] (Fig. 1).

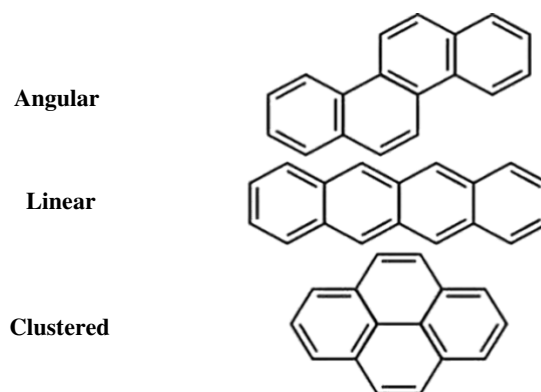


Fig. 1 Molecular arrangement of PAHs

The number of rings of each PAH affects its physicochemical properties, although all of them generally present high boiling and melting points, and low vapour pressure. PAHs having high molecular weight (4 or more aromatic rings) exhibit very low vapour pressure and are insoluble in water, therefore they are mostly found adsorbed on the surface of the particulate matter in the environment. Instead, low molecular weight PAHs (2-3 rings) present a higher vapour pressure and a slight solubility in water, so they could also be found in the vapour phase or in solution in aqueous matrices [18]. In this respect, the octanol-water partition coefficient (K_{ow}) is a physicochemical property useful for modeling the fate and transport of PAHs in the aquatic environment and terrestrial environment. As shown in Table 1, the log K_{ow} values for these compounds ranged from 3.30 (naphthalene) to 6.70 (indeno[1,2,3-cd]pyrene).

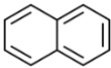
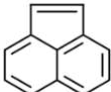
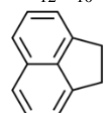
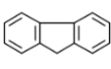
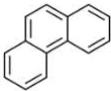
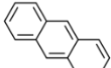
Based on the type of emission source, PAHs are divided into three main categories: biogenic, petrogenic and pyrogenic. The biogenic PAHs derive from biological processes and include e.g. retene and perylene. Petrogenic PAHs are present in petroleum and its refining products, and could enter the environment due to use and spill of oil. Mostly alkylated lighter PAHs, such as alkylphenanthrenes, are part of this group [19]. Pyrogenic PAHs originate from the incomplete combustion of organic materials under condition of oxygen scarcity and could have both natural (volcanic eruption and forest fire) or anthropogenic sources (biomass and fossil fuel combustion) [20]. Due to their release into the atmosphere, they could be dispersed globally [21]. Pyrosynthesis and pyrolysis are the main formation mechanisms of these compounds.

Introduction

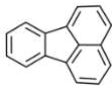


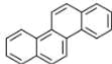
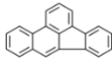
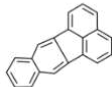
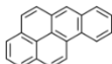
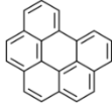
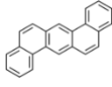

During combustion, at temperatures between 400 and 500 °C, hydrocarbons undergo cracking which leads to the formation of smaller and unstable molecules (pyrolysis). These fragments, mostly radicals, could recombine to produce polycyclic aromatic hydrocarbons (pyrosynthesis) whose formation is thermodynamically favored [22].

After industrialization most of the PAHs emissions are considered to be of anthropogenic origin [3], thus making this class of compounds an evident tracer of human activity [13]. As a result of the increased content of PAHs in the environment, these pollutants received great attention due to their toxic potential, and some of them were recognized to be carcinogenic to humans or possibly carcinogenic to humans [23]. Therefore, 16 PAHs were regulated by the United States Environmental Protection Agency (US EPA) as priority organic pollutants [24], and eight of these PAHs are classified as carcinogens of category 1B (European Union, 2013) [25]. The 16 priority PAHs represent the target analytes in this Thesis (Table 1).

Table 1 Name, CAS and formulas of the US-EPA 16 priority pollutant PAHs. The molecular weight (MW) and the octanol-water partition coefficient (Log K_{ow}) are also shown

Name	CAS#	Formula	MW	Log K_{ow}
Naphthalene Nap	000091-20-3	$C_{10}H_8$ 	128.17	3.30
Acenaphthylene Acy	000208-96-8	$C_{12}H_8$ 	152.19	4.00
Acenaphthene Ace	000083-32-9	$C_{12}H_{10}$ 	154.21	3.92
Fluorene Flu	000086-73-7	$C_{13}H_{10}$ 	166.22	4.18
Phenanthrene Phe	000085-01-8	$C_{14}H_{10}$ 	178.23	4.57
Anthracene Ant	000120-12-7	$C_{14}H_{10}$ 	178.23	4.54

Introduction

Fluoranthene Flt	000206-44-0	$C_{16}H_{10}$ 	202.25	5.18
Pyrene Py	000129-00-0	$C_{16}H_{10}$ 	202.25	5.22
Benzo[a]anthracene BaA	000056-55-3	$C_{18}H_{12}$ 	228.29	5.91
Chrysene Chr	000218-01-9	$C_{18}H_{12}$ 	228.29	5.91
Benzo[b]fluoranthene BbF	000205-99-2	$C_{20}H_{12}$ 	252.31	5.80
Benzo[k]fluoranthene BkF	000207-08-9	$C_{20}H_{12}$ 	252.31	6.00
Benzo[a]pyrene BaP	00050-32-08	$C_{20}H_{12}$ 	252.31	5.91
Benzo[ghi]perylene BghiP	000191-24-2	$C_{22}H_{12}$ 	276.33	6.63
Dibenzo[a,h]anthracene DiahA	000053-70-3	$C_{22}H_{14}$ 	278.35	6.50
Indeno[1,2,3-cd]pyrene InPy	000193-39-5	$C_{22}H_{12}$ 	276.33	6.70

1.1 PAHs IN REMOTE REGIONS

Arctic and Antarctica, as well as high-altitude glaciers, are characterized by lower levels of contaminants than other parts of the planet due to their remote location, thus they play an important role for studying possible sources of pollutants and assessing their distribution on a time scale [5,7].

Introduction

The first paleoenvironmental ice core record of PAHs was reported in 1994 by Kawamura et al. [26]. Analysis of the 400-year-old ice core from Greenland revealed a presence of PAHs related to fossil fuel combustion and crude oils. Moreover, the historical trend of the levels of PAHs detected showed an increase in the anthropogenic pollutant concentrations after the 1930s, likely associated with the increase in emissions from the mid-latitudes of the Northern Hemisphere. The results achieved highlighted that the distribution of PAHs in Arctic regions is strongly influenced by long-distance transport mechanisms.

The presence of persistent organic pollutants has also been detected in Antarctica, although its geographical position is more isolated from developed countries compared to the Arctic. This indicates that global transport mechanisms of anthropogenic pollutants operate also in the Southern Hemisphere, but the concentration levels in Antarctica were generally lower than in Arctic [27]. Fuoco et al. [5] reported PAH and PCB concentrations from a snow/firn four-century record at Talos Dome on the East Antarctic Plateau. After the 1930s, a significant increase in the PAHs concentration was observed in relation to anthropogenic activities, thus confirming the exponential increase in emissions from anthropogenic combustion sources in the 20th century. In addition, the highest PAHs concentration was found at depth profile corresponding to the Tambora eruption, the largest volcanic eruption in recorded history. Therefore, it is clear that volcanic eruptions also contribute to the peak of atmospheric PAHs concentration, but certainly in a limited time.

PAHs undergo LRAT based on their physicochemical properties and environmental conditions [28]. PAHs volatilize in their source regions and once in the atmosphere they are subject to dry or wet deposition. However, PAHs could re-volatilize and be transported to remote locations adsorbed on aerosol particles through a number of deposition/volatilization cycles, termed as the “grasshopper effect” (Fig. 2).

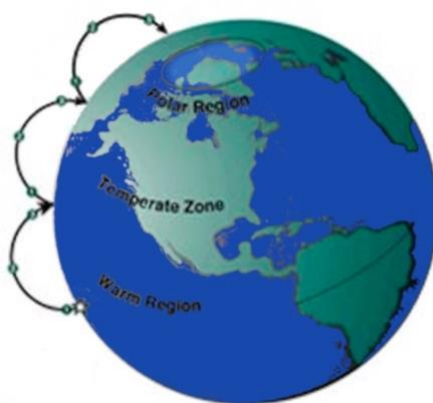


Fig. 2 The grasshopper effect

Introduction

In remote regions, the low temperatures make deposition processes more intense than evaporation, so resulting in PAHs accumulation in the local environments [28,29]. Several atmospheric transport models were developed to investigate the global distribution of PAHs and their transport potential, using also the evaluation of parameters such as the gas/particle partitioning, the photochemical degradation processes and the reactivity of PAHs in the atmosphere [29,30].

Although PAHs resulting from anthropogenic combustion in low latitudes are the main input of these contaminants in remote regions [29], PAHs pollution related to human activities was also found at a local scale. In particular, the Arctic has important sources of local contamination due to the presence of permanent population, military bases and coal-mining activities. Rose et al. [31], for instance, identified the coal combustion occurring in the Isfjord power stations (Svalbard) as significant local emission sources of PAHs. They also showed that the pattern of coal consumption during the winter months reflects peak concentrations of some PAHs. Conversely, Antarctica could be considered almost free from any source of local contamination due to anthropogenic contribution, with the exception of research stations and related activities [27]. Kukučka et al. [15] analyzed a snow pit from the Ekström Ice Shelf and ascribed the detected PAHs contamination to sources present in the polar region. Based on the air mass trajectories, it was assumed that the same PAH concentrations were found near the coastal area where the research stations are mostly located.

In general, the analysis of PAHs may present some issues and challenges related to their determination in snow and ice samples at ultra-trace levels, which could result in poor analyte recovery or the use of large sample volumes [5,10,14,15,26]. In fact, the determination of PAHs as organic tracers in ice core samples requires high sensitivity and selectivity due to the presence of these compounds at ultra-trace levels. In addition, despite the large volume requirements, the volume of sample available would be in the order of tens of mL to obtain a good temporal resolution for paleoclimatic reconstruction [1].

Therefore, the development of new sensitive analytical techniques is demanded for quantifying the full range of 16 US EPA PAHs, in order to investigate snow and ice records in areas considered to be the most pristine on the planet.

2 MINIATURIZED SAMPLE TREATMENT TECHNIQUES

Most methods that address the analysis of PAHs in polar snow and ice samples include a pre-concentration step due to the presence of targets at trace and ultra-trace levels. Sample pre-treatment techniques are used to increase the selectivity and sensitivity of the method by removing potential interferents and concentrating the analytes, respectively. A correct approach to sample preparation is essential to obtain valid results from analytical measurements [32].

Solid-phase extraction (SPE) and liquid-liquid extraction (LLE) were the most commonly used sample preparation procedures as they allow to obtain excellent recovery and LOD values [3,5,10,11,33]. However, these techniques have several drawbacks: the most common involve the use of large volumes of sample and organic solvents and, consequently, the need for evaporation of the solvent entails the risk of losing the lower molecular weight analytes [34]. Furthermore, the generation of toxic residues has side effects for both operators and the environment.

Miniaturization of analytical methodologies has improved dramatically in recent years as innovative approach in sample preparation, by reducing solvent consumption according to the principles of green analytical chemistry [35,36]. Microextraction techniques require a smaller sample volume than conventional ones and eliminate or reduce the use of organic solvents to desorb analytes. In addition, they are less time-consuming and allow for automation and integration of multiple steps in a single operation, thus minimizing sample handling and the risk of contamination [34,36]. The latter is critical for ice core and snow samples as they require careful handling to avoid external contamination that could affect the results due to the presence of the analytes at very low concentrations [3].

This section introduces the miniaturized techniques that have been investigated in this Thesis for the development of methods to analyze PAHs at the ultra-trace level in polar snow samples.

2.1 SOLID-PHASE MICROEXTRACTION

In 1990 Pawliszyn and Arthur developed solid-phase microextraction (SPME) as a fast and solvent-free technique based on the extraction of analytes using a fused silica fiber externally coated with a small amount of adsorbent stationary phase exposed to the sample (Fig. 3) [37]. This solvent-free sample preparation technique offers the advantage of integrating sample

Introduction

collection, extraction, analyte enrichment, and isolation from sample matrices in one step, thermal desorption of analytes taking place directly in the gas chromatograph injector.

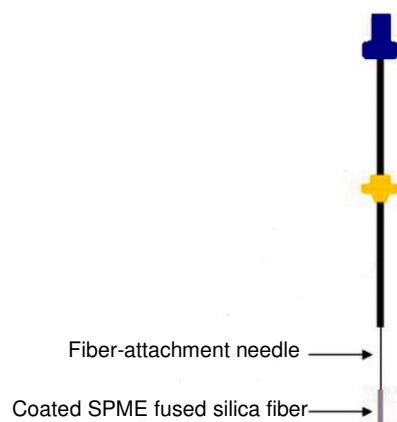


Fig. 3 SPME device

The extraction can be carried out by direct immersion (DI-SPME) or by headspace extraction (HS-SPME). In DI-SPME, the fiber is immersed in the liquid sample and the analytes are transported directly from the matrix to the fiber providing good precision. In HS-SPME the analytes are extracted from the gas phase in equilibrium with the sample. This approach is recommended in case of complex matrix analysis or sample modifications, e.g. adjusting the pH or salting the matrix without the risk of damaging the fiber (Fig. 4).

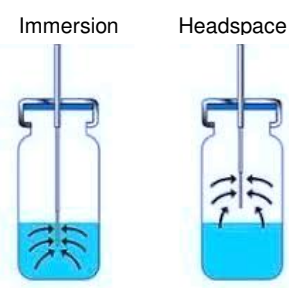


Fig. 4 SPME sampling modes

During extraction process, the analytes are partitioned between the sample and the fiber until the equilibrium is reached. Once in the equilibrium, the exposure of the fiber for a longer time does not cause an increase in the extraction yield. In general, setting the conditions of the SPME technique represents a compromise between sensitivity, speed and precision. As stated above, both sensitivity and accuracy are higher under equilibrium conditions. However, the time necessary to reach this equilibrium often is not feasible in practice. Sample agitation contributes to accelerate the partitioning process by promoting the mass transfer and the mobility of low diffusion compounds from aqueous sample to fiber, avoiding the formation of analyte-depleted

Introduction

areas near the fiber. The use of extraction temperatures higher than room temperature also increases the extraction rate. On the other hand, since extraction is an exothermic process, the increase in temperature favors desorption of the compounds from the fiber with consequent lower recovery of analytes. It is clear that the selection of appropriate extraction conditions should consider the behaviors of all target analytes, particularly when analyzing a group of compounds with different physicochemical properties, such as the 16 PAHs [38].

The type of stationary phase is another important factor affecting the sensitivity and repeatability of the SPME method as the extraction efficiency is a function of the mutual affinity between analytes and coating material. The fiber coating surface can interact with the analytes via π - π interactions, hydrogen bonds or van der Waals forces. In general, the selection of the most suitable materials for a specific application takes into account the characteristics of the analytes, such as molecular size, volatility and polarity, as well as the complexity of the matrix [39].

Several commercial coatings and devices have been developed that allow a wide range of SPME applications. Among commercial fibers, polydimethylsiloxane (PDMS) fibers proved to be the most suitable for the extraction of PAHs from aqueous matrices, so that some standard and official methods are based on their use [39–42]. Nevertheless, commercially available fibers have limitations related to low thermal stability, short lifetime and poor selectivity. New advances in the development of techniques and sorbent materials for use as coatings allowed to enhance the SPME capabilities [43]. The sol-gel technique led to major improvements in the thermal, physical and chemical stability of SPME fibers and was applied to extract a wide range of compounds including PAHs [44,45]. Molecularly-imprinted polymers (MIPs)-based fibers combine the high selectivity of the recognition cavities towards target analytes with chemical and thermal stability [46]. However, the steric recognition of PAHs in MIP cavities implies lower selectivity than compounds having functional groups that tend to interact via hydrogen bonds with specific sites in the cavity [47]. Nanoparticles (NPs) are known to exhibit exceptional properties for extracting PAHs such as a large surface area that results in a great sorption capacity. Several types of NPs have been applied as coatings for SPME fibers in the analysis of PAHs, including metal organic frameworks (MOFs) and carbon nanoparticles, which also provided stability to the fibers [48,49]. The performance and applicability of carbon-based sorbent materials used as fiber coatings to extract PAHs from polar snow samples were demonstrated in this Thesis.

2.2 DISPERSIVE MICRO-SOLID-PHASE EXTRACTION

Dispersive solid-phase extraction (DSPE) is an alternative technique to classical SPE and involves the use of a sorbent phase or a combination of different phases, dispersed in a liquid sample. Firstly, the purpose of the DSPE was to selectively retain potential interference, as in the case of the technique known as QuEChERS (an acronym to summarize the proposed advantages: Quick, Easy, Cheap, Effective, Rugged, and Safe) developed in 2003 by Anastassiades et al. for the multiresidue extraction of pesticides from fruit and vegetable samples [50]. Afterward, the potential of dispersion was used for the microextraction of contaminants such as PAHs, mycotoxins and residues of veterinary drugs from different food matrices, and this approach is commonly referred to as dispersive micro-solid-phase extraction (D- μ -SPE) [51]. The kinetics of the sorption of D- μ -SPE is favored by the close contact between the sorbent particles and the analytes in the sample solution. However, an external energy source is fundamental to accelerate extraction by enhancing the dispersion of the sorbent as well as the diffusion of the analytes. Ultrasound and vortex are generally used for these purposes as they could promote mass transfer and disaggregate particles to increase their overall size. Elution is carried out by using an appropriate desorption solvent before instrumental analysis. The choice of sorbent is fundamental for achieving high performance and depends on the nature of the analytes and the sample matrix. In addition, the reversibility of the interaction should be considered in order to effectively desorb the analytes from the phase by using few microliters of eluting solvent. The high area-volume ratio gives the NPs an excellent sorption capacity, and the potential for functionalization and magnetization increased their range of applications in D- μ -SPE. In particular, magnetization allows for feasible recovery of the sorbent after extraction and desorption using an external magnetic field without the need for filtration or centrifugation [52]. Many authors developed methods based on magnetic NPs-carbon nanotubes for the determination of PAHs in different matrices, showing the advantages of this simple, fast and efficient extraction technique [53–55]. In this work, a magnetic nanocomposite based on carbon nanotubes and cyclodextrins was studied for the extraction of PAHs at ultra-trace level from aqueous matrix.

2.3 MICROEXTRACTION BY PACKED SORBENT

Microextraction by packed sorbent (MEPS) was introduced in 2004 by Abdel-Rehim as a miniaturization of the classical SPE technique, developing a single device that integrated

Introduction

sample extraction, pre-concentration and cleaning [56,57]. The microextraction is performed using 1-4 mg of sorbent material packed in a syringe as a plug or in a cartridge called Barrel Insert and Needle (BIN) [58]. The microextraction can be fully automated using the syringe coupled with autosampler used in gas-chromatography (GC) or liquid-chromatography (LC) apparatus. Sampling can also be performed with a semi-automatic procedure using the eVol[®] system compatible for use with BIN (Fig. 5). Both methodologies allow to set parameters such as the number of loading/ejecting steps, the sampling volume and the speed.

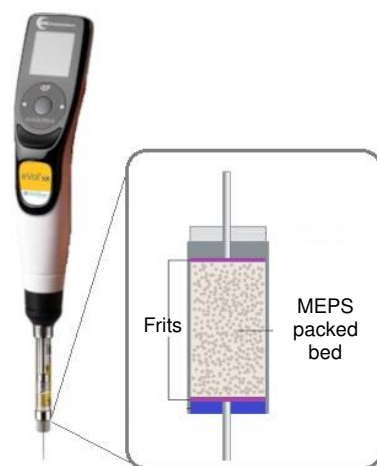


Fig. 5 eVol™ Handheld Automated Analytical Syringe and schematic MEPS BIN

The main advantage of this technique is the possibility of extracting a very low sample volume. Therefore, MEPS immediately found wide application in bioanalysis, since the sample volume of body fluids is usually limited [59–61]. However, environmental analysis also benefited from the performance of MEPS by reducing the extraction time and improving both automation and sensitivity [62,63]. The MEPS technique can be performed using two different microextraction modes, selected in relation to recovery values, reliability and analysis time. The "Draw-eject" mode consists of a sequence of aspiration and ejection cycles of sample aliquots in the same vial. In the "extract-discard" mode each aliquot of aspirated sample is discarded as waste [64]. Since the analytes are adsorbed on a small amount of sorbent, they are eluted using a few microliters of organic solvent, thus allowing MEPS to be coupled online with GC or LC. In addition, the consumption of limited quantities of solvents makes the technique more cost-effective and environmentally friendly than SPE and LLE. The evaluation of both number of sampling and elution cycles is fundamental to carry out a fast, sensitive and selective procedure. When analyzing complex matrices, a washing step may be required between loading and elution steps to remove interfering compounds retained in the sorbent. However, decreases in recovery

Introduction

were observed, so the need for this step should be assessed individually for each extraction [57,58].

The miniaturized features of the MEPS allow for easy reduction or elimination of carryover by washing the sorbent bed between runs with an appropriate solvent, thus enabling reuse of the same cartridge for multiple extractions. In particular, the number of reuses for the solid phase depends on the complexity of the sample matrix, namely for the analysis of water samples a BIN can perform up to 300 injections. Cartridge lifetime is shorter for non-centrifuged plasma, as the quality of matrix may alter the sorbent surface and affect the retention of the analytes [57].

Similarly to other sample preparation techniques, the type of sorbent is a crucial factor for MEPS selectivity [65]. A wide range of materials can be used as sorbents, some of which are commonly applied in SPE as well, e.g. materials based on silica (C2, C8 and C18), ion exchange (SCX), polystyrene-divinylbenzene copolymers (PS-DVB) and mixed mode sorbents. MEPS also takes advantage of using non-commercial materials, including MIPs, nanoporous and graphitic sorbents, but the feasibility provided by the use of commercial phases integrated into BINs is not negligible, especially when automation is required to extract sample volumes in the order of mL [58]. In addition, reversed phase separation has been shown to be suitable for the extraction of hydrophobic compounds such as PAHs from water samples. To date, the development of several MEPS-based methods for the analysis of PAHs in aqueous matrix has been reported in the literature, however the potential of this technique has not been used for paleoclimatic purposes [64,66,67]. Based on these considerations, in this Thesis, a MEPS-based method was developed for the first time to extract PAHs from Antarctic snow samples.

3 SORBENT MATERIALS FOR THE EXTRACTION OF PAHs

This section provides a description of the main features and the most common uses of carbon nanotubes, silica-based bonded phase and cyclodextrins, i.e. the groups of materials including the sorbents investigated in the present Thesis for the extraction of PAHs from snow samples.

3.1 CARBON NANOTUBES

The term carbon nanotubes (CNTs) refers to a group of materials discovered in 1991 by Iijima showing unique physicochemical properties such as a large surface area and high thermal stability [68]. The CNTs are divided into two categories depending on whether they are formed by a single or several sheets of graphene. Single-walled carbon nanotubes (SWCNTs) have diameters of 1-2 nm, while multi-walled carbon nanotubes (MWCNTs) have larger diameters (5-50 nm) (Fig. 6).

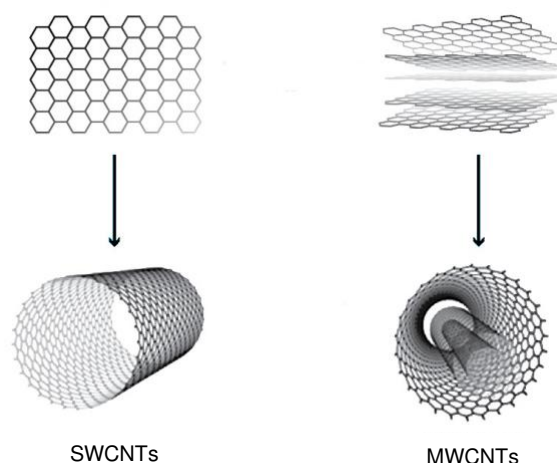


Fig. 6 Molecular structure of SWCNTs and MWCNTs

SWCNTs show excellent electric properties, in particular they exhibit electrical conductivity having semiconductor or metallic behavior. These properties make SWCNTs suitable in the field of nanoelectrodes and sensors [69]. MWCNTs have been very useful in many analytical fields, such as separation and sample preparation techniques. Although sample pre-treatment techniques also involve SWCNTs, MWCNTs have received more attention because being made up of several rolled-up sheets they show a greater surface area and consequently a higher adsorption capacity of organic compounds [70].

Introduction

The adsorption mechanisms that characterize CNTs are different depending on the type of targets. The affinity potential of CNTs towards chemicals is due to the hydrophobic interactions and π - π bonds between the CNTs and organic compounds having π electrons, i.e. molecules with carbon-carbon double bonds or aromatic rings [71]. Hydrogen bonds and electrostatic interactions are also used to predict the relations between organic substances and CNTs due to the functional groups and charges present on the CNT surface, respectively. In particular, the presence of specific functional groups and charges can affect the hydrophilicity of CNTs thus determining chemical polarity. For example, the presence of functional groups on the surface of CNTs that increase the oxygen content, are able to reduce the available surface area, thus interfering with the hydrophobic interactions between CNTs and non-polar chemicals. The presence of functional groups on CNTs (e.g. hydroxyl, carboxyl or carbonyl) can be the result of synthesis and purification procedures or can be incorporated on CNT by oxidation processes; their removal from CNTs can occur by means of heat-treatments [72]. Besides the influence on adsorption capability, the presence of functional groups also allows for synthesis of new composite sorbents by bonding CNTs with other materials such as polypyrrole or cyclodextrins in order to enhance the analytical performance [73,74].

In general, different adsorption processes operating simultaneously and dependent on the properties of both CNTs and chemicals can predict interactions between CNTs and organic compounds. These mechanisms could also show opposite effects to consider when investigating a carbon sorbent: i.e., CNTs with smaller diameter have a greater surface curvature that results in a higher number of multilayers and a greater adsorption capacity for molecular species. Nevertheless, molecules with planar structures such as benzene show better affinity for CNTs with larger diameters due to the flatter surface that provide higher contact [72].

PAHs having an aromatic ring structure and relatively high hydrophobic partition coefficients are known to show a strong interaction towards CNTs [71]. Therefore, in this Thesis the capabilities of four groups of commercially available MWCNTs, including one functionalized with carboxylic moieties (COOH-MWCNT) and one with helical configuration (HMWCNT) were evaluated as selective coatings for SPME extraction and subsequent GC-MS analysis of the 16 PAHs at ultra-trace in aqueous samples. The results showed greater extraction efficiency in adsorption and recovery of analytes using the SPME fiber coated with HMWCNT.

Furthermore, in this Thesis the capabilities of a type of composite material based on functionalized MWCNT and cyclodextrins as innovative materials were investigated.

3.2 BONDED SILICA PHASES

In this work, commercial silica-based materials, i.e., C2, C8 and C18, were studied as sorbents for the MEPS technique. C2, C8 and C18 have alkyl chains of different lengths (ethyl, octyl, octadecyl, respectively) which are covalently bonded to an inert matrix of silica (Fig. 7).

These sorbents are examples of silica-based materials used in the reverse phase separation mode (RP). As is known, the retention of organic compounds is mainly due to hydrophobic interactions and Van der Waals forces between the analytes and the stationary phase.

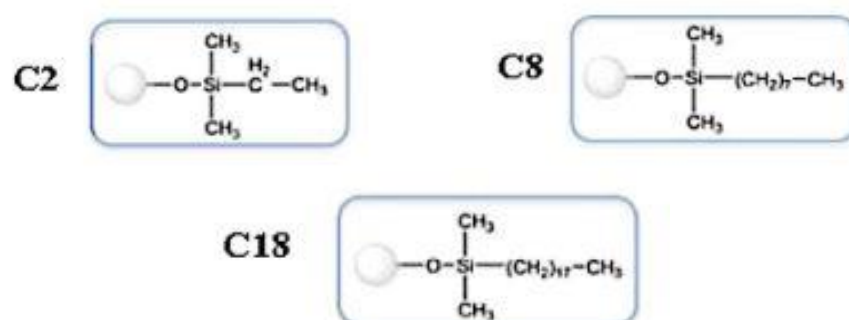


Fig. 7 Structures of the silica bonded phases studied in the present study

According to the increase of the retention capacity of the phase with the chain length, C18 is the phase with the highest hydrophobicity able to adsorb even weak hydrophobic analytes from the aqueous solution. C8 is a moderately hydrophobic phase used for methods that require less analyte retention. C2 is the phase with less hydrophobicity than C18 and C8 [75]. The main applications of this type of sorbents concern the extraction of drugs and their metabolites in biological fluids as well as organics at trace and ultra-trace levels in environmental aqueous samples. In particular, these phases are considered suitable for the extraction of PAHs from water samples due to hydrophobic interactions [65].

On this basis, in the present work of the Thesis an innovative method based on the MEPS technique with GC-MS analysis for the extraction of US-EPA PAHs was developed: for this purpose, in a preliminary phase, efficiency of microextraction using C2, C8 and C18 packed sorbents was evaluated.

3.3 CYCLODEXTRINS

Cyclodextrins (CDs) are natural compounds having cyclic structure made up of glucopyranose units linked by α -(1,4) bonds. CDs include three main types of oligosaccharides that differ in the number of glucose residues, namely α -CD (six) β -CD (seven) and γ -CD (eight) [76]. The

Introduction

secondary hydroxyl groups of glucopyranose (C₂ and C₃) are found at the margin that delineates the wider end of the ring whereas the primary hydroxyl groups (C₆) are found around the bottom edge. Since the primary hydroxyl groups can freely rotate, the diameter of the bottom side is reduced compared to the face that hosts the secondary hydroxyl groups (Fig. 8).

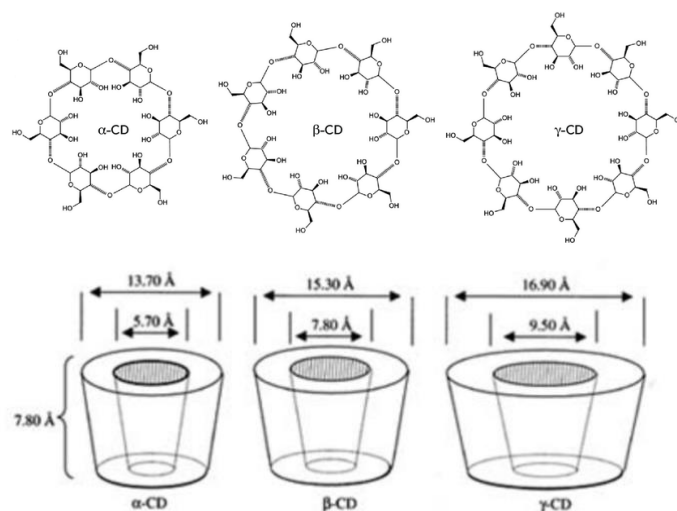


Fig. 8 Structures of cyclodextrins

The cyclic structure has a hydrophobic cavity bounded by the glycosidic H and O atoms. The non-bonding electrons of the glycosidic oxygen located at the level of the cavity originate a high electron density which gives CDs Lewis base properties. The hydroxyl group on the C₂ of glucopyranose can form a hydrogen bond with the hydroxyl group on the C₃ of the adjacent unit. The formation of these hydrogen bonds supports the rigid structure of CDs and results in the low solubility of β -CD in water. This formation of hydrogen bonds is partial in α -CD because a glucopyranose unit is in a distorted position so that only four hydrogen bonds can be formed. The γ -CD has a more flexible non-planar structure which makes them more soluble in water than α -CD and β -CD [77].

In aqueous solution the cavity of the CD is occupied by water molecules. However, the interaction between polar and non-polar molecules is energetically disadvantaged, therefore the water molecules are replaced by lower polarity compounds. CDs have the ability to form host-guest inclusion complexes with a wide range of molecules. The driving force for the formation of the complex is determined by entropic factors (displacement of water molecules) and enthalpy factors (hydrophobic interactions between the CD cavity and the guest). The complex is stabilized by Van der Waals forces and hydrogen bonds in a dynamic equilibrium. The affinity of a molecule for the CD cavity is a function of two elements. The first is steric, as α -, β -, and γ -CD have different diameters so they can include molecules based on their fitting,

Introduction

whereas the second depends on the thermodynamic interaction between the different components of the system, i.e. CDs, guest and solvent [78].

Inclusion in the cavity of CD causes significant changes in the physicochemical properties of the guest molecules. Changes that would be difficult to achieve otherwise include e.g. increased solubility of insoluble guests, stabilization against the degrading effects of oxygen and light, control of volatility and sublimation, physical isolation of compounds, chromatographic separations, masking of flavours and smells, and controlled delivery of drugs. Therefore, these attributes make CDs and their derivatives suitable for applications in different fields such as pharmaceuticals and analytical chemistry [77].

In particular, the potential of CDs has recently been used in combination with other materials to prepare sorbents for sample preparation techniques [79]. β - and γ -CD have been the most used in environmental analysis due to the size of their cavity capable of complexing analytes such as PAHs and phenolic compounds [80–82].

In this Thesis β - and γ -CD were used for preparation of composites with functionalized MWCNTs as innovative materials for the efficient extraction of PAHs in water samples. At first, the sorbents were studied using the magnetic D- μ -SPE technique, but poor recovery efficiency was achieved. Therefore, the nanocomposites were successfully used to develop a SPME-GC-MS method for the analysis of 16 US-EPA PAHs in water samples.

MATERIALS AND METHODS

4 CHEMICALS AND MATERIALS

Hexane (puriss. p.a., ACS reagent, $\geq 99.0\%$ GC), acetonitrile (ACN) (suitable for HPLC, gradient grade, $\geq 99.9\%$), dichloromethane (DCM) (puriss., meets analytical specification of Ph. Eur., NF, $\geq 99\%$ GC), and ethyl acetate (EtAc) (puriss. p.a. ACS, Reag. Ph. Eur., Reag. ISO) were supplied by Sigma-Aldrich Chemie GmbH (Steinheim, Germany). Methanol (MeOH) ($\geq 99.7\%$ purity) was supplied by Honeywell Riedel-de Haën (Seelze, Germany).

Four different types of carbon nanotubes, i.e. HMWCNTs 100–200 nm OD, length: 1–10 μm ; MWCNTs > 50 nm OD, length: 10–20 μm (50MWCNTs); MWCNTs < 8 nm OD, length: 10–50 μm (8MWCNTs) and one type of functionalized COOH-MWCNTs: > 50 nm OD, length: 10–20 μm were purchased from Cheap Tubes Inc. (Cambridgeport, USA).

Five mg of γ -cyclodextrin were purchased by Fluorochem (UK).

One cm SPME bare fused silica and 1 cm-30 μm PDMS fibers were provided by Supelco (Bellefonte, PA, USA). Duralco 4460 epoxy glue was purchased by Cotronics Corp. (Brooklyn, NY, USA).

Ultrapure water was produced by a Millipore Milli-Q Element A10 Water Purification System (Merck-Millipore, Milan, Italy).

5 INSTRUMENTAL EQUIPMENT

The research activity was carried out in the Analytical Chemistry Laboratories of the Department of Chemistry, Life Sciences and Environmental Sustainability of the University of Parma. The synthesis and characterization of MWCNT-CD nanocomposites were conducted in the Laboratory 83 of Inorganic and Bioinorganic Chemistry under the supervision of Prof. F. Bisceglie.

5.1 GAS CHROMATOGRAPHY-MASS SPECTROMETRY

Analyses of the 16 US-EPA PAHs were performed using a HP 6890 Series Plus gas chromatograph (Agilent Technologies, Milan, Italy) supplied with a PAL Combi-xt autosampler (CTC Analytics AG, Switzerland) and coupled to a MSD 5973 mass spectrometer (Agilent Technologies).

The GC used is equipped with a S/SL (Agilent Technologies) injection port: all the analyses were carried out by operating in splitless mode, and helium was used as carrier gas at a constant flow rate of 1.0 mL min⁻¹. The mass spectrometer was equipped with an electron ionization (EI) ion source and an electron energy of 70 eV was always used. The transfer line and the ion source were maintained at 280 °C and 150 °C, respectively. Preliminarily, full scan mass spectra were recorded in the 40–400 amu range (scan time: 2 scan s⁻¹) to select a list of both qualifier and quantifier ions per target analyte. GC-MS analyses were carried out under selected ion monitoring (SIM) conditions. The SIM mode was used for quantitative measurements setting a dwell time of 30 ms for each ion. The selected ions are listed in Table 2. The ChemStation (Agilent Technologies) was used for signal acquisition and data processing.

Taking into account that the GC column has been replaced over the three years of this work, the GC runs are described later in each method section, as well as time windows of quantifier ions.

Table 2 Ions monitored for target PAHs (quantifier ions are underlined) in SIM mode.

PAHs	Qualifier and quantifier ions (<i>m/z</i>)
Nap-d8	<u>136</u> , 137, 108
Nap	<u>128</u> , 127, 102
Acy-d8	<u>160</u> , 158, 161
Acy	<u>152</u> , 151, 76

Materials and methods

Ace-d10	<u>162</u> , 164, 160
Ace	<u>153</u> , 154, 76
Flu-d10	<u>176</u> , 174, 175
Flu	<u>166</u> , 165, 139
Phe-d10	<u>188</u> , 189, 184
Phe	<u>178</u> , 176, 152
Ant-d10	<u>188</u> , 189, 184
Ant	<u>178</u> , 176, 152
Flt-d10	<u>212</u> , 208, 213
Flt	<u>202</u> , 200, 101
Py-d10	<u>212</u> , 211, 208
Py	<u>202</u> , 200, 101
BaA-d12	<u>240</u> , 236, 241
BaA	<u>228</u> , 226, 113
Chr-d12	<u>240</u> , 236, 241
Chr	<u>228</u> , 226, 113
BbF-d12	<u>264</u> , 265, 260
BbF	<u>252</u> , 253, 126
BkF-d12	<u>264</u> , 265, 263
BkF	<u>252</u> , 253, 126
BaP-d12	<u>264</u> , 265, 260
BaP	<u>252</u> , 253, 126
InPy-d12	<u>288</u> , 289, 144
DiahA-d14	<u>292</u> , 288, 293
InPy	<u>276</u> , 279, 278, 277, 139
DiahA	<u>278</u> , 279, 277, 276, 139
BghiP-d12	<u>288</u> , 287, 289
BghiP	<u>276</u> , 279, 278, 277, 139

5.2 CHARACTERIZATION OF MATERIALS: INSTRUMENTS

- Thermogravimetric analysis (TGA) was performed using a TGA 7 instrument (PerkinElmer, Waltham, MA).
- Morphological characterization was performed using an environmental scanning electron microscope (ESEM) Quanta TM 250 FEG (FEI, Hillsboro, OR, US).

Materials and methods

- Fourier transform infrared (FTIR) spectra were recorded by a Spectrum Two™ FT-IR Spectrometer (PerkinElmer).
- Raman spectra were recorded by using a Renishaw System-1000 spectrometer (Renishaw, UK).
- Zeta-potential (ζ -potential) measurements were performed by Dynamic Light Scattering (DLS) using a Zetasizer-Nano ZSP (Malvern Panalytical, Worcestershire, UK).

6 METHOD VALIDATION

The developed methods were validated according to EURACHEM guidelines [83].

Detection (y_D) and quantitation (y_Q) limits were expressed as signals based on the mean blank (x_b) and the standard deviation of blank responses (s_b) as follows:

$$y_D = x_b + 3 s_b$$

$$y_Q = x_b + 10 s_b$$

The value of x_b and s_b were calculated carrying out 10 blank measurements. The concentration values of the limit of detection (LOD) and limit of quantitation (LOQ) were obtained by projection of the corresponding signals y_D and y_Q through a calibration plot $y = f(x)$ onto the concentration axis.

Calibration curves were constructed performing 3 replicate measurements on six concentration levels spaced across the range of interest evaluating at least over 1 order of magnitude. Homoscedasticity was verified by applying the Bartlett's test ($\alpha = 0.05$). Linearity was evaluated by applying the Mandel's fitting test ($\alpha = 0.01$), whereas the Lack-of-fit was performed to evaluate the goodness of the fit ($\alpha = 0.05$). The significance of the intercept (significance level 5%) was established by running a Student's t -test.

Precision defined as repeatability and intermediate precision was calculated in terms of relative standard deviation (RSD) % on three concentration levels performing six replicates at each level. Intermediate precision was estimated over three days proving homoscedasticity of data and carrying out ANOVA at 95% confidence level.

Trueness was evaluated in terms of recovery rate (RR%) calculated as follows:

$$RR\% = \frac{c_1}{c_2} \times 100$$

where c_1 is the measured concentration and c_2 is the concentration calculated from the amount spiked into the sample. For each concentration level 10 replicated measurements were carried out.

7 METHODS

As mentioned in the Introduction, the contamination control strategy plays an important role in extracting reliable data from polar samples due to the expected low level of analyte concentration. In fact, awareness of the importance of contamination control has increased over the past few decades and therefore clean materials, reagents and careful procedures have been developed, allowing pristine and detailed records to be extracted from polar samples [4].

In this work, after washing and drying, all glassware was thoroughly rinsed three times using hexane as an ultrapure special grade non-polar solvent is recommended to remove residual organic contaminants when the target analytes are POPs, including PAHs [10].

7.1 SPME-GC-MS METHOD USING HMWCNTs AS FIBER COATING

This section provides the description of each step of the development and validation of the analytical method for the SPME-GC-MS analysis of the 16 PAHs proposing, for the first time, HMWCNTs as novel SPME coating. The developed method was the subject of the research paper entitled “*Helical multi-walled carbon nanotube-coated fibers for solid-phase microextraction determination of polycyclic aromatic hydrocarbons at ultra-trace levels in ice and snow samples*” by Arcoletto et al. (2020), published in *Journal of Chromatography A* [84].

7.1.1 Analytical standards and reagents

EPA 525 PAH Mix A including Nap (99% purity), Ace (99% purity), Flt (98% purity), Acy, Flu, Phe, Ant, Py, BaA, Chr, BbF, BkF, BaP, InPy, DiahA, BghiP (certified reference material, 500 $\mu\text{g mL}^{-1}$ each component in dichloromethane), and perdeuterated PAHs including Nap-d8 (>99% atom D), Ace-d10 (>99% atom D), Phe-d10 (>98% atom D), Py-d10 (>98% atom D), BaA-d12 (>98% atom D), BaP-d12 (>98% atom D), BghiP-d12 (>98% atom D) were purchased from Sigma-Aldrich (Milan, Italy).

Native and deuterated PAHs stock solutions containing each analyte/deuterated standard at the concentration of 10 mg L^{-1} were prepared in MeOH and kept at 4 °C in darkness. The working solutions were prepared by proper dilution of the stock solutions.

7.1.2 Fiber preparation and characterization

Materials and methods

The MWCNTs fiber coatings were obtained by dipping 1 cm portion of the silica substrate of the fibers into the Duralco 4460 epoxy glue and, after 2 min, into 1 g of each MWCNT powder for three times.

TGA of HMWCNTs was performed in the 50–600 °C temperature range (heating rate: 10 °C min⁻¹) under inert (N₂) atmosphere.

7.1.3 SPME procedure

Before use, each fiber was conditioned at 270 °C in the GC inlet for 2 h under a helium flow in order to remove impurities.

All of the experiments were performed by direct immersion technique in a 10 mL glass vial containing 9.5 mL of the sample solution spiked with internal standards each at the concentration of 10 ng L⁻¹. Vials were fitted with crimped aluminium caps lined with PTFE septa. Desorption was carried out at the temperature of 310 °C for 5 min.

7.1.4 GC-MS conditions

Separation was performed on a Rxi–17Sil MS capillary column (30 m x 0.25 mm i.d., 0.25 µm film thickness) (Restek, Bellefonte, PA, USA). A Rxi-5Sil MS capillary column (30 m x 0.25 mm i.d, 0.25 µm film thickness) (Restek, Bellefonte, PA, USA) was used for confirmation purposes.

Table 3 Time windows of the monitored ions

PAHs	Time window (min)
Nap, Nap-d8	2.00-5.00
Acy, Ace, Flu, Ace-d10	5.00-8.50
Phe, Ant, Phe-d10	8.50-11.00
Flt, Py, Py-d10	11.00-17.00
BaA, Chr, BaA-d12	17.00-22.00
BbF, BkF, BaP, BaP-d12	22.00-30.00
InPy, DiahA, Bghi, BghiP-d12	30.00-37.33

The S/SL (Agilent Technologies) injector was set at 310 and 270 °C for the desorption of the HMWCNTs and 30 µm PDMS fibers, respectively. The temperature program for the

chromatographic run was as follows: 110 °C; 15 °C min⁻¹ up to 220 °C, 4 °C min⁻¹ up to 320 °C, 320 °C for 5 min. The time windows of the monitored ions are summarized in Table 3.

7.1.5 Extraction optimization by experimental design

Variables such as extraction temperature (T) and extraction time (t) were optimized using a 2² full factorial design (FFD). Low and high levels in the experimental domain were T = 40–80 °C and t = 15–60 min, respectively. This experimental plan allows the evaluation of the effects of both the main factors and their interactions [85]. In order to evaluate the experimental error, four replicates at the center of the experimental domain were carried out. For the experiments, standard solutions at the concentration of 50 ng L⁻¹ for each PAH were used.

A *F*-test was performed to evaluate the existence of relevant quadratic effects comparing the experimental and calculated responses at the center of the experimental domain and a star design was added to the factorial design experiments. The final regression models were then calculated by a forward search stepwise variable selection algorithm and the optimal conditions were assessed by using the multicriteria method of the desirability functions [85,86].

All statistical analyses were performed by using the statistical package SPSS Statistics 23.0 (IBM, Milan, Italy).

7.1.6 Validation

Calibration curves were prepared by spiking the appropriate amount of analytes into 9.5 mL of groundwater in order to obtain the 1.5–30 ng L⁻¹ concentration range. Deuterated PAHs (used as internal standards) were added at 10 ng L⁻¹.

Precision was calculated at 3, 10 and 30 ng L⁻¹. Two concentration levels at 5 and 30 ng L⁻¹ for each analyte were analyzed to calculate RR%.

7.1.7 Enrichment factors

The enrichment factors (EFs) were calculated for both HMWCNTs-coated and commercial 30 µm PDMS fibers using a concentration of 10 ng L⁻¹ for each PAH. EFs were calculated as the ratio of the concentration of the analyte extracted onto the fiber surface to that of the analyte in the standard mixture, i.e. using the ratio of the chromatographic peak area of each analyte after SPME compared to that obtained by the direct injection of a standard solution at 10 µg L⁻¹ [87]. Three replicated measurements were performed.

7.2 MEPS-GC-MS METHOD

The herein described MEPS-GC-MS method resulted in the publication of a research paper in *Chemosphere*, entitled “A sensitive microextraction by packed sorbent-gas chromatography-mass spectrometry method for the assessment of polycyclic aromatic hydrocarbons contamination in Antarctic surface snow”, by Arcoleo et al. (2021) [88].

7.2.1 Analytical standards and reagents

The standard mixture of 16 PAHs Nap, Ace, Flt, Acy, Flu, Phe, Ant, Py, BaA, Chr, BbF, BkF, BaP, InPy, DiahA and BghiP (each component at a concentration of 100 $\mu\text{g mL}^{-1}$ in acetonitrile), and deuterated PAHs internal standard (IS) containing Nap-d8, Ace-d10, Phe-d10, Ant-d10, BaA-d12, Chr-d12, BghiP-d12, DiahA-d14, Acy-d8, Flu-d10, Flt-d10, Py-d10, BaP-d12, BbF-d12, BkF-d12 and InPy-12 (each component at a concentration of 10 $\mu\text{g mL}^{-1}$ in acetonitrile) were purchased from Neochema (Bodenheim, Germany) and were stored in the absence of light at 4 °C.

Intermediate stock solutions of native and deuterated PAHs, each at 1 mg L^{-1} , were prepared in MeOH. Daily, standard native and deuterated PAHs working solutions were prepared by proper dilution of the stock solutions before use.

7.2.2 Environmental snow sample collection

Surface snow samples collected on the coastal area of Victoria Land (Antarctica) during the 2020–2021 austral summer were kindly provided by the National Antarctic Research Program (PNRA). Samples were maintained at $-20\text{ }^{\circ}\text{C}$ until analysis, then they were thawed in the laboratory at room temperature preventing exposure to solar irradiation and subjected to MEPS procedure.

7.2.3 Semi-automated MEPS procedure

Microextractions were carried out using the hand-held digital device eVol[®] Sample Dispensing System equipped with a 50 μL syringe. This device allows for using commercially available BINs. In this work the BINs packed with 4 mg of phases C2, C8 and C18 respectively were used. The entire apparatus was purchased from SGE Analytical Science (SGE Analytical Science Pty Ltd., Victoria, Australia).

Materials and methods

Prior to first use, each BIN was activated three times with 50 μL of MeOH followed by the same volume of ultrapure water at a speed of $10 \mu\text{L s}^{-1}$.

The sample (4 mL) was extracted from a 10 mL glass vial by 80 loading steps of 50 μL each at a speed of $12.50 \mu\text{L s}^{-1}$ and all portions were discarded into the waste. Then the sorbent was dried by 10 cycles of pulling and pushing air at a flow rate of $25.00 \mu\text{L s}^{-1}$.

Based on the assumption that small aliquots commonly elute analytes of interest more efficiently than one large aliquot [89], the adsorbed PAHs were collected in three fractions (10 μL each) by eluting with EtAc at the speed of $1.67 \mu\text{L s}^{-1}$. The eluate was spiked with IS at the concentration of $10 \mu\text{g L}^{-1}$ and 1 μL of the solution was injected into the GC-MS. After the elution step, the sorbent was washed with EtAc, MeOH and ultrapure water (50 μL each) to avoid any carryover and to condition the solid phase before the next extraction.

7.2.4 GC-MS conditions

The injection port temperature was set at $300 \text{ }^\circ\text{C}$. Separation was achieved on a Rxi-5Sil MS capillary column (30 m \times 0.25 mm i.d, 0.25 μm film thickness) (Restek, Bellefonte, PA, USA). The GC oven temperature program was as follows: $70 \text{ }^\circ\text{C}$; $15 \text{ }^\circ\text{C min}^{-1}$ to $290 \text{ }^\circ\text{C}$ (held for 4 min) for a total run time of 19.17 min. The time windows of the selected ions are listed in Table 4.

Table 4 Time window for target PAHs

PAHs	Time window (min)
Nap, Nap-d8	3.90-5.50
Acy, Ace, Acy-d8, Ace-d10	5.50-7.60
Flu, Flu-d10	7.60-9.00
Phe, Ant, Phe-d10, Ant-d10	9.00-10.50
Flt, Py, Flt-d10, Py-d10	10.50-12.50
BaA, Chr, BaA-d12, Chr-d12	12.50-14.50
BbF, BkF, BaP, BbF-d12, BkF-d12, BaP-d12	14.50-16.50
InPy, DiahA, Bghi, InPy-d12, DiahA-d14, BghiP-d12	16.50-19.17

7.2.5 Selection of the sorbent and elution solvent

The method was developed using uncontaminated snow from Antarctic Plateau as blank matrix. Three reversed-phase sorbent materials (silica-C2, silica-C8 and silica-C18) were evaluated and compared for the enrichment of the target PAHs from water samples. For each sorbent the extraction of three independent replicate sample solutions spiked with PAHs at 500 ng L⁻¹ was performed.

After the optimization of best sorbent material, the effect of three different elution solvents (DCM, EtAc and MeOH) on PAHs desorption from C8-BIN was investigated performing extraction of three independent sample solutions spiked with PAHs at 250 ng L⁻¹ for each solvent.

The performance of both the sorbents and the elution solvents was expressed in terms of relative chromatographic peak areas using the formula:

$$\text{Area ratio} = A(\text{spike, net})/A(\text{internal standard})$$

where: A(spike, net) is the net chromatographic peak area of the compound in a spiked “blank” sample which was subjected to MEPS; A(internal standard) is the chromatographic peak area of the internal standard added after sample extraction.

7.2.6 Optimization of the MEPS procedure by experimental design

For the optimization of the experimental parameters, measurements were carried out on blank water obtained by melting uncontaminated snow spiked with PAHs mixture at 250 ng L⁻¹. The influence of two factors and of their interactions on MEPS performance was studied using a full centred design (FCD). The investigated factors were the following: the number of loading cycles (x_1) and the number of eluting cycles (x_2). Low and high levels were: $x_1 = 40-80$, $x_2 = 3-10$. Four replicates at the centre point were considered to estimate the experimental variability.

The FCD was used to calculate the final regression models which were used to identify the optimal conditions by means of the multicriteria method of the desirability functions [86]. The software package SPSS Statistics 23.0 (IBM, Milano, Italy) was used for statistical calculations.

7.2.7 Validation

Calibration curves were constructed on six concentration levels in the LOQ–150 ng L⁻¹ range by spiking uncontaminated snow from Antarctic Plateau used as blank samples.

15, 50 and 150 ng L⁻¹ were the concentration levels used to calculate repeatability and intermediate precision over three days. Trueness was assessed at 20, 70 and 130 ng L⁻¹.

Before each injection, IS was added at 10 µg L⁻¹ to the PAH standard solutions and to samples after extraction.

7.2.8 Enrichment factors

The enrichment capabilities of semi-automated MEPS-C8 were evaluated in terms of EFs. Under the optimized conditions, EFs were calculated as the ratio of the concentration of the analytes at 20 and 50 ng L⁻¹ extracted by MEPS to that obtained by the direct injection of 1 µL of standard solution of PAHs at 10 µg L⁻¹. Experimentally, the ratio of the chromatographic peak area for each analyte after MEPS was compared to that obtained by direct injection and corrected by using the proper response factor. Three replicate measurements were carried out.

7.3 SPME-GC-MS METHOD USING MWCNT-CD NANOCOMPOSITE AS FIBER COATING

This experimental section describes the second SPME-GC-MS method developed in this Thesis. The method makes use of nanocomposites based on functionalized COOH-MWCNT and β- and γ-cyclodextrins (β- and γ-CD), respectively, as fiber coatings for the extraction of the 16 PAHs. The MWCNT-CD based materials combine the thermal and chemical stability of MWCNTs with the ability of CDs to complex analytes within their hydrophobic cavity.

The analytical standards and the information regarding both the preparation of the working solutions and the utilised GC-MS conditions were already described in paragraphs 7.2.1 and 7.2.4, respectively.

7.3.1 Preparation of SPME coatings

The synthesis and characterization of nanocomposites were carried out by the group of Inorganic and Bioinorganic Chemistry of the Department of Chemistry, Life Sciences and Environmental Sustainability under the supervision of Prof. Franco Bisceglie. The commercial COOH-MWCNTs were subjected to two types of oxidative treatment by using nitric acid and ammonium hydroxide/hydrogen peroxide, respectively, in order to increase the concentration of carboxylic functions on the graphitic surface. Chemical oxidation was performed according to the procedure described by Datsyuk et al. [90] with minor modifications. Briefly, 500 mg of

CNTs were dispersed in 40 mL of either nitric acid and of a mixture of ammonium hydroxide/hydrogen peroxide (1/1 v/v) and maintained at room temperature for 72 h. The subsequent addition of β -CD and γ -CD was carried out as reported by Cheng et al. [91]. Therefore, four types of nanocomposites were obtained, namely MWCNT-HNO₃- β -CD, MWCNT-HNO₃- γ -CD, MWCNT-H₂O₂- β -CD and MWCNT-H₂O₂- γ -CD.

7.3.2 Characterization and fiber preparation

The four types of nanocomposites were characterized by FTIR, TGA and X-ray photoelectron spectroscopy (XPS), the latter being carried out thanks to a collaboration with the Institute of Nanosciences of the National Research Council of Modena. Oxidized and untreated COOH-MWCNTs were subjected to ζ -potential measurement by DLS technique. In addition, Raman spectra of MWCNT-HNO₃ and MWCNT-H₂O₂ reduced with hydrazine hydrate and their unreduced analogues were recorded.

The MWCNT-CD and COOH-MWCNT coatings of the fibers were obtained by dipping a 1 cm portion of the bare fused silica fibers in Duralco 4460 epoxy glue and, after 2 minutes, in 100 mg of each powder of MWCNT-CD and COOH-MWCNTs for three times.

7.3.3 Optimization of the SPME procedure

The experimental plan was obtained by applying a central composite design (CCD) consisting of a 2³ FFD, four replicates at the center point and a star design [92]. Three variables were investigated, namely desorption time (x_1), extraction temperature (x_2) and extraction time (x_3). The experimental domain was: $x_1 = 3$ -5 min, $x_2 = 40$ -60 °C and $x_3 = 40$ -80 min. For this purpose, standard solutions spiked with PAH standards mixture at the concentration of 50 ng L⁻¹ were used.

The presence of relevant quadratic effects was evaluated using an *F*-test comparing the experimental and calculated responses at the center of the experimental domain. The identification of the optimal conditions was assessed using the desirability function method. Statistical analysis carried out by using the software package SPSS Statistics 23.0 (IBM, Milano, Italy).

7.3.4 SPME procedure

Before use, each fiber was conditioned in the GC injection port at 270 °C for 1 h under a helium flow.

The experiments were performed using the direct immersion mode under the optimized conditions. Ten mL glass vial containing 9.5 mL of the sample solution spiked with internal standard at the concentration of 10 ng L⁻¹ were used. Desorption was carried out at the temperature of 270 °C.

7.3.5 Validation

Calibration curves in the LOQ–30 ng L⁻¹ range were obtained by spiking the appropriate amount of standard PAH mix in Antarctic Plateau snow used as blank matrix.

Precision was calculated at 2, 15 and 30 ng L⁻¹. RR% values were assessed by performing the analyses at 3, 10 and 20 ng L⁻¹.

7.3.6 Enrichment factors

The MWCNT-H₂O₂- γ -CD fiber was used to calculate EFs by operating under the optimized conditions. A standard solution spiked with PAHs at the concentration of 10 ng L⁻¹ was used and 3 replicate measurements were performed. The ratio of chromatographic peak areas obtained for each PAH after SPME were compared to that obtained by the direct injection of 1 μ L of standard solution of PAHs at 10 μ g L⁻¹ and corrected by using the proper response factor.

7.3.7 Solution for the preparation of co-crystals

Solid state experiments to investigate the ability of CDs to complex PAHs were carried out. For this purpose, γ -CD (50 mg) and pyrene (8 mg) were dissolved in 9 mL of water and MeOH, respectively. After the two solutions were combined, they were stirred for two hours at room temperature. Two hundred mL of acetonitrile were added to the solution. The mixture was evaporated at room temperature and when it reached approximately 20 mL it was placed under magnetic stirring at 70 °C for two days. The temperature was progressively lowered to room temperature by 2 degrees at a time.

RESULTS AND DISCUSSION

8 SPME-GC-MS METHOD USING HMWCNTs AS FIBER COATING

8.1 FIBER COATING SELECTION

The four types of MWCNTs investigated as SPME fiber coating for the ultra-trace extraction of the 16 PAHs are depicted in Fig. 9.

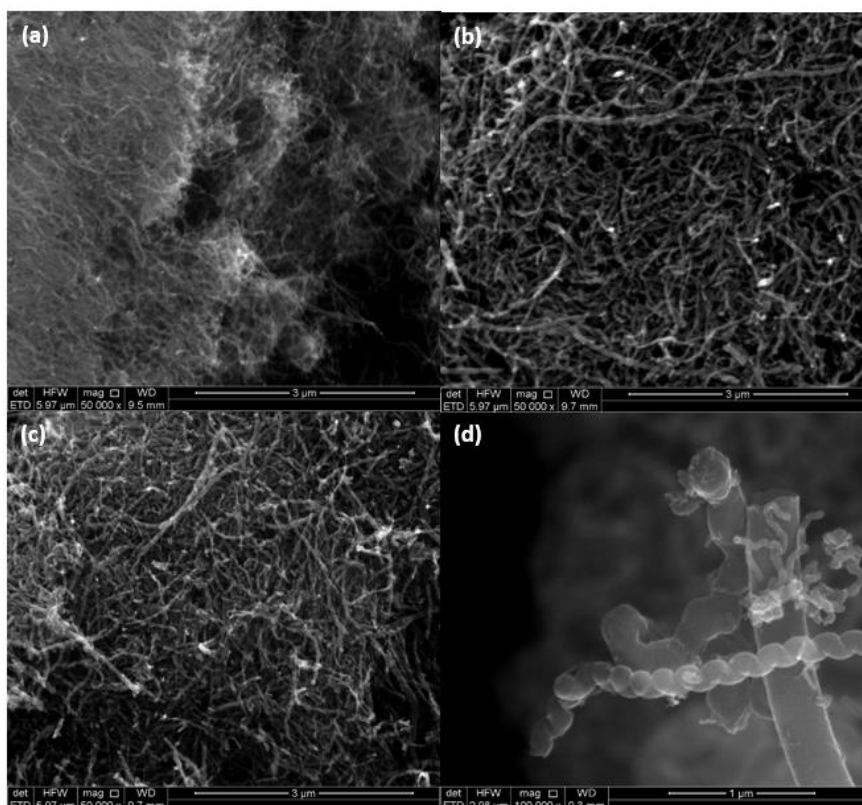


Fig. 9 SEM images of the MWCNTs under study (a) 8MWCNTs, (b) 50MWCNTs, (c) COOH-MWCNTs and (d) HMWCNTs.

As observed from the SEM images, the MWCNTs under study have different morphologies and external diameters, which influence the adsorption of PAHs along with other parameters such as the presence of functional groups on the surface.

The potential of wide applications in separation science for carbon nanotubes is due to non-covalent forces including hydrogen bonding, electrostatic forces, π - π stacking, hydrophobic interactions and van der Waals forces, thus making MWCNTs effective sorbents for the extraction and preconcentration of organic compounds [93]. In addition, their chemical and physical properties make them stable materials suitable for application as coating for SPME fibers [94]. The assessment of the four types of MWCNTs tested as coating in this work and a commercial 30 μ m-PDMS fiber is shown in Fig. 10.

Results and discussion

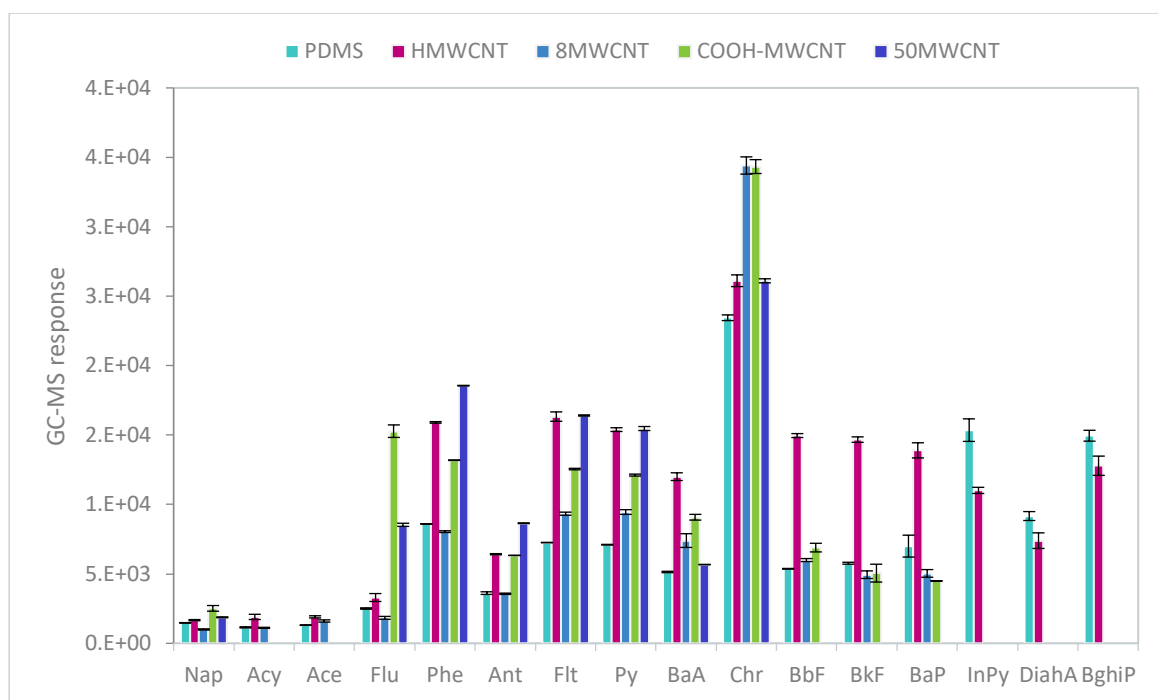


Fig. 10 Evaluation of extraction efficiency of a commercial 30 μm PDMS fiber and four different MWCNTs coated fibers for the extraction of 16 PAHs from water samples spiked with 16 PAHs at the concentration of 50 ng L^{-1} each ($n=3$). SPME conditions: sample volume, 9.5 mL; extraction temperature, 60 $^{\circ}\text{C}$; extraction time, 30 min; desorption temperature, 270 $^{\circ}\text{C}$, desorption time, 2 min.

The comparison of the fibers showed that the one coated with HMWCNT exhibited the highest GC-MS response for most PAHs compared to the other MWCNTs tested, especially for PAHs with 5 and more aromatic rings. This result is consistent with other studies in which HMWCNTs were used as sorbent to extract PAHs by DSPE [95,96]. In fact, HMWCNTs have a larger external diameter (100–200 nm) than 8MWCNT (< 8 nm) and 50MWCNT (> 50 nm), which results in better contact between planar PAHs and the flat surface of the nanotube and therefore a better extraction efficiency [72]. Concerning 50MWCNT, this material showed very good extraction efficiency for several 3 and 4-rings PAHs (Flu, Phe, Ant, Flt and Py).

As for the COOH-MWCNTs, the functionalization of the nanotube surface generally implies a reduction of the surface available for the adsorption of the analytes and this effect is even more evident when extracting planar molecules [97]. This finding could explain the absence of GC-MS response in this study for InPy, DiahA and BghiP when using COOH-MWCNTs-coated fiber.

Commercial PDMS fiber allowed for the highest extraction yield for InPy, DiahA and BghiP as it allowed for more effective desorption of the heavier PAHs. Conversely, strong adsorption occurs through the π - π interactions between PAHs with higher molecular weight and CNTs, thus making desorption more difficult [98].

Since HMWCNT fiber was shown to be the most effective for extracting most PAHs exhibiting up to 3 times higher GC responses than PDMS fiber, it was selected for method optimization and validation.

8.2 CARRYOVER EFFECT

After the selection of the fiber coated with HMWCNTs, the thermal stability of the material was investigated to evaluate the most suitable desorption conditions.

Commonly, the carryover effect is known to influence subsequent SPME analyses due to the memory effect of the analytes adsorbed on the coating, especially in the case of low volatile compounds [38]. This could compromise the extraction efficiency, therefore longer desorption times and higher desorption temperatures may be necessary [99,100].

A TGA of the HMWCNTs was performed to determine the optimal injection port temperature and desorption time values. The analysis showed that HMWCNTs are stable at temperatures below 350 °C (Fig. A1). Based on these results, a desorption temperature of 310 °C was selected to achieve desorption of all PAHs without damaging the fiber coating. The effect of desorption time was also studied in the 2 – 5 min range, resulting in a time of 5 minutes to completely desorb the analytes. These desorption conditions were found to be suitable for not observing the carryover effect.

8.3 SPME OPTIMIZATION

The extraction conditions of the HMWCNT coated fiber were optimized by running a CCD to investigate the effects of both extraction temperature and extraction time as main factors.

The experimental domain was selected taking into consideration the properties of the analytes and the feasibility of the analysis. As for the extraction temperature, values below 40 °C were not investigated as they were not sufficient to allow the extraction of the heaviest target PAHs, while values above 80 °C could favor the volatilization of the lightest analytes. As regards the extraction time, a time range suitable for routine analyses was chosen (40-60 min).

Table 5 shows the regression models calculated for each PAH. A decrease in the GC-MS response was observed for the more volatile PAHs at higher temperature values, while longer extraction times favor the adsorption of higher molecular weight PAHs (having five or six rings).

Results and discussion

The optimal conditions for the simultaneous extraction of all PAHs studied were found using the multi-criteria method of desirability functions. An extraction temperature of 68 °C and an extraction time of 60 min were calculated as optimal conditions. Furthermore, a global desirability value $D = 0.86$ and good single desirability values were obtained, thus confirming a suitable procedure for the simultaneous extraction of the 16 PAHs.

Table 5 Regression coefficients of the polynomial functions calculated by optimization procedure

PAHs	Regression models
Nap	$y = 13750 (\pm 1310) + 2730 (\pm 1210)Tt - 3040 (\pm 1390)T^2$
Acy	$y = 15130 (\pm 1340) - 3670 (\pm 1890)T^2$
Ace	$y = 13390 (\pm 1180) - 3830 (\pm 1670)T^2$
Flu	$y = 26560 (\pm 2050) - 6290 (\pm 2900)T^2$
Phe	$y = 75330 (\pm 3920) + 9630(\pm 3510)T + 18040(\pm 3510)t - 11590 (\pm 5270)T^2 - 13020(\pm 5270)t^2$
Ant	$y = 84210 (\pm 4240) + 14800 (\pm 4240)T + 25260 (\pm 4240)t - 9990 (\pm 5200)Tt - 20030 (\pm 6000)t^2$
Flt	$y = 101430 (\pm 3770) + 24020 (\pm 3750)T + 36820 (\pm 3750)t - 17770 (\pm 4590)Tt - 23470 (\pm 5300)t^2$
Py	$y = 101440 (\pm 3560) + 22420 (\pm 3560)T + 37420 (\pm 3560)t - 18060 (\pm 4360)Tt - 24260 (\pm 5030)t^2$
BaA	$y = 79150 (\pm 5090) + 37660 (\pm 7200)t - 17010 (\pm 8820)Tt$
Chr	$y = 80490 (\pm 5490) + 32560 (\pm 5490)t - 13900 (\pm 6720)Tt - 15820 (\pm 7760)t^2$
BbF	$y = 96650 (\pm 8980) + 54290 (\pm 12690)t$
BkF	$y = 92880 (\pm 8730) + 53430 (\pm 12350)t$
BaP	$y = 97060 (\pm 9670) + 57110 (\pm 13680)t$
InPy	$y = 176330 (\pm 18030) + 117950 (\pm 25490)t$
DiahA	$y = 156760 (\pm 15590) + 99730 (\pm 22040)t$
BghiP	$y = 120220 (\pm 12130) + 80370 (\pm 17150)t$

8.4 METHOD VALIDATION

The SPME-GC-MS method based on the use of HMWCNT coated fiber was validated using groundwater spiked with the standard solution of PAH, and deuterated PAH as internal standards. The HMWCNTs showed excellent capability as sorbent material for the

Results and discussion

determination of PAHs in water at ultra-trace levels, since excellent results were achieved with LOD and LOQ values at low ng L⁻¹ level for all analytes (Table 6).

Table 6 Validation parameters of the HMWCNT-SPME-GC-MS method

Compound	LOD	LOQ	$b_0(\pm s_{b_0})$	$b_1(\pm s_{b_1})$	Linear range
	ng L ⁻¹		ng L ⁻¹		
Nap	0.8	2.6	1.0 (±0.2)	0.07 (±0.01)	3 – 30
Acy	1.2	3.0	-	0.128 (±0.004)	3 – 30
Ace	1.1	3.0	-	0.093 (±0.004)	3 – 30
Flu	0.6	2.0	-	0.226 (±0.005)	3 – 30
Phe	0.1	0.4	0.8 (±0.1)	0.202(±0.009)	1.5 – 30
Ant	0.3	0.8	-	0.195 (±0.004)	1.5 – 30
Flt	0.3	0.8	-	0.173 (±0.002)	1.5 – 30
Py	0.2	0.7	0.15 (±0.05)	0.158 (±0.003)	1.5 – 30
BaA	0.7	2.2	-	0.189 (±0.004)	3 – 30
Chr	0.5	1.5	0.41 (±0.09)	0.171 (±0.005)	1.5 – 30
BbF	0.2	0.8	0.29 (±0.06)	0.162 (±0.004)	1.5 – 30
BkF	0.7	2.2	-	0.156 (±0.002)	3 – 30
BaP	0.4	1.4	0.14 (±0.04)	0.169 (±0.002)	1.5 – 30
InPy	0.3	1.0	0.5 (±0.1)	0.208 (±0.008)	1.5 – 30
DiahA	0.2	0.8	-	0.176 (±0.004)	1.5 – 30
BghiP	0.9	2.9	0.39 (±0.09)	0.192 (±0.006)	3 – 30

(-): not significant.

Regression equation: $y = b_0 + b_1 \cdot x$

Mandel's fitting test was applied in the range 3–30 ng L⁻¹ for Nap, Acy, Ace, Flu, BaA, BkF and DiahA and in the range 1.5–30 ng L⁻¹ for the other analytes, demonstrating good linearity.

Regarding repeatability, at the lowest concentration (3 ng L⁻¹) the calculated RSDs were in the range of 1.5–15% and at the highest concentration level (30 ng L⁻¹) in the range of 1.1– 11.7%. RSD values always lower than 22% were obtained for the intermediate precision (Table 7).

Results and discussion

Table 7 Repeatability and intermediate precision of the HMWCNT-SPME-GC-MS method ($n=6$)

PAHs	Repeatability (RSD%)			Intermediate precision (RSD%)		
	3 ng L ⁻¹	10 ng L ⁻¹	30 ng L ⁻¹	3 ng L ⁻¹	10 ng L ⁻¹	30 ng L ⁻¹
Nap	6	13	12	9	14	14
Acy	4	10	6	21	20	9
Ace	8	3	5	18	5	6
Flu	7	13	5	10	9	5
Phe	13	13	4	18	1	3
Ant	10	8	6	14	16	6
Flt	7	0.2	2	19	2	6
Py	7	1	2	10	7	7
BaA	6	7	5	8	16	10
Chr	6	14	5	3	13	4
BbF	12	2	5	16	22	6
BkF	2	4	3	5	9	6
BaP	2	0.1	2	10	1	2
InPy	15	3	2	9	7	11
DiaA	14	5	3	11	9	2
BghiP	5	1	1	7	5	9

For all PAHs, recovery rates were obtained in the range 92.5 (± 0.4)–119.7 (± 0.2)% calculated at concentration levels of 5 ng L⁻¹ and 30 ng L⁻¹, thus demonstrating that the analytical procedure has a suitable level of trueness even at levels close to the LOQ of the analytes (Table 8).

The excellent extraction efficiency of the fiber is also evaluated on the basis of comparison with methods developed by other authors using different coatings to determine PAHs in water samples [49,99,101–108]. The LODs provided by the developed method are appreciably lower than most of those obtained in other studies, also in relation to the type of separation or detection technique used (Table 9).

Results and discussion

Table 8 Recovery rates ($n=10$) of the HMWCNT-SPME-GC-MS method

PAHs	RR% ($\pm s_{RR\%}$)	
	5 ng L ⁻¹	30 ng L ⁻¹
Nap	118.6 (± 0.1)	108.3 (± 0.4)
Acy	105.89 (± 0.04)	102.7 (± 0.2)
Ace	118.81 (± 0.03)	101.4 (± 0.1)
Flu	109.9 (± 0.20)	102.0 (± 0.3)
Phe	100.30 (± 0.07)	98.9 (± 0.2)
Ant	117.40 (± 0.03)	98.8 (± 0.3)
Flt	95.43 (± 0.03)	101.1 (± 0.1)
Py	94.65 (± 0.03)	99.0 (± 0.1)
BaA	97.94 (± 0.01)	101.9 (± 0.3)
Chr	100.94 (± 0.01)	100.8 (± 0.3)
BbF	98.4 (± 0.1)	99.3 (± 0.2)
BkF	94.6 (± 0.1)	99.1 (± 0.1)
BaP	98.04 (± 0.03)	100.3 (± 0.1)
InPy	96.01 (± 0.06)	101.1 (± 0.2)
DiahA	92.5 (± 0.4)	99.7 (± 0.2)
BghiP	119.7 (± 0.2)	102.7 (± 0.1)

It should also be emphasized that the high sensitivity of the method developed in this Thesis concerns the 16 US-EPA PAHs which have different volatility and water solubility, while many other studies have focused only on a part of them.

Finally, the developed method can also be defined cost-effective as the fiber coated with HMWCNT proved to be reused up to 200 times without a significant loss of the extraction performance due to its thermal stability.

Results and discussion

Table 9 Comparison of LOD values achieved in this work with those of previous studies for the determination of PAHs

Coating	Analytes	LODs	Method	Technique	Reference
		ng/L			
MWCNT/ZrO ₂	6 PAHs	33 – 160	HF ^a -SPME	HPLC-UV	[99]
MWCNTs/PoPD ^b	7 PAHs	20 – 90	HS-SPME	GC-FID	[101]
MWCNTs	5 PAHs	9 – 13	HF-SPME	GC-FID	[102]
PoPD-co-PoT ^c /MCNTs	8 PAHs	1 – 6	HS-SPME	GC-MS	[49]
MWCNTs/PoAP ^d	7 PAHs	2 – 10	HS-SPME	GC-MS	[103]
MWCNTs	6 PAHs	30 – 70	HS-SPME	GC-MS	[104]
PA ^e	8 PAHs	0.05 – 5	HS-SPME	GC-HRMS	[105]
PEDOT@AuNPs ^f	5 PAHs	2.5 – 25	HS-SPME	GC-FID	[106]
PTMS-SBA-15 ^g	8 PAHs	5.1 – 37.2	HS-SPME	GC-MS	[107]
MIL-53(AI) ^h	16 PAHs	0.1 – 0.73	DI-SPME	GC- MS/MS	[108]
HMWCNTs	16 PAHs	0.1 – 1.2	DI-SPME	GC-MS	This work

^a Hollow fiber-SPME

^b Poly-ortho-phenylenediamine

^c Poly(o-phenylenediamine-co-o-toluidine)

^d Poly-ortho-aminophenol

^e Polyacrilate

^f Poly(3,4-ethylenedioxythiophene)@Au nanoparticles

^g Nanoporous phenyltrimethoxysilane functionalized silica

^h Material Institut Lavoisier

8.5 ENRICHMENT FACTORS

The HMWCNT coated SPME fiber showed a good enrichment capability in terms of EFs with values in the range 2670 (\pm 290) – 142120 (\pm 580).

The comparison with the commercial 30 μ m PDMS fiber showed that the EFs achieved with HMWCNTs were higher for most of the analytes investigated, with the exception of the heaviest PAHs (InPy, DiahA and BghiP) (Fig. 11).

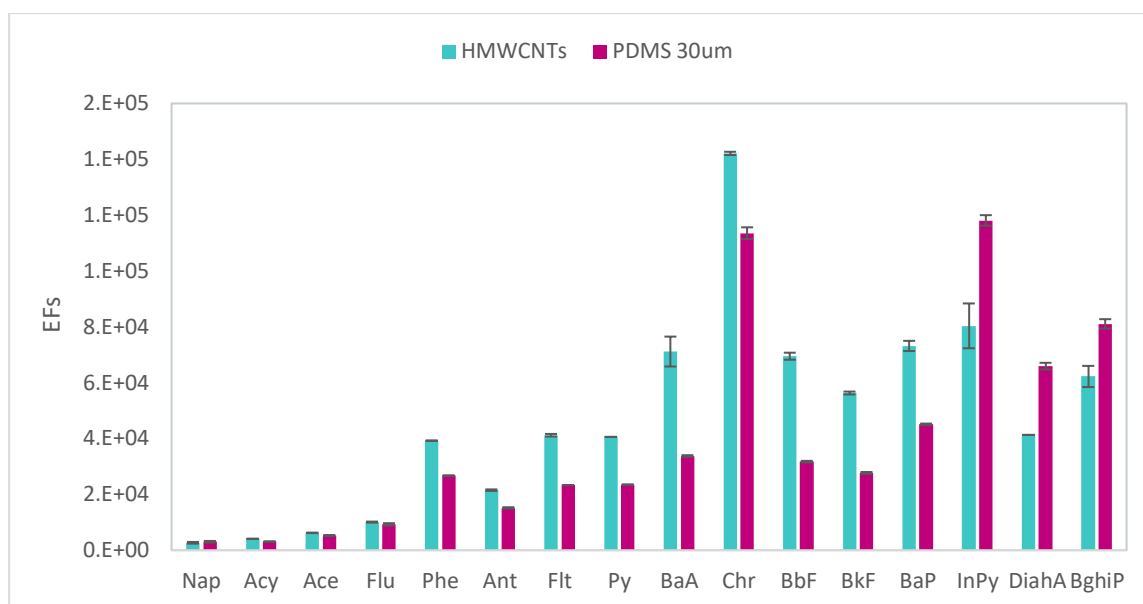


Fig. 11 EFs of the HMWCNTs-based coating vs commercial 30 µm PDMS coating ($n=3$).

As already stated, the results achieved could be explained by considering the strong adsorption of the high-molecular weight PAHs with the surface of the CNTs, making the desorption process more critical.

As shown in the figure, the highest EFs were calculated for BaA, BbF and BaP, the latter classified by the International Cancer Agency as a human carcinogen (Group 1) [23].

Getting better EFs is fundamental to achieving lower detection and quantification limits. In this perspective, the development of coatings characterized by a high extraction performance is a key point for the detection of organic compounds at ultra-trace levels, thus making the SPME technique a promising tool for paleoclimatic investigation.

8.6 REAL SNOW SAMPLES ANALYSIS

The method was successfully applied to the analysis of four surface snow samples from Ny-Ålesund (Svalbard) for the determination of PAHs at the ultra-trace level. The samples were collected in April 2019 at three sampling sites: the Austre Brøggerbreen (BRG) and Midtre Lovénbreen (MDB) glaciers, and the area of the Gruvebadet Aerosol Laboratory (GVB1 and GVB2) located near the village of Ny-Ålesund.

As shown in Table 10, Flu, Flt, InPy and BghiP represent the 67% of the Σ_{16} PAHs concentration and were detected in all samples with the following concentration ranges: 3.86–13.1 ng L⁻¹ (Flu), 2.1–2.8 ng L⁻¹ (Flt), 1.06–3.0 ng L⁻¹ (InPy) and 0.86–1.87 ng L⁻¹ (BghiP).

Results and discussion

Table 10 Concentrations of PAHs determined in Arctic snow samples from Svalbard islands

PAHs	BRG	MDB	GVB1	GVB2
	ng L ⁻¹			
Nap	4.1 (±0.5)	8.9 (±0.1)	n.d	9.9 (±0.3)
Acy	n.d	n.d	n.d	n.d
Ace	n.d	n.d	n.d	n.d
Flu	3,86 (±0.01)	5.3 (±0.1)	13.1 (±1.3)	4.2 (±0.5)
Ph	n.d	0.40 (±0.03)	1.0 (±0.1)	n.d.
An	n.d	n.d	n.d	n.d
Flt	2.6 (±0.3)	2.1 (±0.3)	2.4 (±0.3)	2.8 (±0.5)
Py	n.d.	n.d	0.8 (±0.1)	n.d.
BaA	n.d	n.d	n.d	n.d
Chry	n.d	n.d	n.d	n.d
BbF	n.d	n.d	n.d	n.d
BkF	n.d	n.d	n.d	n.d
Bap	n.d	n.d	n.d	n.d
InPy	1.06 (±0.01)	1.6 (±0.2)	3.0 (±0.1)	1.68 (±0.02)
DiahA	n.d	n.d	n.d	n.d
BghiP	0.86 (±0.05)	1.1 (±0.2)	1.87 (±0.04)	0.9 (±0.03)

(n.d.): not detected.

Nap and Phe were detected in at least 50% of the samples. Furthermore, Nap which is considered the main pollutant in the environment of Svalbard [109] when observed, was detected at the highest concentration level compared to the other PAHs.

The Σ_{16} PAHs concentration determined in the BRG sample (12.5 ng L⁻¹) had a value similar to that found in the top layer of snow by Vecchiato et al. [14], which hypothesized combustion as the main source of PAHs in the snows of Austre Brøggerbreen.

9 MEPS-GC-MS METHOD

9.1 DEVELOPMENT OF MEPS PROCEDURE

MEPS was performed by using the extract-discard extraction mode in agreement with other studies that demonstrated the best performance of this procedure in terms of recovery and sensitivity compared to the draw-eject mode [63,64]. In addition, Prieto et al. reported that by applying the extract-discard mode an improvement in the lifetime of the MEPS syringe was observed as a consequence of the reduction of the mechanical stress of the syringe plunger [63,110].

Once the extraction mode was selected, the effect of other parameters on the extraction efficiency of the MEPS technique was investigated, e.g. the type of absorbent material and the type of elution solvent [65,66]. Although a washing step may be required between sample loading and analyte elution [58], this was avoided because the wash step could adversely affect analyte recovery and because the matrix blank chromatogram showed the absence of interferent peaks in the matrix (Fig. A2).

Sample loading and analyte elution rates were also investigated (data not shown). Particular attention was paid to reach a good compromise between an effective extraction yield and obtain suitable timing for routine analyses. The speeds available on the eVol® device equipped with a 50 μL syringe are in the range of 1.67–25.00 $\mu\text{L s}^{-1}$, so the most suitable extraction and elution rates for the extraction of PAHs were found in correspondence of 12.50 $\mu\text{L s}^{-1}$ and 1.67 $\mu\text{L s}^{-1}$, respectively. In fact, an extraction rate in the range 10–20 $\mu\text{L s}^{-1}$ is considered appropriate to obtain excellent interactions between analytes and sorbent [58,63]. On the other hand, the choice of the lowest elution rate allowed a good elution of the analyte despite the use of a very small volume of solvent [63].

9.2 PERFORMANCE OF C2, C8 AND C18 SORBENTS ON PAHs MICROEXTRACTION

In general, the type of sorbent suitable for obtaining adequate recovery depends on the nature of the analytes as well as the sample matrix [57,59,62,65,110]. In this study, three different types of silica-based sorbent phase C2, C8 and C18 packed in MEPS BINs were evaluated for the extraction of the analytes from water samples. In the preliminary phase of the study, dichloromethane was used as an elution solvent, since previous studies reported its high elution

efficiency for the determination of PAHs in water samples [66,96,111]. The effect of other elution solvents on recovery for the selected sorbent phase was then evaluated.

As shown in Fig. 12 the best performance for most analytes was achieved using C8-BIN, especially for two-, three- and four-ring PAHs due to the highest sorption/partition potential, whereas C2-BIN demonstrated the highest yield for InPy, DiahA and BghiP. The lowest extraction yields for higher molecular weight PAHs using C8-BIN are likely due to the less effective elution process related to stronger retention of heavier PAHs on the C8 sorbent compared to C2.

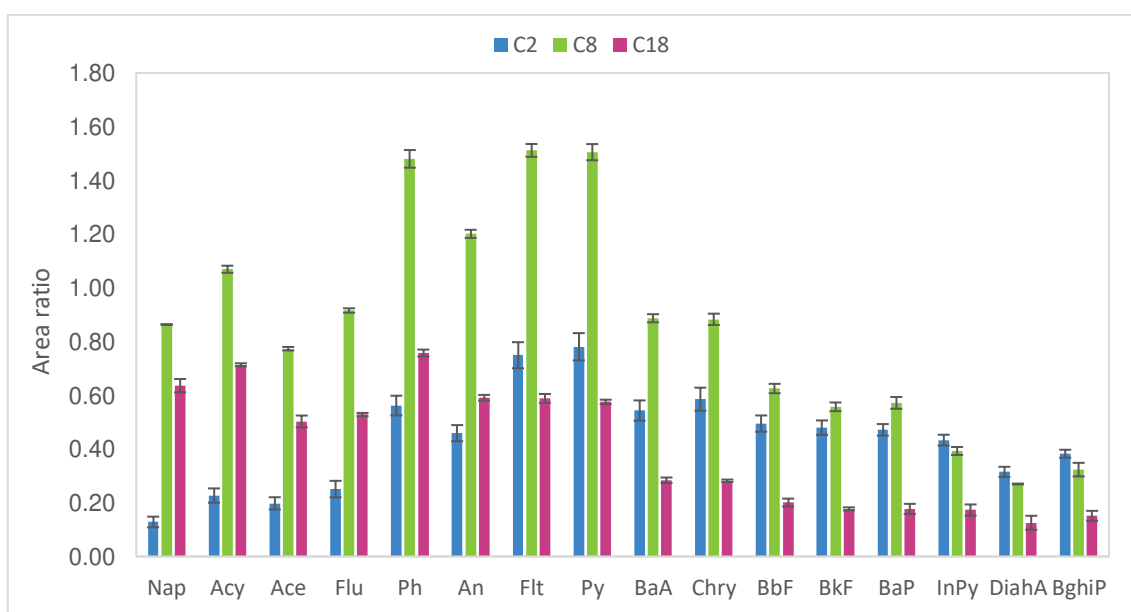


Fig. 12 Comparison of extraction efficiency of the MEPS sorbents C2-BIN, C8-BIN and C18-BIN ($n=3$). Sample PAHs concentration, 500 ng L^{-1} ; pump cycles of sample loading, $40 \times 50 \text{ }\mu\text{L}$; speed of sample loading, $12.50 \text{ }\mu\text{L s}^{-1}$; pump cycles of eluent, $10 \times 10 \text{ }\mu\text{L}$; elution solvent, DCM; speed of eluent, $1.67 \text{ }\mu\text{L s}^{-1}$.

As expected, C18-BIN was the phase that exhibited the lowest yields for PAHs with four or more aromatic rings. In fact, the C18 phase, which is characterized by a longer alkyl chain, provides a greater retention of more hydrophobic compounds and consequently a poor recovery when eluting with a small volume of organic solvent [112,113].

Therefore, C8-BIN was selected as the most suitable MEPS sorbent having more balanced performance for this application compared to C2-BIN and C18-BIN, considering the wide range of $\log K_{ow}$ values of the analytes considered in this study.

9.3 EFFECT OF DESORPTION SOLVENTS ON PAHs MICROEXTRACTION

Since the type of eluting solvent is also a fundamental parameter for the performance of MEPS

[57], DCM, EtAc and MeOH were studied for the elution of the 16 PAHs from C8-BIN. Fig. 13 shows that EtAc determined the best recovery for all target analytes except Nap. The lowest response obtained by DCM is probably due to residual water on the sorbent particles packed in the BIN after sample loading despite the drying step. This could result in a poor recovery of PAHs being DCM immiscible with water. Regarding MeOH, other works proposed it as elution solvent for PAHs desorption from silica-based BIN [64,66,67,114]. However, in the present study MeOH showed lower responses than EtAc with the exception of Nap. In fact, Nap which has the lowest K_{ow} has a more effective desorption by MeOH. Finally, the effect of the solvents was tested by performing a one-way ANOVA followed by Bonferroni t -test for multiple comparisons. The presence of significant differences ($p < 0.05$) between the mean responses was demonstrated by ANOVA. The better extraction yield of EtAc for all PAHs (except Nap) compared to MeOH was confirmed by the t -test ($p < 0.05$). Based on these findings, EtAc was applied in the overall MEPS experiments.

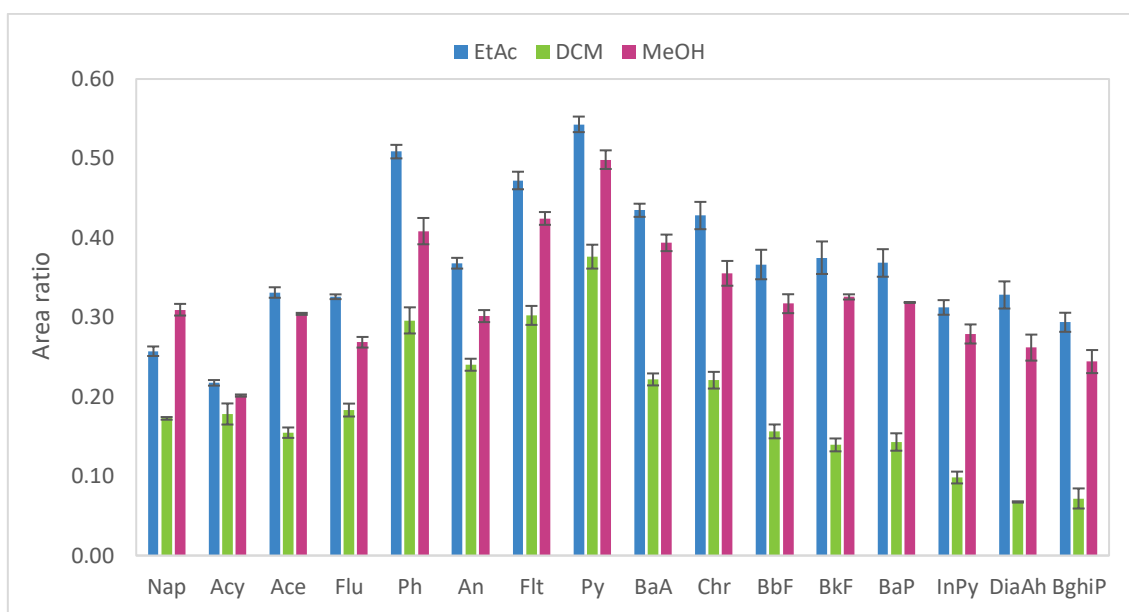


Fig. 13 Comparison of performance of elution solvent (DCM, EtAc, MeOH) ($n=3$). Sample PAHs concentration, 250 ng L^{-1} ; pump cycles of sample loading, $40 \times 50 \text{ }\mu\text{L}$; speed of sample loading, $12.50 \text{ }\mu\text{L s}^{-1}$; pump cycles of eluent, $10 \times 10 \text{ }\mu\text{L}$; speed of eluent; $1.67 \text{ }\mu\text{L s}^{-1}$; sorbent, C8.

9.4 MEPS OPTIMIZATION

After establishing the loading and elution rates and selecting the appropriate sorbent and elution solvent, an FCD was run to optimize the number of loading and elution cycles. The number of loading cycles should ideally be sufficient to reach a suitable concentration factor while avoiding prolonged extraction times [115].

Table 11 shows the calculated regression models used to estimate the optimal extraction

Results and discussion

conditions for the 16 PAHs.

Table 11 Regression model for each analyte

PAHs	Regression models
Nap	$y = 574 (\pm 30) + 118 (\pm 39)x_1 - 230 (\pm 39)x_2$
Acy	$y = 666 (\pm 34) + 104 (\pm 43)x_1 - 283 (\pm 43)x_2$
Ace	$y = 499 (\pm 27) + 96 (\pm 34)x_1 - 200 (\pm 34)x_2$
Flu	$y = 569 (\pm 32) + 111 (\pm 40)x_1 - 240 (\pm 40)x_2$
Phe	$y = 848 (\pm 50) + 152 (\pm 64)x_1 - 375 (\pm 64)x_2$
Ant	$y = 640 (\pm 41) + 122 (\pm 51)x_1 - 296 (\pm 51)x_2$
Flt	$y = 798 (\pm 46) + 145 (\pm 58)x_1 - 359 (\pm 58)x_2$
Py	$y = 819 (\pm 46) + 138 (\pm 58)x_1 - 350 (\pm 58)x_2$
BaA	$y = 489 (\pm 34) - 193 (\pm 43)x_2$
Chr	$y = 495 (\pm 34) - 199 (\pm 43)x_2$
BbF	$y = 304 (\pm 28) + 74 (\pm 35)x_1 - 198 (\pm 35)x_2$
BkF	$y = 301 (\pm 28) + 74 (\pm 35)x_1 - 173 (\pm 35)x_2$
BaP	$y = 325 (\pm 34) - 181 (\pm 43)x_2$
InPy	$y = 201 (\pm 23) - 204 (\pm 29)x_2$
DiaA	$y = 133 (\pm 25) - 159 (\pm 31)x_2$
BghiP	$y = 212 (\pm 23) - 216 (\pm 29)x_2$

x_1 : number of loading cycles.

x_2 : number of elution cycles.

The variable x_1 , when significant, shows an increase in the GC-MS response of analytes for a high number of loading cycles, on the contrary a reduced number of elution cycles is adequate to achieve satisfactory recovery.

Finally, the multicriteria method of desirability functions allowed to identify the optimal conditions for the simultaneous extraction of the PAHs studied, namely 80 loading cycles and 3 elution cycles.

The global desirability was $D = 0.91$ with also good single desirability values always higher than 0.9. The developed method therefore proved to be feasible for the simultaneous extraction of target analytes. Furthermore, the method can also be considered time efficient having an

Results and discussion

average time of 20 minutes *per* sample compared to MEPS procedures reported by other authors, which require a greater number of loading and eluting cycles [64,67].

9.5 METHOD VALIDATION

Under the above mentioned optimal extraction conditions, linearity, LOD, LOQ, trueness and precision were evaluated as validation parameters for the developed MEPS-GC-MS method.

In addition, the extraction potential of the C8 sorbent was also assessed by calculating the EFs exhibiting good results ranging from 64 (± 7) for Ace to 129 (± 18) for Phe.

Table 12 Validation parameters of the developed MEPS-GC-MS method

Compound	LOD	LOQ	$b_0(\pm s_{b_0})$	$b_1(\pm s_{b_1})$	Linear range
	ng L ⁻¹				ng L ⁻¹
Nap	1	4	0.088 (± 0.003)	0.00248 (± 0.00004)	LOQ – 150
Acy	1	4	0.026 (± 0.005)	0.0023 (± 0.0001)	LOQ – 150
Ace	1	5	-	0.0036 (± 0.0001)	LOQ – 150
Flu	1	2	0.03 (± 0.01)	0.0027 (± 0.0001)	LOQ – 150
Phe	0.3	1	0.17 (± 0.01)	0.0029 (± 0.0001)	LOQ – 150
Ant	1	4	0.07 (± 0.01)	0.0030 (± 0.0001)	LOQ – 150
Flt	0.3	1	0.05 (± 0.01)	0.0039 (± 0.0002)	LOQ – 150
Py	0.4	1	0.06 (± 0.02)	0.0044 (± 0.0002)	LOQ – 150
BaA	1	2	0.04 (± 0.01)	0.0036 (± 0.0001)	LOQ – 150
Chr	1	2	0.04 (± 0.01)	0.0061 (± 0.0001)	LOQ – 150
BbF	3	8	0.06 (± 0.02)	0.0032 (± 0.0002)	LOQ – 150
BkF	3	8	-	0.0064 (± 0.0002)	LOQ – 150
BaP	4	13	0.09 (± 0.02)	0.0040 (± 0.0003)	LOQ – 150
InPy	3	12	0.05 (± 0.01)	0.0034 (± 0.0001)	LOQ – 150
DiahA	5	15	-	0.0042 (± 0.0001)	LOQ – 150
BghiP	4	14	0.07 (0.02)	0.0037 (± 0.0002)	LOQ – 150

(-): not significant.

Regression equation: $y = b_0 + b_1 \cdot x$

Results and discussion

Table 12 shows the excellent LOD values at the low level of ng L^{-1} for all target PAHs provided by the developed method, thus demonstrating fitness for purpose for the analysis of the analytes at ultra-trace levels.

These values are comparable with those reported in previous works [64,67], which validated the methods using spiked ultrapure water, while in the present study the validation was carried out using uncontaminated snow from Antarctic Plateau as blank sample. Good linearity in the LOQ – 150 ng L^{-1} range for all PAHs was verified by applying the Mandel fitting test.

Table 13 Repeatability and intermediate precision of the MEPS-GC-MS method ($n=6$)

PAHs	Repeatability (RSD%)			Intermediate precision (RSD%)		
	15 ng L^{-1}	50 ng L^{-1}	150 ng L^{-1}	15 ng L^{-1}	50 ng L^{-1}	150 ng L^{-1}
Nap	2	0,4	2	5	4	6
Acy	0,3	2	1	9	7	3
Ace	3	4	4	10	12	12
Flu	4	4	10	13	9	10
Phe	7	2	1	6	5	0,4
Ant	5	2	1	11	4	6
Flt	4	4	0,1	3	9	5
Py	1	0,8	2	9	9	2
BaA	10	0,3	4	8	2	12
Chr	11	8	2	12	13	9
BbF	3	6	3	15	15	1
BkF	2	10	5	12	11	13
BaP	5	4	9	14	14	15
InPy	1	10	1	7	15	8
DiahA	5	11	7	9	11	6
BghiP	11	9	6	15	11	11

Precision in terms of repeatability was calculated showing RSDs% in the range 0.3-11% at the lowest concentration (15 ng L^{-1}) and in the range 0.1-10% at the highest concentration level (150 ng L^{-1}). As regards the three-day intermediate precision, RSD values were always lower

Results and discussion

than 15% (Table 13).

Recovery rates in the range of 77.6 (± 0.1)–120.8 (± 0.1)% were achieved, thus demonstrating the good trueness of the developed method (Table 14).

Table 14 Recovery rates ($n=10$) of the MEPS-GC-MS method

PAHs	RR% ($\pm s_{RR\%}$)		
	20 ng L ⁻¹	70 ng L ⁻¹	130 ng L ⁻¹
Nap	117.05 (± 0.02)	99.96 (± 0.02)	89.65 (± 0.02)
Acy	110.9 (± 0.1)	119.33 (± 0.03)	111.5 (± 0.1)
Ace	81.46 (± 0.01)	93.00 (± 0.01)	87.63 (± 0.01)
Flu	120.8 (± 0.1)	119.58 (± 0.03)	120.1 (± 0.1)
Phe	100.31 (± 0.01)	112.18 (± 0.01)	105.38 (± 0.01)
Ant	108.63 (± 0.04)	115.86 (± 0.02)	108.06 (± 0.04)
Flt	104.56 (± 0.03)	118.96 (± 0.02)	112.03 (± 0.03)
Py	104.32 (± 0.01)	110.23 (± 0.01)	102.66 (± 0.01)
BaA	80.13 (± 0.01)	77.86 (± 0.01)	79.37 (± 0.01)
Chr	111.61 (± 0.02)	95.83 (± 0.02)	86.03 (± 0.02)
BbF	78.07 (± 0.04)	81.66 (± 0.02)	85.63 (± 0.04)
BkF	101.3 (± 0.1)	82.46 (± 0.04)	83.2 (± 0.1)
BaP	106.4 (± 0.1)	87.29 (± 0.04)	77.6 (± 0.1)
InPy	101.70 (± 0.03)	94.34 (± 0.02)	85.95 (± 0.03)
DiahA	95.02 (± 0.04)	78.93 (± 0.02)	79.80 (± 0.04)
BghiP	98.92 (± 0.04)	100.25 (± 0.03)	92.74 (± 0.04)

Furthermore, it should be emphasized the high analytical performance of this method demonstrated suitable for the determination of all 16 PAHs, i.e., compounds very different in terms of physical and chemical properties, while other MEPS methods mainly concerned only low molecular weight PAHs [66,114], with the exception of the previously commented MEPS-GC-MS methods [64,67].

It should also be noted that these results were obtained by extracting a sample volume of 4 mL,

representing a further result for the purposes of paleoclimatic temporal resolution, unlike other studies on PAH contamination in polar sites based on the use of very large sample volumes (7 – 10 L) [5,10].

9.6 REAL SNOW SAMPLE ANALYSIS

The determination of PAHs in five surface snow samples kindly provided by the PNRA project “Emerging COntaminants in Antarctic Snow: sources and TRAnsport” demonstrated the applicability of the developed MEPS-based method.

Samples were collected at four sites on the coast of Victoria Land (Antarctica) during the austral summer 2020-2021 (Fig. 14).

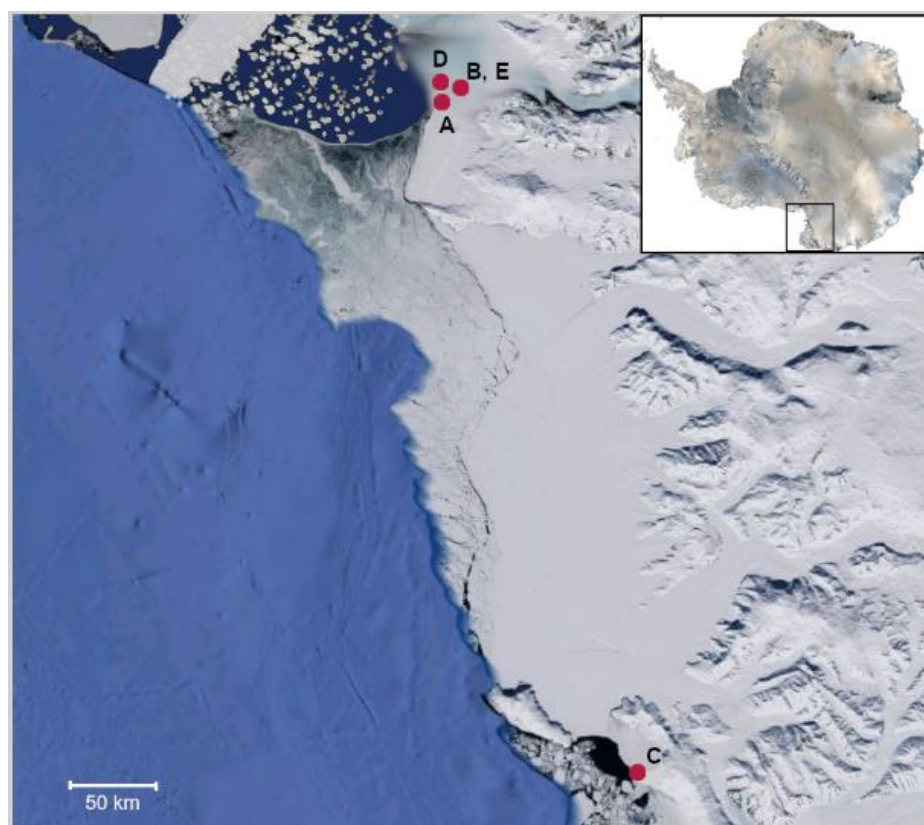


Fig. 14 Sampling sites in Antarctica of the snow samples analysed in this study

Sample A was from the Icaro Camp meteorological station area ($74^{\circ} 42'37''$ S, $164^{\circ} 07'05''$ E); samples B and E were collected near the “Enigma Lake” scientific research base ($74^{\circ} 43'$ S, $164^{\circ} 01'$ E); samples C and D were sampled near Cape Phillips ($73^{\circ} 03'$ S, $169^{\circ} 36'$ E) and Adélie Cove ($74^{\circ} 45'$ S, $164^{\circ} 00'$ E) respectively. The latter is a colony of around 13 – 15 thousands Adélie penguin nests.

PAHs with more than four aromatic rings were not detected in the samples analysed (Table 15).

Results and discussion

This could be explained considering the low presence of high molecular weight PAHs in the snow matrix as they are more lipophilic and less water soluble than lighter PAHs [116]. Values ranging from 24 to 39 ng L⁻¹ for Σ_{16} PAH concentrations were detected in each sample, with the lowest concentration detected at the site near Adélie Cove (D). In general, the concentrations of Σ_{16} PAHs showed comparable values among the different areas considered, including even the most isolated sampling site (Cape Phillips).

Table 15 Concentrations of PAHs determined in the Antarctic snow samples

PAHs	Icaro (A)	Enigma (B)	Cape Phillips (C)	Adélie Cove (D)	Enigma2 (E)
	ng L ⁻¹				
Nap	11.2	8.8	7.8	6.7	6.0
Acy	n.d.	n.d.	7.1	n.d.	7.4
Ace	n.d.	n.d.	n.d.	n.d.	n.d.
Flu	10.1	7.8	8.1	7.7	8.5
Phe	n.d.	n.d.	n.d.	n.d.	n.d.
Ant	n.d.	n.d.	n.d.	n.d.	n.d.
Flt	5.2	6.2	5.2	5.1	5.3
Py	4.3	5.7	4.2	4.4	4.2
BaA	n.d.	6.9	n.d.	n.d.	n.d.
Chr	n.d.	3.5	n.d.	n.d.	n.d.
BbF	n.d.	n.d.	n.d.	n.d.	n.d.
BkF	n.d.	n.d.	n.d.	n.d.	n.d.
BaP	n.d.	n.d.	n.d.	n.d.	n.d.
InPy	n.d.	n.d.	n.d.	n.d.	n.d.
DiahA	n.d.	n.d.	n.d.	n.d.	n.d.
BghiP	n.d.	n.d.	n.d.	n.d.	n.d.

(n.d.): not detected.

The compounds that exhibited the highest concentration level compared to the other analytes for all sampling sites were Nap and Flu (41 and 42% of the total Σ_{16} PAH, respectively). They are also the main components of diesel fuel [117], therefore these results confirmed other

Results and discussion

studies describing the presence of regional environmental pollution around scientific stations due to naval operations and fuel combustion [8,10,15]. Furthermore, the mean concentration of $\Sigma_{16}\text{PAHs}$ of the analysed samples is 32 ng L^{-1} , very similar to that described by Vecchiato et al. [10], who hypothesized a contamination due to distribution of PAHs by wind from a twin-otter refueling point since an anomalous concentration of Nap was detected in the sample collected at Mid Point. These considerations further support the description of PAH contamination phenomena due to local sources in Antarctica.

As stated in the Introduction, Antarctica could be regarded as the most pristine region compared to other remote areas [27]. For comparison purposes, the concentrations of PAHs determined in this work were compared with those found in other remote areas, such as Caucasus and Alps. The concentrations of PAHs found in the ice core drilled in 2009 at the western Elbrus plateau showed a concentration range of $112\text{--}166 \text{ ng L}^{-1}$ in the upper and hence more recent part of the core [2].

The seasonal snowpack of the eastern Italian Alps corresponding to 2004–2005 was examined by Gabrieli et al. [118]. High altitude sites ($> 1700 \text{ m a.s.l.}$) revealed ΣPAH concentrations ranging from 20 to 59 ng L^{-1} . As regards the urban area of the valley bottom, the highest concentration of ΣPAH was found, i.e. 290 ng L^{-1} .

Therefore, as evidenced by comparing different remote environments, the differences in the level of contamination reflect the influence for each sampling site of their regional sources, as well as of PAH deposition and distribution phenomena.

10 SPME-GC-MS METHOD USING MWCNT-CD NANOCOMPOSITE AS FIBER COATING

10.1 CHARACTERIZATION OF THE MWCNT-CD NANOCOMPOSITES

As already reported, the determination of PAHs in polar snow and ice samples presents issues due to the high sensitivity and selectivity required by the analytical methods to allow the detection of the analytes at ultratrace levels. This condition is particularly truthful for PAHs with 4 or more aromatic rings since these compounds are more lipophilic than lighter PAHs [116]. Therefore, in order to increase the extraction efficiency of MWCNTs towards the heavier PAHs, nanocomposites based on MWCNTs and CDs (β - and γ -) were prepared. The choice of β -CD and γ -CD, respectively is related to the presence of cavities suitable for the complexation of PAHs, thus allowing to improve the interactions between the sorbent and the target analytes [73,80].

The effect of oxidation treatments on the MWCNTs was evaluated by means of ζ -potential measurements on the concentration of carboxylic functionalization on the graphitic surface. More negative ζ -potential values compared to the untreated COOH-MWCNT were observed when the oxidation treatments were performed, thus suggesting an increased presence of OH groups on the surface of the nanotubes (Table A1).

Subsequent reduction of oxidized MWCNTs with hydrazine hydrate was performed to reduce defects on the MWCNTs. Raman spectra (Fig. A3) show that the R-value representing the intensity of the band ratio I_D/I_G was slightly lower for reduced systems, thus suggesting a decrease of the defects on the surface of the MWCNT after the reduction process.

The presence of CDs onto the surface of the MWCNTs was assessed also by FTIR (Fig. A5) and XPS (Figg. A6-A7) analyses. Fig. A6 shows the XPS spectra related to C1s and O1s of the COOH-MWCNT, MWCNT-HNO₃- γ -CD and MWCNT-H₂O₂- γ -CD samples. A higher intensity of the peak of the structures with high binding energies is observed in the samples containing CDs compared to the reference COOH-MWCTN sample, thus confirming that the supramolecular receptors are able to interact with the MWCNTs mainly via H-bonding

Finally, the TGA curves (Fig. A4) confirmed the thermal stability of the materials, thus assessing the reliability for SPME applications.

10.2 PERFORMANCE STUDY OF DIFFERENT MWCNT-CD NANOCOMPOSITES AS FIBER COATINGS

As mentioned in the introduction, the MWCNT-CD based nanocomposite was initially evaluated as sorbent material for magnetic D- μ -SPE. However, poor recovery values were obtained (data not shown), probably due to issues related to not exhaustive elution using a few μ L of organic solvent. Therefore, the evaluation of the nanocomposites was carried out using the SPME technique, which involves the thermal desorption of analytes [119].

The performance of the MWCNT-HNO₃- β -CD, MWCNT-HNO₃- γ -CD, MWCNT-H₂O₂- β -CD, MWCNT-H₂O₂- γ -CD and original COOH-MWCNTs fibers were compared in terms of GC-MS response (Fig. 15).

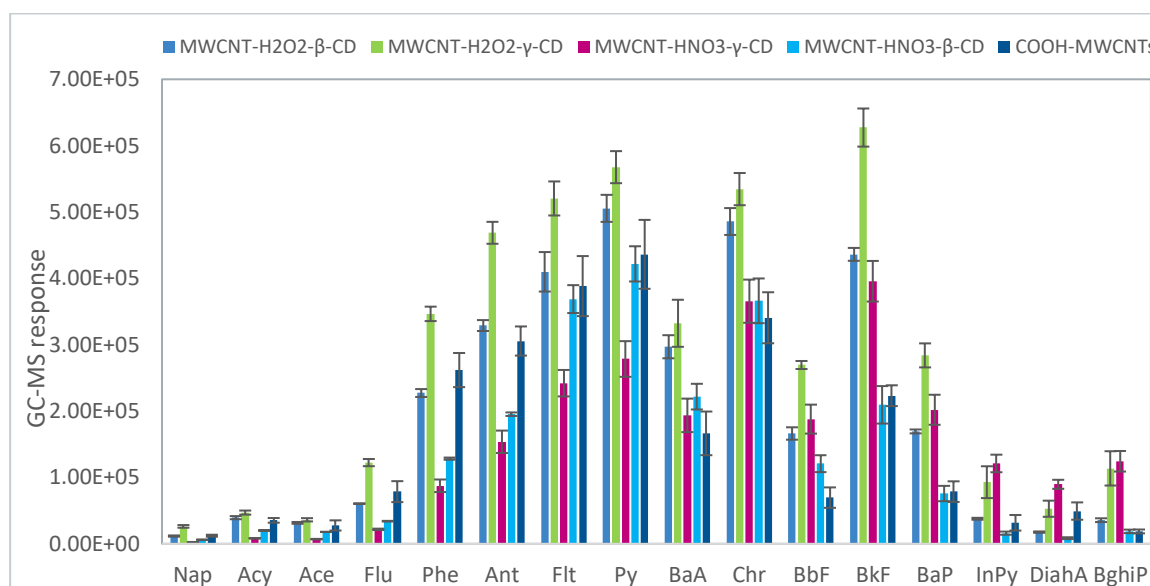


Fig. 15 Comparison of the responses of the four MWCNT-CD nanocomposites coatings and COOH-MWCNTs for the DI-SPME-GC-MS analysis of the investigated PAHs (extraction time: 60 min, extraction temperature: 68 °C; desorption temperature, 270 °C, desorption time, 2 min) ($n=3$).

The sorption mechanism of PAHs by COOH-MWCNTs was previously discussed in paragraph 8.1. As for the COOH-MWCNT fiber a significant decrease of the extraction performance (up to 7 times in terms of GC-MS response) was observed after nine extraction cycles. This behaviour can be ascribed to the decarboxylation of the coating when exposed to the high temperatures of the GC injector required for desorption of the analytes [120]. By contrast, fibers coated with MWCNT-CD based materials proved to be stable up to 270 °C with a weight loss of about 7% and 1% for β -CD and γ -CD based coating, respectively (Fig. A4).

In general, the best extraction performance for most of the investigated PAHs were obtained using the fibers coated with the materials subjected to H₂O₂ treatment. As reported by Datsyuk et al. it could be hypothesised that the use of strong oxidizing agents, such as HNO₃, lead to

exfoliation and fragmentation of the material itself. On the contrary, a lower degree of damage is obtained when the H₂O₂ treatment is applied [90].

Although in this work the MWCNT-HNO₃ have undergone to a less extreme treatment (not refluxed), compared to the procedure reported in literature [90], the material was likely affected by damage to the graphitic integrity as well, with a consequent increase in carbon defects. This was confirmed by the most negative ζ -potential value obtained compared to MWCNT-H₂O₂ and pristine COOH-MWCNTs (Table A1). Hence, the H₂O₂ treatment proved to be more effective providing a gentler oxidation of CNTs.

Among the fibers coated with nanocomposites and synthesized starting from MWCNT-H₂O₂, the MWCNT-H₂O₂- γ -CD provided the best extraction performance. This may be the result of the ability of γ -CD to better complex PAHs, especially the higher molecular weight PAHs. These findings are in agreement with the results achieved by Belenguer-Sapiña et al. which obtained better extraction performance for the investigated PAHs using γ -CD compared to β -CD [80]. This behavior was attributed to the cavity size of the CDs. In fact, the greater interaction between PAHs and γ -CD is related to the possibility for the molecules to fit completely in the cavity and not only with a part of them [80,81]. More precisely, the ability of CD to form an inclusion complex with a guest molecule is mainly due to steric factors, i.e. it depends on both the size of the CD cavity and the size of the guest molecule as well as on the orientation of the molecule in the CD cavity and the overall hydrophobicity of the guest. Therefore, only compounds with similar or smaller molecular size and adequate structure have the possibility of being included within the cavities of CDs by means of hydrophobic interactions or Van der Waals forces [81,121]. In order to confirm the complexation capability of the γ -CD towards the investigated PAHs further studies based on ¹H-NMR are in progress.

It should be considered that, in addition to the complexation capability of CDs, MWCNTs also promote the extraction of PAHs mainly via π - π interactions. The performance of the developed CD-based materials was compared with those achieved using the other materials tested during the PhD research activity. The performance of the nanocomposites obtained from MWCNT-H₂O₂ resulted to be significantly higher than those of the COOH-MWCNT fiber (Fig. 15). In particular, the MWCNT-H₂O₂- γ -CD coated fiber showed GC-MS responses up to 6 times higher than the COOH-MWCNT fiber for all the 16 PAHs. This result is even more remarkable if we consider that the COOH-MWCNT fiber showed an evident decrease in the extraction performance after 6 extraction cycles due to the decarboxylation of the sorbent. Therefore, the MWCNT-H₂O₂- γ -CD coated fibers were selected for method optimization and validation

purposes.

10.3 SPME OPTIMIZATION

Both the extraction and desorption conditions were optimized by applying a CCD. Similarly to the case of the SPME-GC-MS method based on the use of HMWCNTs, the selected extraction parameters were extraction temperature and extraction time.

Table 16 Regression model for each analyte

PAHs	Regression models
Nap	$y = 10278 (\pm 636) - 1307 (\pm 511)x_2$
Acy	$y = 28400 (\pm 2436) - 13177 (\pm 1958)x_2$
Ace	$y = 24104 (\pm 1474) - 11319 (\pm 1185)x_2$
Flu	$y = 73865 (\pm 3807) - 18240 (\pm 3060)x_2$
Phe	$y = 215426 (\pm 13529) + 28655 (\pm 10875)x_3$
Ant	$y = 329525 (\pm 13761) + 65539 (\pm 11062)x_2 + 44989 (\pm 11062)x_3 - 29824 (\pm 12367)x_2x_3$
Flt	$y = 350403 (\pm 10879) + 143907 (\pm 9730)x_2 + 89682 (\pm 9730)x_3 + 38395 (\pm 14595)x_3^2$
Py	$y = 375910 (\pm 9323) + 168742 (\pm 7738)x_2 + 102450 (\pm 7738)x_3 + 38202 (\pm 13898)x_2^2 + 33028 (\pm 13898)x_3^2$
BaA	$y = 136219 (\pm 13237) + 75300 (\pm 11840)x_2 + 68400 (\pm 11840)x_3 + 70949(\pm 17760)x_2^2$
Chr	$y = 386033(\pm 19288) + 118321(\pm 16009)x_2 + 127226(\pm 16009)x_3 - 71651 (\pm 28753)x_1^2 + 141084 (\pm 28753)x_2^2$
BbF	$y = 134342 (\pm 22614) + 46482 (\pm 15105)x_3$
BkF	$y = 474448 (\pm 67769) + 149182 (\pm 45266)x_3$
BaP	$y = 122203 (\pm 17018) + 44173 (\pm 13680)x_3 + 89557 (\pm 26280)x_2^2$
InPy	$y = 133868 (\pm 19778) + 42874 (\pm 13211)x_3$
DiaHA	$y = 132997 (\pm 20563) + 40591 (\pm 13735)x_3 - 68914 (\pm 26750)x_1^2$
BghiP	$y = 167597 (\pm 17969) + 47667 (\pm 12002)x_3 - 68801 (\pm 23375)x_1^2$

x₁: desorption time

x₂: extraction temperature

x₃: extraction time

Taking into account that the desorption of the higher molecular weight PAHs requires high

desorption temperatures, the desorption time was considered as additional variable to be optimised (in the 3-5 min range) in order to identify the most suitable condition for obtaining an efficient recovery of the analytes without excessive stress on the fiber.

Table 16 shows the regression models calculated for each PAH. Response surfaces for Ant, Py and BaP are also presented in Fig. 16. As expected, the low molecular weight PAHs show a negative coefficient in correspondence with the extraction temperature, whereas, a longer extraction time positively affects the extraction of higher molecular weight PAHs.

Using the desirability function method, the optimal conditions resulted in a desorption time of 4 min, an extraction temperature of 40 °C and an extraction time of 80 min, with a global desirability $D = 0.81$. The results showed that a low temperature extraction and a prolonged extraction time were required in order to promote the adsorption of the analytes on the fiber coating. Desorbing PAHs for 4 min at 270 °C allowed to achieve the complete recovery of the extracted analytes, in fact no carryover was observed after desorption.

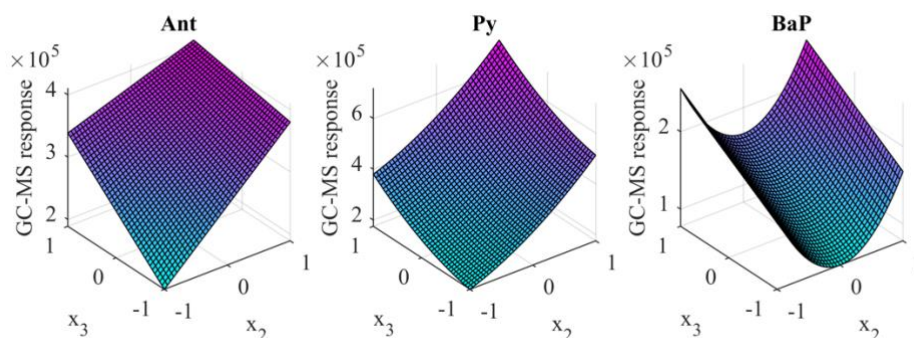


Fig. 16 Response surfaces of Ant, Py and Ba. depicted by representing the temperature (x_2) and extraction time (x_3) vs. GC-MS response

10.4 METHOD VALIDATION

Under optimized conditions, the method was validated showing excellent LOD and LOQ values in the low ng L^{-1} (Table 17). The LODs obtained were lower than those achieved using the HMWCNT coated fiber (Table 18). The capability of determining lower concentrations levels, especially for heavier PAHs, plays a very important role in paleoclimatic investigations. In fact, PAHs with 4 or more rings are more lipophilic and less soluble in water than PAHs having low molecular weight, therefore their concentrations in aqueous matrices are even lower. Good linearity for over an order of magnitude in the LOQ – 30 ng L^{-1} range was demonstrated by applying the Mandel's fitting test. Excellent trueness was confirmed in terms of RR in the 88 (± 2) – 119.8 (± 0.4)% range, calculated at 3, 10 and 20 ng L^{-1} (Table 19). Furthermore,

Results and discussion

satisfactory precision was calculated in terms of repeatability and intermediate precision over three days, always exhibiting RSD within 21% also at the lowest level (Table 20).

Table 17 Validation parameter of the developed method

Compound	LOD	LOQ	$b_0(\pm s_{b_0})$	$b_1(\pm s_{b_1})$	Linear range
	ng L ⁻¹		ng L ⁻¹		
Nap	0.7	2.3	0.15 (± 0.1)	0.015 (± 0.001)	LOQ–30
Acy	0.7	2.2	0.07 (± 0.2)	0.062 (± 0.001)	LOQ–30
Ace	0.4	1.4	-	0.058 (± 0.001)	LOQ–30
Flu	0.2	0.8	0.32 (± 0.9)	0.14 (± 0.1)	LOQ–30
Phe	0.1	0.3	0.32 (± 0.5)	0.036 (± 0.009)	LOQ–30
Ant	0.2	0.7	0.20 (± 0.3)	0.042 (± 0.002)	LOQ–30
Flt	0.1	0.2	-	0.41 (± 0.01)	LOQ–30
Py	0.1	0.3	1.2 (± 0.4)	0.44 (± 0.02)	LOQ–30
BaA	0.2	0.6	0.2 (± 0.1)	0.151 (± 0.005)	LOQ–30
Chr	0.1	0.5	-	0.64 (± 0.01)	LOQ–30
BbF	0.2	0.8	-	0.175 (± 0.004)	LOQ–30
BkF	0.3	0.9	-	0.86 (± 0.02)	LOQ–30
BaP	0.3	1.0	-	0.36 (± 0.01)	LOQ–30
InPy	0.2	0.6	-	0.30 (± 0.01)	LOQ–30
DiahA	0.3	0.9	0.4 (± 0.2)	0.30 (± 0.01)	LOQ–30
BghiP	0.3	0.9	0.5 (± 0.1)	0.35 (± 0.01)	LOQ–30

(-): not significant.

Regression equation: $y = b_0 + b_1 \cdot x$

Results and discussion

Table 18 Comparison of performance of the validated SPME-GC-MS methods under study

Fiber coatings	LODs (ng L ⁻¹)	Recovery rate (%)*	Intermediate precision (RSD%)**
HMWCNTs	0.1–1.2	92.5 (±0.4)–119.7 (±0.2)	≤22
MWCNT-H ₂ O ₂ -γ-CD	0.1–0.7	88 (±2) – 119.8 (±0.4)	≤21

*(n=10)

***(n=6) Over three days

Table 19 Recovery rates (n=10) of the MWCNT-H₂O₂-γ-CD-SPME-GC-MS method.

PAHs	RR% (±s _{RR%})		
	3 ng L ⁻¹	10 ng L ⁻¹	20 ng L ⁻¹
Nap	87.8 (±0.2)	91.0 (±0.1)	91.45 (±0.26)
Acy	111.31 (±0.04)	94.3 (±0.1)	91.19 (±0.18)
Ace	110.57 (±0.06)	91.1 (±0.1)	91.87 (±0.29)
Flu	109.9 (±0.1)	95.3 (±0.2)	94.85 (±0.29)
Phe	112.72 (±0.07)	119.7 (±0.1)	117.56 (±0.19)
Ant	89.1 (±0.1)	90.4 (±0.1)	91.7 (±0.1)
Flt	119.80 (±0.04)	90.80 (±0.04)	97.8 (±0.3)
Py	90.38 (±0.06)	92.26 (±0.03)	97.28 (±0.39)
BaA	96.17 (±0.06)	95.7 (±0.1)	98.8 (±0.5)
Chr	119.33 (±0.01)	93.40 (±0.04)	96.11 (±0.18)
BbF	104.16 (±0.08)	105.1 (±0.1)	105.2 (±0.2)
BkF	107.15 (±0.03)	97.7 (±0.1)	100.9 (±0.3)
BaP	95.51 (±0.03)	91.4 (±0.1)	94.1 (±0.2)
InPy	109.07 (±0.18)	100.56 (±0.19)	97.98 (±0.16)
DiahA	115.19 (±0.09)	90.11 (±0.9)	99.01 (±0.02)
BghiP	90.7 (±0.3)	88.09 (±0.05)	90.3 (±0.1)

Results and discussion

Table 20 Repeatability and intermediate precision of the MWCNT-H₂O₂- γ -CD-SPME-GC-MS method ($n=6$)

PAHs	Repeatability (RSD%)			Intermediate precision (RSD%)		
	2 ng L ⁻¹	15 ng L ⁻¹	30 ng L ⁻¹	2 ng L ⁻¹	15 ng L ⁻¹	30 ng L ⁻¹
Nap	11	7	4	20	17	18
Acy	7	6	5	16	11	10
Ace	14	11	8	13	18	14
Flu	14	5	7	13	9	10
Phe	20	14	9	17	18	8
Ant	19	10	8	17	10	7
Flt	13	12	8	16	17	12
Py	11	11	9	16	18	14
BaA	7	11	5	18	13	11
Chr	14	2	3	21	13	8
BbF	6	13	4	14	20	7
BkF	20	11	7	18	13	6
BaP	19	11	5	20	13	17
InPy	14	11	7	11	17	10
DiahA	18	5	5	18	18	15
BghiP	18	6	3	17	16	13

10.5 ENRICHMENT FACTORS

The enrichment capability of the fiber coated with the MWCNT-H₂O₂- γ -CD nanocomposite was investigated and good enrichment factors in the 3770 (\pm 259) – 113349 (\pm 3058) range were obtained. The result was compared with EFs calculated using HMWCNTs coated fiber (Fig. 17).

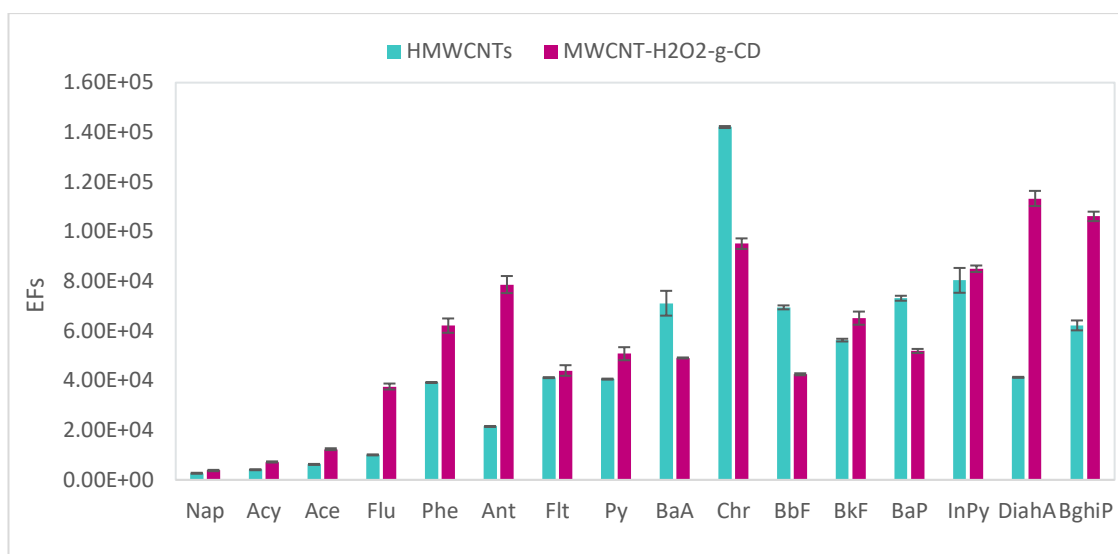


Fig. 17 Enrichment factors of the MWCNT-H₂O₂- γ -CD coating vs HMWCNTs coating

As shown in the figure, both coatings exhibited excellent enrichment capabilities. It should also be noted that MWCNT-H₂O₂- γ -CD fiber showed higher EFs for heavier PAHs than HMWCNTs fiber (up to 3 times for DiahA). As already pointed out, the greater extraction efficiency for higher molecular weight PAHs provided by CDs results in an important improvement in the paleoclimatic studies of organic pollutants since the heavier PAHs are particularly lipophilic and their determination in aqueous matrices requires very sensitive detection of analytes.

Unfortunately, the reliability of the validated method could not be tested on real samples as research expeditions in remote regions were postponed due to the Covid-19 pandemic.

10.6 SOLID STATE INVESTIGATION

To get a better insight into the interactions taking place between γ -CD and PAHs, solid-state investigations were carried out by growing co-crystals for X-ray diffraction analysis. A search using the Cambridge Structural Database (Version 5.42, September 2021, [122]) for generic co-crystals of cyclodextrins with molecules containing at least one benzene ring yielded 399 entries. Only two of them contained a PAH in the structure: [bis(β -cyclodextrin) octanol clathrate pyrene hydrate] (refcode PUKPIU) and [bis(β -cyclodextrin) tris(cyclohexanol) clathrate pyrene hydrate] (refcode PUKPOA) [123]. A portion of their crystal structure is shown in Fig. 18.

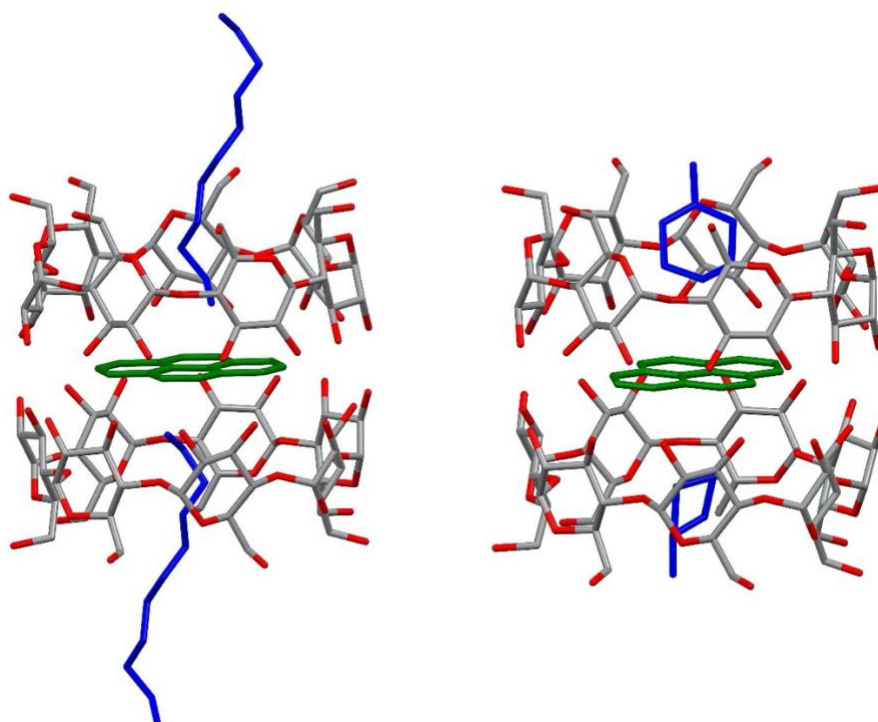


Fig. 18 Perspective view of the crystal structure of PUKPIU (left) and PUKPOA (right). Alcohol molecules and pyrene units are represented in blue and green, respectively. Hydrogen atoms and lattice solvent molecules were omitted for clarity.

In both cases, the alcohol (coloured in blue) forms a host-guest complex with the macrocycle, while pyrene (in green) is sandwiched between two β -CDs by means of dispersion interactions. Inspired by these results, crystallization experiments with γ -CD and pyrene were set up.

The crystals obtained were analysed through X-ray diffraction methods. Intensity data and cell parameters were recorded at 200(2) K on a Bruker D8 Venture PhotonII diffractometer (CuK α radiation $\lambda = 1.54178 \text{ \AA}$). The raw frame data were processed using SAINT and SADABS to yield the reflection data files [124,125]. The structures were solved by Direct Methods using the SIR2019 program [126] and refined on F_o^2 by full-matrix least-squares procedures, using SHELXL-2018 [127,128] in the WinGX suite v.2014.1 [129]. The structure was solved in the tetragonal space group P4₂i2, with cell parameters $a = b = 23.7980(7)$, $c = 31.6880(7)$ and $\alpha = \beta = \gamma = 90^\circ$.

Fig. 20 shows a portion of the crystal structure. The macrocycle skeleton is clearly visible, and several water molecules are present in the lattice (not shown in the figure for clarity). No other definite molecular group could be properly modelled, but the main residual electron density (green mesh in the figure) is sandwiched between two cyclodextrins, similarly to the position of pyrene in the example of the β -cyclodextrin clathrates previously discussed. Further attempts to grow better quality crystals are ongoing.

Results and discussion

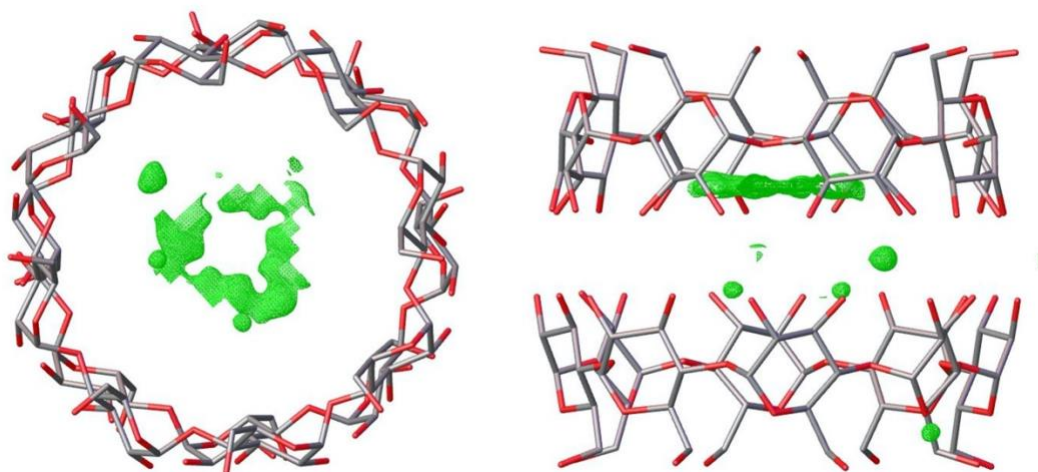


Fig. 19 Top (left) and side (right) view of the crystal structure containing γ -CD. Hydrogen atoms and lattice water molecules are not shown for clarity. The residual electron density is represented as a green mesh.

CONCLUSIONS

Conclusions

The goal of the PhD Thesis was the development of innovative analytical methods based on the use of miniaturized sample treatment techniques for the analysis of 16 US EPA priority PAHs as environmental proxies at the ultratrace level in polar snow and ice samples to support paleoclimatic research. All methods were optimized by applying the chemometric approach of the experimental design, obtaining excellent LOD values at the minimum ng L^{-1} level for all target compounds and demonstrating their ability to analyze these proxies at ultratrace levels with the advantage of extracting a few mL of sample.

Regarding the SPME-GC-MS method, HMWCNT was proposed for the first time as a coating of the SPME fiber, proving higher extraction efficiency than commercially available $30\ \mu\text{m}$ PDMS fiber and other MWCNTs tested as coatings. The fully automated method was developed and validated demonstrating adequate sensitivity and selectivity for the determination of the analytes. Furthermore, the proposed HMWCNT-SPME-GC-MS method proved to be suitable for the analysis of PAHs from Arctic snow samples.

Reliable and rapid determination of PAHs from Antarctic snow samples at ultratrace levels was achieved using the MEPS-GC-MS method developed and validated in this work. The method was based on the use of the silica-C8 sorbent, which under optimized conditions showed a high extraction efficiency and selectivity towards PAHs. High precision was provided due to the use of the semi-automatic device which also allowed for reduced sample handling, which is a fundamental prerequisite to avoid potential sources of sample contamination during extraction. Furthermore, the MEPS-based method achieved high sensitivity by extracting 4 mL of sample volume, representing a promising tool for the analysis of chemical records in paleoclimate research. Finally, the method proved to be suitable for the analysis of ultratrace PAHs in snow samples collected in Antarctica, highlighting the likely contribution of PAH contamination from local pollution sources.

Finally, another aspect addressed in the Thesis concerned a study of the inclusion properties of CD with PAHs and the development of a new MWCNT- H_2O_2 - γ -CD nanocomposite as a SPME fiber coating for the GC-MS analysis of PAHs. This method has allowed to improve the extraction efficiency of the analytes, obtaining LOD at the level of ng L^{-1} lower than reported in the previous methods discussed in the Thesis. In particular, an enhanced sensitivity towards high molecular weight PAHs was obtained.

On the basis of these promising results and to investigate the complexation of PAHs with CDs, a co-crystallization study was carried out. To gain more insight on the formation of inclusion

Conclusions

complexes of PAHs with cyclodextrins, investigations based on $^1\text{H-NMR}$ and fluorescence spectroscopy are also in progress.

It can be concluded that the methods developed in this Thesis revealed to be promising tools for the ultra-trace analysis of PAHs as organic markers in snow/firn and ice cores from polar regions. The future application of these methods to the paleoclimate research could provide paleoenvironmental records to assess occurrence and global contamination with PAHs and other chemical proxies.

REFERENCES

References

- [1] C. Barbante, A. Spolaor, W.R. Cairns, C. Boutron, Man's footprint on the Arctic environment as revealed by analysis of ice and snow, *Earth-Science Rev.* 168 (2017) 218–231. <https://doi.org/10.1016/j.earscirev.2017.02.010>.
- [2] M. Vecchiato, A. Gambaro, N.M. Kehrwald, P. Ginot, S. Kutuzov, V. Mikhaleiko, C. Barbante, The Great Acceleration of fragrances and PAHs archived in an ice core from Elbrus, Caucasus, *Sci. Rep.* 10 (2020) 10661. <https://doi.org/10.1038/s41598-020-67642-x>.
- [3] J. Gabrieli, P. Vallelonga, G. Cozzi, P. Gabrielli, A. Gambaro, M. Sigl, F. Decet, M. Schwikowski, H. Gäggeler, C. Boutron, P. Cescon, C. Barbante, Post 17th-Century Changes of European PAH Emissions Recorded in High-Altitude Alpine Snow and Ice, *Environ. Sci. Technol.* 44 (2010) 3260–3266. <https://doi.org/10.1021/es903365s>.
- [4] P. Gabrielli, P. Vallelonga, Contaminant Records in Ice Cores, in: J.P. Smol, J.M. Blais, M.R. Rosen (Eds.), *Environ. Contam. Dev. Paleoenviron. Res.*, Springer Science+Business Media Dordrecht, 2015; pp. 393–430. https://doi.org/10.1007/978-94-017-9541-8_14.
- [5] R. Fuoco, S. Giannarelli, M. Onor, S. Ghimenti, C. Abete, M. Termine, S. Francesconi, A snow/firn four-century record of polycyclic aromatic hydrocarbons (PAHs) and polychlorobiphenyls (PCBs) at Talos Dome (Antarctica), *Microchem. J.* 105 (2012) 133–141. <https://doi.org/10.1016/j.microc.2012.05.018>.
- [6] A.M. Grannas, C. Bogdal, K.J. Hageman, C. Halsall, T. Harner, H. Hung, R. Kallenborn, P. Klán, J. Klánová, R.W. Macdonald, T. Meyer, F. Wania, The role of the global cryosphere in the fate of organic contaminants, *Atmos. Chem. Phys.* 13 (2013) 3271–3305. <https://doi.org/10.5194/acp-13-3271-2013>.
- [7] L.A. Barrie, D. Gregor, B. Hargrave, R. Lake, D. Muir, R. Shearer, B. Tracey, T. Bidleman, Arctic contaminants: sources, occurrence and pathways, *Sci. Total Environ.* 122 (1992) 1–74. [https://doi.org/10.1016/0048-9697\(92\)90245-N](https://doi.org/10.1016/0048-9697(92)90245-N).
- [8] R. Bargagli, Environmental contamination in Antarctic ecosystems, *Sci. Total Environ.* 400 (2008) 212–226. <https://doi.org/10.1016/j.scitotenv.2008.06.062>.
- [9] S. Cao, G. Na, R. Li, L. Ge, H. Gao, S. Jin, C. Hou, Y. Gao, Z. Zhang, Fate and deposition of polycyclic aromatic hydrocarbons in the Bransfield Strait, Antarctica, *Mar. Pollut. Bull.* 137 (2018) 533–541. <https://doi.org/10.1016/j.marpolbul.2018.10.045>.

References

- [10] M. Vecchiato, E. Argiriadis, S. Zambon, C. Barbante, G. Toscano, A. Gambaro, R. Piazza, Persistent Organic Pollutants (POPs) in Antarctica: Occurrence in continental and coastal surface snow, *Microchem. J.* 119 (2015) 75–82. <https://doi.org/10.1016/j.microc.2014.10.010>.
- [11] S. Giannarelli, A. Ceccarini, C. Tiribilli, R. Spreafico, S. Francesconi, R. Fuoco, Paleo-environmental record of polycyclic aromatic hydrocarbons and polychlorobiphenyls at the peripheral site GV7 in Victoria Land (East Antarctica), *Chemosphere*. 174 (2017) 390–398. <https://doi.org/10.1016/j.chemosphere.2017.01.126>.
- [12] A.T. Lebedev, D.M. Mazur, O.V. Polyakova, D.S. Kosyakov, A.Y. Kozhevnikov, T.B. Latkin, I. Andreeva Yu, V.B. Artaev, Semi volatile organic compounds in the snow of Russian Arctic islands: Archipelago Novaya Zemlya, *Environ. Pollut.* 239 (2018) 416–427. <https://doi.org/10.1016/j.envpol.2018.03.009>.
- [13] J.L. Jaffrezo, M.P. Clain, P. Masclet, Polycyclic aromatic hydrocarbons in the polar ice of greenland. Geochemical use of these atmospheric tracers, *Atmos. Environ.* 28 (1994) 1139–1145. [https://doi.org/10.1016/1352-2310\(94\)90291-7](https://doi.org/10.1016/1352-2310(94)90291-7).
- [14] M. Vecchiato, E. Barbaro, A. Spolaor, F. Burgay, C. Barbante, R. Piazza, A. Gambaro, Fragrances and PAHs in snow and seawater of Ny-Ålesund (Svalbard): Local and long-range contamination, *Environ. Pollut.* 242 (2018) 1740–1747. <https://doi.org/10.1016/j.envpol.2018.07.095>.
- [15] P. Kukučka, G. Lammel, A. Dvorská, J. Klánová, A. Möller, E. Fries, Contamination of Antarctic snow by polycyclic aromatic hydrocarbons dominated by combustion sources in the polar region, *Environ. Chem.* 7 (2010) 504. <https://doi.org/10.1071/EN10066>.
- [16] C. Giorio, N. Kehrwald, C. Barbante, M. Kalberer, A.C.F. King, E.R. Thomas, E.W. Wolff, P. Zennaro, Prospects for reconstructing paleoenvironmental conditions from organic compounds in polar snow and ice, *Quat. Sci. Rev.* 183 (2018) 1–22. <https://doi.org/10.1016/j.quascirev.2018.01.007>.
- [17] H.I. Abdel-Shafy, M.S.M. Mansour, A review on polycyclic aromatic hydrocarbons: Source, environmental impact, effect on human health and remediation, *Egypt. J. Pet.* 25 (2016) 107–123. <https://doi.org/10.1016/j.ejpe.2015.03.011>.
- [18] A.L.C. Lima, J.W. Farrington, C.M. Reddy, Combustion-Derived Polycyclic Aromatic Hydrocarbons in the Environment—A Review, *Environ. Forensics.* 6 (2005) 109–131.

References

- <https://doi.org/10.1080/15275920590952739>.
- [19] S. Boitsov, H.K.B. Jensen, J. Klungsøyr, Natural background and anthropogenic inputs of polycyclic aromatic hydrocarbons (PAH) in sediments of South-Western Barents Sea, *Mar. Environ. Res.* 68 (2009) 236–245. <https://doi.org/10.1016/j.marenvres.2009.06.013>.
- [20] N.D. Dat, M.B. Chang, Review on characteristics of PAHs in atmosphere, anthropogenic sources and control technologies, *Sci. Total Environ.* 609 (2017) 682–693. <https://doi.org/10.1016/j.scitotenv.2017.07.204>.
- [21] P. Fernández, G. Carrera, J.O. Grimalt, M. Ventura, L. Camarero, J. Catalan, U. Nickus, H. Thies, R. Psenner, Factors Governing the Atmospheric Deposition of Polycyclic Aromatic Hydrocarbons to Remote Areas, *Environ. Sci. Technol.* 37 (2003) 3261–3267. <https://doi.org/10.1021/es020137k>.
- [22] K. Ravindra, R. Sokhi, R. Van Grieken, Atmospheric polycyclic aromatic hydrocarbons: Source attribution, emission factors and regulation, *Atmos. Environ.* 42 (2008) 2895–2921. <https://doi.org/10.1016/j.atmosenv.2007.12.010>.
- [23] Some non-heterocyclic polycyclic aromatic hydrocarbons and some related exposures., *IARC Monogr. Eval. Carcinog. Risks to Humans.* 92 (2010) 1–853.
- [24] U.S. Environmental Protection Agency, Priority Pollutant List, in: Washington DC, 2014. <https://www.epa.gov/eg/toxic-and-priority-pollutants-under-clean-water-act>.
- [25] <https://eur-lex.europa.eu/legal-content/EN/TXT/PDF/?uri=CELEX:32013R1272&from=EN> (accessed 03 April 2022).
- [26] K. Kawamura, I. Suzuki, Y. Fuji, O. Watanabe, Ice core record of polycyclic aromatic hydrocarbons over the past 400 years, *Naturwissenschaften.* 81 (1994) 502–505. <https://doi.org/10.1007/BF01132682>.
- [27] J.S. Poland, M.J. Riddle, B.A. Zeeb, Contaminants in the Arctic and the Antarctic: a comparison of sources, impacts, and remediation options, *Polar Rec. (Gr. Brit).* 39 (2003) 369–383. <https://doi.org/10.1017/S0032247403002985>.
- [28] T. Gouin, D. Mackay, K.C. Jones, T. Harner, S.N. Meijer, Evidence for the “grasshopper” effect and fractionation during long-range atmospheric transport of organic contaminants, *Environ. Pollut.* 128 (2004) 139–148.

References

- <https://doi.org/10.1016/j.envpol.2003.08.025>.
- [29] J.E. Balmer, H. Hung, Y. Yu, R.J. Letcher, D.C.G. Muir, Sources and environmental fate of pyrogenic polycyclic aromatic hydrocarbons (PAHs) in the Arctic, *Emerg. Contam.* 5 (2019) 128–142. <https://doi.org/10.1016/j.emcon.2019.04.002>.
- [30] A. Zelenyuk, D. Imre, J. Beránek, E. Abramson, J. Wilson, M. Shrivastava, Synergy between Secondary Organic Aerosols and Long-Range Transport of Polycyclic Aromatic Hydrocarbons, *Environ. Sci. Technol.* 46 (2012) 12459–12466. <https://doi.org/10.1021/es302743z>.
- [31] N.L. Rose, C.L. Rose, J.F. Boyle, P.G. Appleby, Lake-Sediment Evidence for Local and Remote Sources of Atmospherically Deposited Pollutants on Svalbard, *J. Paleolimnol.* 31 (2004) 499–513. <https://doi.org/10.1023/B:JOPL.0000022548.97476.39>.
- [32] R.M. Smith, Before the injection—modern methods of sample preparation for separation techniques, *J. Chromatogr. A.* 1000 (2003) 3–27. [https://doi.org/10.1016/S0021-9673\(03\)00511-9](https://doi.org/10.1016/S0021-9673(03)00511-9).
- [33] G. Na, C. Liu, Z. Wang, L. Ge, X. Ma, Z. Yao, Distribution and characteristic of PAHs in snow of Fildes Peninsula, *J. Environ. Sci.* 23 (2011) 1445–1451. [https://doi.org/10.1016/S1001-0742\(10\)60605-5](https://doi.org/10.1016/S1001-0742(10)60605-5).
- [34] L. Ramos, J.J. Ramos, U.A.T. Brinkman, Miniaturization in sample treatment for environmental analysis, *Anal. Bioanal. Chem.* 381 (2005) 119–140. <https://doi.org/10.1007/s00216-004-2906-5>.
- [35] D. Fatta-Kassinos, A. Nikolaou, L. Ioannou-Ttofa, Advances in Analytical Methods for the Determination of Pharmaceutical Residues in Waters and Wastewaters, in: *Environ. Heal.*, Elsevier, 2019: pp. 1–12. <https://doi.org/10.1016/B978-0-12-409548-9.11247-3>.
- [36] J. Płotka-Wasyłka, N. Szczepańska, M. de la Guardia, J. Namieśnik, Miniaturized solid-phase extraction techniques, *TrAC Trends Anal. Chem.* 73 (2015) 19–38. <https://doi.org/10.1016/j.trac.2015.04.026>.
- [37] C.L. Arthur, J. Pawliszyn, Solid phase microextraction with thermal desorption using fused silica optical fibers, *Anal. Chem.* 62 (1990) 2145–2148. <https://doi.org/10.1021/ac00218a019>.

References

- [38] J. Pawliszyn, *Applications of Solid Phase Microextraction*, Royal Society of Chemistry, Cambridge, 2007. <https://doi.org/10.1039/9781847550149>.
- [39] J. Pawliszyn, *Handbook of Solid Phase Microextraction*, Elsevier, 2012. <https://doi.org/10.1016/C2011-0-04297-7>.
- [40] R. Doong, S. Chang, Y. Sun, Solid-phase microextraction for determining the distribution of sixteen US Environmental Protection Agency polycyclic aromatic hydrocarbons in water samples, *J. Chromatogr. A.* 879 (2000) 177–188. [https://doi.org/10.1016/S0021-9673\(00\)00347-2](https://doi.org/10.1016/S0021-9673(00)00347-2).
- [41] H. Piri-Moghadam, M.N. Alam, J. Pawliszyn, Review of geometries and coating materials in solid phase microextraction: Opportunities, limitations, and future perspectives, *Anal. Chim. Acta.* 984 (2017) 42–65. <https://doi.org/10.1016/j.aca.2017.05.035>.
- [42] USEPA (U.S. Environmental Protection Agency), Method 8272, (2007). <https://www.epa.gov/sites/production/files/2015-12/documents/8272.pdf>.
- [43] E.A. Souza Silva, S. Risticovic, J. Pawliszyn, Recent trends in SPME concerning sorbent materials, configurations and in vivo applications, *TrAC Trends Anal. Chem.* 43 (2013) 24–36. <https://doi.org/10.1016/j.trac.2012.10.006>.
- [44] S.L. Chong, D. Wang, J.D. Hayes, B.W. Wilhite, A. Malik, Sol–Gel Coating Technology for the Preparation of Solid-Phase Microextraction Fibers of Enhanced Thermal Stability, *Anal. Chem.* 69 (1997) 3889–3898. <https://doi.org/10.1021/ac9703360>.
- [45] A. Amiri, Solid-phase microextraction-based sol–gel technique, *TrAC Trends Anal. Chem.* 75 (2016) 57–74. <https://doi.org/10.1016/j.trac.2015.10.003>.
- [46] A. Sarafraz-Yazdi, N. Razavi, Application of molecularly-imprinted polymers in solid-phase microextraction techniques, *TrAC Trends Anal. Chem.* 73 (2015) 81–90. <https://doi.org/10.1016/j.trac.2015.05.004>.
- [47] S. Ncube, L. Madikizela, E. Cukrowska, L. Chimuka, Recent advances in the adsorbents for isolation of polycyclic aromatic hydrocarbons (PAHs) from environmental sample solutions, *TrAC Trends Anal. Chem.* 99 (2018) 101–116. <https://doi.org/10.1016/j.trac.2017.12.007>.
- [48] F. Bianchi, A. Pankajakshan, F. Fornari, S. Mandal, P. Pelagatti, A. Bacchi, P.P. Mazzeo,

References

- M. Careri, A zinc mixed-ligand microporous metal-organic framework as solid-phase microextraction coating for priority polycyclic aromatic hydrocarbons from water samples, *Microchem. J.* 154 (2020) 104646. <https://doi.org/10.1016/j.microc.2020.104646>.
- [49] M. Kazemipour, M. Behzadi, R. Ahmadi, Poly(o-phenylenediamine-co-o-toluidine)/modified carbon nanotubes composite coating fabricated on a stainless steel wire for the headspace solid-phase microextraction of polycyclic aromatic hydrocarbons, *Microchem. J.* 128 (2016) 258–266. <https://doi.org/10.1016/j.microc.2016.05.004>.
- [50] M. Anastassiades, S.J. Lehotay, D. Štajnbaher, F.J. Schenck, Fast and Easy Multiresidue Method Employing Acetonitrile Extraction/Partitioning and “Dispersive Solid-Phase Extraction” for the Determination of Pesticide Residues in Produce, *J. AOAC Int.* 86 (2003) 412–431. <https://doi.org/10.1093/jaoac/86.2.412>.
- [51] A. Chisvert, S. Cárdenas, R. Lucena, Dispersive micro-solid phase extraction, *TrAC Trends Anal. Chem.* 112 (2019) 226–233. <https://doi.org/10.1016/j.trac.2018.12.005>.
- [52] M.S. Cárdenas Aranzana, Dispersive Solid-Phase (Micro)Extraction, in: *Encycl. Anal. Chem.*, Wiley, 2010. <https://doi.org/10.1002/9780470027318.a9167>.
- [53] A.I. Corps Ricardo, F.J. Guzmán Bernardo, M. Zougagh, R.C. Rodríguez Martín-Doimeadios, Á. Ríos, Magnetic nanoparticles—carbon nanotubes hybrid composites for selective solid-phase extraction of polycyclic aromatic hydrocarbons and determination by ultra-high performance liquid chromatography, *Anal. Bioanal. Chem.* 409 (2017) 5125–5132. <https://doi.org/10.1007/s00216-017-0459-7>.
- [54] M. Moazzen, R. Ahmadkhaniha, M.E. Gorji, M. Yunesian, N. Rastkari, Magnetic solid-phase extraction based on magnetic multi-walled carbon nanotubes for the determination of polycyclic aromatic hydrocarbons in grilled meat samples, *Talanta*. 115 (2013) 957–965. <https://doi.org/10.1016/j.talanta.2013.07.005>.
- [55] Q. Zhao, F. Wei, Y.-B. Luo, J. Ding, N. Xiao, Y.-Q. Feng, Rapid Magnetic Solid-Phase Extraction Based on Magnetic Multiwalled Carbon Nanotubes for the Determination of Polycyclic Aromatic Hydrocarbons in Edible Oils, *J. Agric. Food Chem.* 59 (2011) 12794–12800. <https://doi.org/10.1021/jf203973s>.
- [56] M. Abdel-Rehim, New trend in sample preparation: on-line microextraction in packed syringe for liquid and gas chromatography applications, *J. Chromatogr. B.* 801 (2004)

References

- 317–321. <https://doi.org/10.1016/j.jchromb.2003.11.042>.
- [57] M.M. Moein, A. Abdel-Rehim, M. Abdel-Rehim, Microextraction by packed sorbent (MEPS), *TrAC - Trends Anal. Chem.* 67 (2015) 34–44. <https://doi.org/10.1016/j.trac.2014.12.003>.
- [58] M. Abdel-Rehim, Microextraction by packed sorbent (MEPS): A tutorial, *Anal. Chim. Acta.* 701 (2011) 119–128. <https://doi.org/10.1016/j.aca.2011.05.037>.
- [59] P. Fernández, M. González, M. Regenjo, A.M. Ares, A.M. Fernández, R.A. Lorenzo, A.M. Carro, Analysis of drugs of abuse in human plasma using microextraction by packed sorbents and ultra-high-performance liquid chromatography, *J. Chromatogr. A.* 1485 (2017) 8–19. <https://doi.org/10.1016/j.chroma.2017.01.021>.
- [60] M.A. Saracino, L. Santarcangelo, M.A. Raggi, L. Mercolini, Microextraction by packed sorbent (MEPS) to analyze catecholamines in innovative biological samples, *J. Pharm. Biomed. Anal.* 104 (2015) 122–129. <https://doi.org/10.1016/j.jpba.2014.11.003>.
- [61] M. Woźniakiewicz, R. Wietecha-Posłuszny, A. Moos, M. Wiczorek, P. Knihnicki, P. Kościelniak, Development of microextraction by packed sorbent for toxicological analysis of tricyclic antidepressant drugs in human oral fluid, *J. Chromatogr. A.* 1337 (2014) 9–16. <https://doi.org/10.1016/j.chroma.2014.02.037>.
- [62] M. Moeder, S. Schrader, U. Winkler, R. Rodil, At-line microextraction by packed sorbent-gas chromatography–mass spectrometry for the determination of UV filter and polycyclic musk compounds in water samples, *J. Chromatogr. A.* 1217 (2010) 2925–2932. <https://doi.org/10.1016/j.chroma.2010.02.057>.
- [63] A. Prieto, S. Schrader, M. Moeder, Determination of organic priority pollutants and emerging compounds in wastewater and snow samples using multiresidue protocols on the basis of microextraction by packed sorbents coupled to large volume injection gas chromatography-mass spectrometry analy, *J. Chromatogr. A.* 1217 (2010) 6002–6011. <https://doi.org/10.1016/j.chroma.2010.07.070>.
- [64] M. Quinto, G. Spadaccino, D. Nardiello, C. Palermo, P. Amodio, D. Li, D. Centonze, Microextraction by packed sorbent coupled with gas chromatography–mass spectrometry: A comparison between “draw-eject” and “extract-discard” methods under equilibrium conditions for the determination of polycyclic aromatic hydrocarbons in water, *J. Chromatogr. A.* 1371 (2014) 30–38.

References

- <https://doi.org/10.1016/j.chroma.2014.10.062>.
- [65] L. Yang, R. Said, M. Abdel-Rehim, Sorbent, device, matrix and application in microextraction by packed sorbent (MEPS): A review, *J. Chromatogr. B.* 1043 (2017) 33–43. <https://doi.org/10.1016/j.jchromb.2016.10.044>.
- [66] S. Fu, J. Fan, Y. Hashi, Z. Chen, Determination of polycyclic aromatic hydrocarbons in water samples using online microextraction by packed sorbent coupled with gas chromatography–mass spectrometry, *Talanta.* 94 (2012) 152–157. <https://doi.org/10.1016/j.talanta.2012.03.010>.
- [67] M. Quinto, P. Amodio, G. Spadaccino, D. Centonze, Development of a mathematical model for online microextraction by packed sorbent under equilibrium conditions and its application for polycyclic aromatic hydrocarbon determination in water by gas chromatography–mass spectrometry, *J. Chromatogr. A.* 1262 (2012) 19–26. <https://doi.org/10.1016/j.chroma.2012.08.098>.
- [68] S. Iijima, Helical microtubules of graphitic carbon, *Nature.* 354 (1991) 56–58. <https://doi.org/10.1038/354056a0>.
- [69] M. Moreno, A. Sánchez Arribas, E. Bermejo, A. Zapardiel, M. Chicharro, Carbon nanotubes as analytical tools in capillary electromigration methods, *Appl. Mater. Today.* 9 (2017) 456–481. <https://doi.org/10.1016/j.apmt.2017.09.008>.
- [70] X. Liang, S. Liu, S. Wang, Y. Guo, S. Jiang, Carbon-based sorbents: Carbon nanotubes, *J. Chromatogr. A.* 1357 (2014) 53–67. <https://doi.org/10.1016/j.chroma.2014.04.039>.
- [71] X.-Y. Song, J. Chen, Y.-P. Shi, Different configurations of carbon nanotubes reinforced solid-phase microextraction techniques and their applications in the environmental analysis, *TrAC Trends Anal. Chem.* 86 (2017) 263–275. <https://doi.org/10.1016/j.trac.2016.11.006>.
- [72] B. Pan, B. Xing, Adsorption Mechanisms of Organic Chemicals on Carbon Nanotubes, *Environ. Sci. Technol.* 42 (2008) 9005–9013. <https://doi.org/10.1021/es801777n>.
- [73] M. Yazdanpanah, S. Nojavan, Micro-solid phase extraction of some polycyclic aromatic hydrocarbons from environmental water samples using magnetic β -cyclodextrin-carbon nano-tube composite as a sorbent, *J. Chromatogr. A.* 1585 (2019) 34–45. <https://doi.org/10.1016/j.chroma.2018.11.066>.

References

- [74] A. Abdar, A. Sarafraz-Yazdi, A. Amiri, N. Bagheri, Magnetic solid-phase extraction of polycyclic aromatic hydrocarbons in water samples by Fe₃O₄@polypyrrole/carbon nanotubes, *J. Sep. Sci.* 39 (2016) 2746–2753. <https://doi.org/10.1002/jssc.201600420>.
- [75] E. Heilweil, F.M. Rabel, Reversed-Phase Thin Layer Chromatography on C₂, C₈, C₁₈, and Diphenyl Bonded Phases, *J. Chromatogr. Sci.* 23 (1985) 101–105. <https://doi.org/10.1093/chromsci/23.3.101>.
- [76] W. Saenger, Cyclodextrin Inclusion Compounds in Research and Industry, *Angew. Chemie Int. Ed. English.* 19 (1980) 344–362. <https://doi.org/10.1002/anie.198003441>.
- [77] E.M.M. Del Valle, Cyclodextrins and their uses: a review, *Process Biochem.* 39 (2004) 1033–1046. [https://doi.org/10.1016/S0032-9592\(03\)00258-9](https://doi.org/10.1016/S0032-9592(03)00258-9).
- [78] K.-H. Frömring, J. Szejtli, Cyclodextrin Inclusion Complexes, in: *Cyclodextrins Pharm.*, 1994: pp. 45–82. https://doi.org/10.1007/978-94-015-8277-3_4.
- [79] A. Gentili, Cyclodextrin-based sorbents for solid phase extraction, *J. Chromatogr. A.* 1609 (2020) 460654. <https://doi.org/10.1016/j.chroma.2019.460654>.
- [80] C. Belenguer-Sapiña, E. Pellicer-Castell, J. El Haskouri, C. Guillem, E.F. Simó-Alfonso, P. Amorós, A. Mauri-Aucejo, Design, characterization and comparison of materials based on β and γ cyclodextrin covalently connected to microporous silica for environmental analysis, *J. Chromatogr. A.* 1563 (2018) 10–19. <https://doi.org/10.1016/j.chroma.2018.05.070>.
- [81] E. Morillo, M.A. Sánchez-Trujillo, J.R. Moyano, J. Villaverde, M.E. Gómez-Pantoja, J.I. Pérez-Martínez, Enhanced Solubilisation of Six PAHs by Three Synthetic Cyclodextrins for Remediation Applications: Molecular Modelling of the Inclusion Complexes, *PLoS One.* 7 (2012) e44137. <https://doi.org/10.1371/journal.pone.0044137>.
- [82] M.A. Sánchez-Trujillo, E. Morillo, J. Villaverde, S. Lacorte, Comparative effects of several cyclodextrins on the extraction of PAHs from an aged contaminated soil, *Environ. Pollut.* 178 (2013) 52–58. <https://doi.org/10.1016/j.envpol.2013.02.029>.
- [83] B. Magnusson, U. Örnemark, eds., *Eurachem Guide: The Fitness for Purpose of Analytical Methods – A Laboratory Guide to Method Validation and Related Topics*, 2nd ed., 2014. <http://www.eurachem.org>.
- [84] A. Arcoledo, F. Bianchi, M. Careri, Helical multi-walled carbon nanotube-coated fibers

References

- for solid-phase microextraction determination of polycyclic aromatic hydrocarbons at ultra-trace levels in ice and snow samples, *J. Chromatogr. A.* 1631 (2020) 461589. <https://doi.org/10.1016/j.chroma.2020.461589>.
- [85] F. Bianchi, M. Careri, Experimental Design Techniques for Optimization of Analytical Methods. Part I: Separation and Sample Preparation Techniques, *Curr. Anal. Chem.* 4 (2008) 55–74. <https://doi.org/10.2174/157341108783339070>.
- [86] L. Vera Candiotti, M.M. De Zan, M.S. Cámara, H.C. Goicoechea, Experimental design and multiple response optimization. Using the desirability function in analytical methods development, *Talanta.* 124 (2014) 123–138. <https://doi.org/10.1016/j.talanta.2014.01.034>.
- [87] N. Riboni, J.W. Trzcinski, F. Bianchi, C. Massera, R. Pinalli, L. Sidisky, E. Dalcanale, M. Careri, Conformationally blocked quinoxaline cavitand as solid-phase microextraction coating for the selective detection of BTEX in air, *Anal. Chim. Acta.* 905 (2016) 79–84. <https://doi.org/10.1016/j.aca.2015.12.005>.
- [88] A. Arcoleo, F. Bianchi, M. Careri, A sensitive microextraction by packed sorbent-gas chromatography-mass spectrometry method for the assessment of polycyclic aromatic hydrocarbons contamination in Antarctic surface snow, *Chemosphere.* 282 (2021) 131082. <https://doi.org/10.1016/j.chemosphere.2021.131082>.
- [89] A. Beyer, M. Biziuk, Comparison of efficiency of different sorbents used during clean-up of extracts for determination of polychlorinated biphenyls and pesticide residues in low-fat food, *Food Res. Int.* 43 (2010) 831–837. <https://doi.org/10.1016/j.foodres.2009.11.018>.
- [90] V. Datsyuk, M. Kalyva, K. Papagelis, J. Parthenios, D. Tasis, A. Siokou, I. Kallitsis, C. Galiotis, Chemical oxidation of multiwalled carbon nanotubes, *Carbon N. Y.* 46 (2008) 833–840. <https://doi.org/10.1016/j.carbon.2008.02.012>.
- [91] J. Cheng, P.R. Chang, P. Zheng, X. Ma, Characterization of magnetic carbon nanotube-cyclodextrin composite and its adsorption of dye, *Ind. Eng. Chem. Res.* 53 (2014) 1415–1421. <https://doi.org/10.1021/ie402658x>.
- [92] R. Leardi, Experimental design in chemistry: A tutorial, *Anal. Chim. Acta.* 652 (2009) 161–172. <https://doi.org/10.1016/j.aca.2009.06.015>.

References

- [93] C. Pan, S. Xu, H. Zou, Z. Guo, Y. Zhang, B. Guo, Carbon nanotubes as adsorbent of solid-phase extraction and matrix for laser desorption/ionization mass spectrometry, *J. Am. Soc. Mass Spectrom.* 16 (2005) 263–270. <https://doi.org/10.1016/j.jasms.2004.11.005>.
- [94] F. Ghaemi, A. Amiri, R. Yunus, Methods for coating solid-phase microextraction fibers with carbon nanotubes, *TrAC Trends Anal. Chem.* 59 (2014) 133–143. <https://doi.org/10.1016/j.trac.2014.04.011>.
- [95] M. Paszkiewicz, M. Caban, A. Bielicka-Giełdoń, P. Stepnowski, Optimization of a procedure for the simultaneous extraction of polycyclic aromatic hydrocarbons and metal ions by functionalized and non-functionalized carbon nanotubes as effective sorbents, *Talanta.* 165 (2017) 405–411. <https://doi.org/10.1016/j.talanta.2016.10.049>.
- [96] M. Paszkiewicz, C. Sikorska, D. Leszczyńska, P. Stepnowski, Helical Multi-walled Carbon Nanotubes as an Efficient Material for the Dispersive Solid-Phase Extraction of Low and High Molecular Weight Polycyclic Aromatic Hydrocarbons from Water Samples: Theoretical Study, *Water, Air, Soil Pollut.* 229 (2018) 253. <https://doi.org/10.1007/s11270-018-3884-0>.
- [97] X.L. Osorio Barajas, T. Hüffer, P. Mettig, B. Schilling, M.A. Jochmann, T.C. Schmidt, Investigation of carbon-based nanomaterials as sorbents for headspace in-tube extraction of polycyclic aromatic hydrocarbons, *Anal. Bioanal. Chem.* 409 (2017) 3861–3870. <https://doi.org/10.1007/s00216-017-0331-9>.
- [98] H.C. Menezes, S.M.R. de Barcelos, D.F.D. Macedo, A.D. Purceno, B.F. Machado, A.P.C. Teixeira, R.M. Lago, P. Serp, Z.L. Cardeal, Magnetic N-doped carbon nanotubes: A versatile and efficient material for the determination of polycyclic aromatic hydrocarbons in environmental water samples, *Anal. Chim. Acta.* 873 (2015) 51–56. <https://doi.org/10.1016/j.aca.2015.02.063>.
- [99] M.N. Yazdi, Y. Yamini, H. Asiabi, Multiwall carbon nanotube- zirconium oxide nanocomposite hollow fiber solid phase microextraction for determination of polyaromatic hydrocarbons in water, coffee and tea samples, *J. Chromatogr. A.* 1554 (2018) 8–15. <https://doi.org/10.1016/j.chroma.2018.04.040>.
- [100] M. Heidari, A. Bahrami, A.R. Ghiasvand, F.G. Shahna, A.R. Soltanian, A needle trap device packed with a sol-gel derived, multi-walled carbon nanotubes/silica composite

References

- for sampling and analysis of volatile organohalogen compounds in air, *Anal. Chim. Acta.* 785 (2013) 67–74. <https://doi.org/10.1016/j.aca.2013.04.057>.
- [101] M. Behzadi, E. Noroozian, M. Mirzaei, A novel coating based on carbon nanotubes/poly-ortho-phenylenediamine composite for headspace solid-phase microextraction of polycyclic aromatic hydrocarbons, *Talanta.* 108 (2013) 66–73. <https://doi.org/10.1016/j.talanta.2013.02.040>.
- [102] A.A. Matin, P. Biparva, M. Gheshlaghi, Gas chromatographic determination of polycyclic aromatic hydrocarbons in water and smoked rice samples after solid-phase microextraction using multiwalled carbon nanotube loaded hollow fiber, *J. Chromatogr. A.* 1374 (2014) 50–57. <https://doi.org/10.1016/j.chroma.2014.11.048>.
- [103] M. Behzadi, M. Mirzaei, M. Daneshpajoo, Carbon nanotubes/poly-ortho-aminophenol composite as a new coating for the headspace solid-phase microextraction of polycyclic aromatic hydrocarbons, *Anal. Methods.* 6 (2014) 9234–9241. <https://doi.org/10.1039/C4AY01926A>.
- [104] S. Maghsoudi, E. Noroozian, HP-SPME of Volatile Polycyclic Aromatic Hydrocarbons from Water Using Multiwalled Carbon Nanotubes Coated on a Steel Fiber through Electrophoretic Deposition, *Chromatographia.* 75 (2012) 913–921. <https://doi.org/10.1007/s10337-012-2283-8>.
- [105] I. Domínguez, F.J. Arrebola, R. Gavara, J.L. Martínez Vidal, A.G. Frenich, Automated and simultaneous determination of priority substances and polychlorinated biphenyls in wastewater using headspace solid phase microextraction and high resolution mass spectrometry, *Anal. Chim. Acta.* 1002 (2018) 39–49. <https://doi.org/10.1016/j.aca.2017.11.056>.
- [106] L. Yang, J. Zhang, F. Zhao, B. Zeng, Electrodeposition of self-assembled poly(3,4-ethylenedioxythiophene) @gold nanoparticles on stainless steel wires for the headspace solid-phase microextraction and gas chromatographic determination of several polycyclic aromatic hydrocarbons, *J. Chromatogr. A.* 1471 (2016) 80–86. <https://doi.org/10.1016/j.chroma.2016.10.041>.
- [107] M. Shamsipur, M.B. Gholivand, M. Shamizadeh, P. Hashemi, Preparation and Evaluation of a Novel Solid-Phase Microextraction Fiber Based on Functionalized Nanoporous Silica Coating for Extraction of Polycyclic Aromatic Hydrocarbons From

References

- Water Samples Followed by GC–MS Detection, *Chromatographia*. 78 (2015) 795–803. <https://doi.org/10.1007/s10337-015-2896-9>.
- [108] X.-F. Chen, H. Zang, X. Wang, J.-G. Cheng, R.-S. Zhao, C.-G. Cheng, X.-Q. Lu, Metal–organic framework MIL-53(Al) as a solid-phase microextraction adsorbent for the determination of 16 polycyclic aromatic hydrocarbons in water samples by gas chromatography–tandem mass spectrometry, *Analyst*. 137 (2012) 5411. <https://doi.org/10.1039/c2an35806a>.
- [109] J. Meng, J. Bu, C. Deng, X. Zhang, Preparation of polypyrrole-coated magnetic particles for micro solid-phase extraction of phthalates in water by gas chromatography–mass spectrometry analysis, *J. Chromatogr. A*. 1218 (2011) 1585–1591. <https://doi.org/10.1016/j.chroma.2011.01.057>.
- [110] A. Prieto, A. Vallejo, O. Zuloaga, A. Paschke, B. Sellergen, E. Schillinger, S. Schrader, M. Möder, Selective determination of estrogenic compounds in water by microextraction by packed sorbents and a molecularly imprinted polymer coupled with large volume injection-in-port-derivatization gas chromatography–mass spectrometry, *Anal. Chim. Acta*. 703 (2011) 41–51. <https://doi.org/10.1016/j.aca.2011.07.007>.
- [111] J. Ma, R. Xiao, J. Li, J. Yu, Y. Zhang, L. Chen, Determination of 16 polycyclic aromatic hydrocarbons in environmental water samples by solid-phase extraction using multi-walled carbon nanotubes as adsorbent coupled with gas chromatography–mass spectrometry, *J. Chromatogr. A*. 1217 (2010) 5462–5469. <https://doi.org/10.1016/j.chroma.2010.06.060>.
- [112] P. Oleszczuk, S. Baran, Application of solid-phase extraction to determination of polycyclic aromatic hydrocarbons in sewage sludge extracts, *J. Hazard. Mater.* 113 (2004) 237–245. <https://doi.org/10.1016/j.jhazmat.2004.06.015>.
- [113] M. Buszewska-Forajta, M.J. Markuszewski, R. Kaliszan, Free silanols and ionic liquids as their suppressors in liquid chromatography, *J. Chromatogr. A*. 1559 (2018) 17–43. <https://doi.org/10.1016/j.chroma.2018.04.002>.
- [114] A. El-Beqqali, A. Kussak, M. Abdel-Rehim, Fast and sensitive environmental analysis utilizing microextraction in packed syringe online with gas chromatography–mass spectrometry, *J. Chromatogr. A*. 1114 (2006) 234–238. <https://doi.org/10.1016/j.chroma.2006.02.024>.

References

- [115] J.A.M. Pereira, J. Gonçalves, P. Porto-Figueira, J.A. Figueira, V. Alves, R. Perestrelo, S. Medina, J.S. Câmara, Current trends on microextraction by packed sorbent – fundamentals, application fields, innovative improvements and future applications, *Analyst*. 144 (2019) 5048–5074. <https://doi.org/10.1039/C8AN02464B>.
- [116] J.B. Korosi, W. Cheng, J.M. Blais, Organic Pollutants in Sediment Core Archives, in: J.P. Smol, J.M. Blais, M.R. Rosen (Eds.), *Environ. Contam. Dev. Paleoenviron. Res.*, Springer Science+Business Media Dordrecht, 2015: pp. 161–185. https://doi.org/10.1007/978-94-017-9541-8_8.
- [117] H.A. Dandajeh, M. Talibi, N. Ladommatos, P. Hellier, Influence of Combustion Characteristics and Fuel Composition on Exhaust PAHs in a Compression Ignition Engine, *Energies*. 12 (2019) 2575. <https://doi.org/10.3390/en12132575>.
- [118] J. Gabrieli, F. Decet, A. Luchetta, M. Valt, P. Pastore, C. Barbante, Occurrence of PAH in the seasonal snowpack of the Eastern Italian Alps, *Environ. Pollut.* 158 (2010) 3130–3137. <https://doi.org/10.1016/j.envpol.2010.06.042>.
- [119] X.-Y. Song, W. Ha, J. Chen, Y.-P. Shi, Application of β -cyclodextrin-modified, carbon nanotube-reinforced hollow fiber to solid-phase microextraction of plant hormones, *J. Chromatogr. A*. 1374 (2014) 23–30. <https://doi.org/10.1016/j.chroma.2014.11.029>.
- [120] S.A. Chernyak, A.S. Ivanov, N.E. Strokova, K.I. Maslakov, S. V. Savilov, V. V. Lunin, Mechanism of Thermal Defunctionalization of Oxidized Carbon Nanotubes, *J. Phys. Chem. C*. 120 (2016) 17465–17474. <https://doi.org/10.1021/acs.jpcc.6b05178>.
- [121] S.-O. Ko, M.A. Schlautman, E.R. Carraway, Partitioning of Hydrophobic Organic Compounds to Hydroxypropyl- β -cyclodextrin: Experimental Studies and Model Predictions for Surfactant-Enhanced Remediation Applications, *Environ. Sci. Technol.* 33 (1999) 2765–2770. <https://doi.org/10.1021/es9813360>.
- [122] C.R. Groom, I.J. Bruno, M.P. Lightfoot, S.C. Ward, The Cambridge Structural Database, *Acta Crystallogr. Sect. B Struct. Sci. Cryst. Eng. Mater.* 72 (2016) 171–179. <https://doi.org/10.1107/S2052520616003954>.
- [123] K.A. Udachin, J.A. Ripmeester, A Novel Mode of Inclusion for Pyrene in β -Cyclodextrin Compounds: The Crystal Structures of β -Cyclodextrin with Cyclohexanol and Pyrene, and with *n*-Octanol and Pyrene, *J. Am. Chem. Soc.* 120 (1998) 1080–1081. <https://doi.org/10.1021/ja972156d>.

References

- [124] S.B. AXS, W. Madison, USA, 2004; SAINT, Software Users Guide, Version 6.0; Bruker Analytical X-ray Systems, Softw. Users Guid. Version 6.0; Bruker Anal. X-Ray Syst. (1999).
- [125] G.M. Sheldrick, SADABS: area-detector absorption correction, v2. 10, Univ. Göttingen, Ger. (1999).
- [126] M.C. Burla, R. Caliendo, B. Carrozzini, G.L. Cascarano, C. Cuocci, C. Giacovazzo, M. Mallamo, A. Mazzone, G. Polidori, Crystal structure determination and refinement via SIR2014, *J. Appl. Crystallogr.* 48 (2015) 306–309. <https://doi.org/10.1107/S1600576715001132>.
- [127] G.M. Sheldrick, A short history of SHELX, *Acta Crystallogr. Sect. A Found. Crystallogr.* 64 (2008) 112–122. <https://doi.org/10.1107/S0108767307043930>.
- [128] G.M. Sheldrick, Crystal structure refinement with SHELXL, *Acta Crystallogr. Sect. C Struct. Chem.* 71 (2015) 3–8. <https://doi.org/10.1107/S2053229614024218>.
- [129] L.J. Farrugia, WinGX suite for small-molecule single-crystal crystallography, *J. Appl. Crystallogr.* 32 (1999) 837–838. <https://doi.org/10.1107/S0021889899006020>.
- [130] M.N. Tahir, Y. Lee, Immobilisation of β -cyclodextrin on glass: Characterisation and application for cholesterol reduction from milk, *Food Chem.* 139 (2013) 475–481. <https://doi.org/10.1016/j.foodchem.2013.01.080>.
- [131] N. Kistamah, C.M. Carr, S. Rosunee, X-ray photoelectron spectroscopic study of Tencel treated with a cationic β -cyclodextrin derivative, *Surf. Interface Anal.* 41 (2009) 710–713. <https://doi.org/10.1002/sia.3076>.

APPENDIX

CONTENTS

Fig. A1 TGA curve of HMWCNTs.

Fig. A2 SPME-GC-(SIM)-MS chromatogram of blank matrix extract.

Fig. A3 Raman spectra of red-MWCNT-HNO₃ and red-MWCNT-H₂O₂ and their untreated counterparts (MWCNT-HNO₃ and MWCNT-H₂O₂)

Fig. A4 TGA curves of COOH-MWCNT and MWCNT-CD nanocomposites

Fig. A5 FTIR spectra showing pristine β - and γ -CD, MWCNT- HNO₃ and MWCNT- H₂O₂ reduced with hydrazine hydrate, and the four nanocomposites evaluated in this work.

Fig. A6 – A7 XPS spectra of COOH-MWCNT and γ -CD-based nanocomposites.

Table A1 ζ -potential values of the acidic, basic and pristine COOH-MWCNTs.

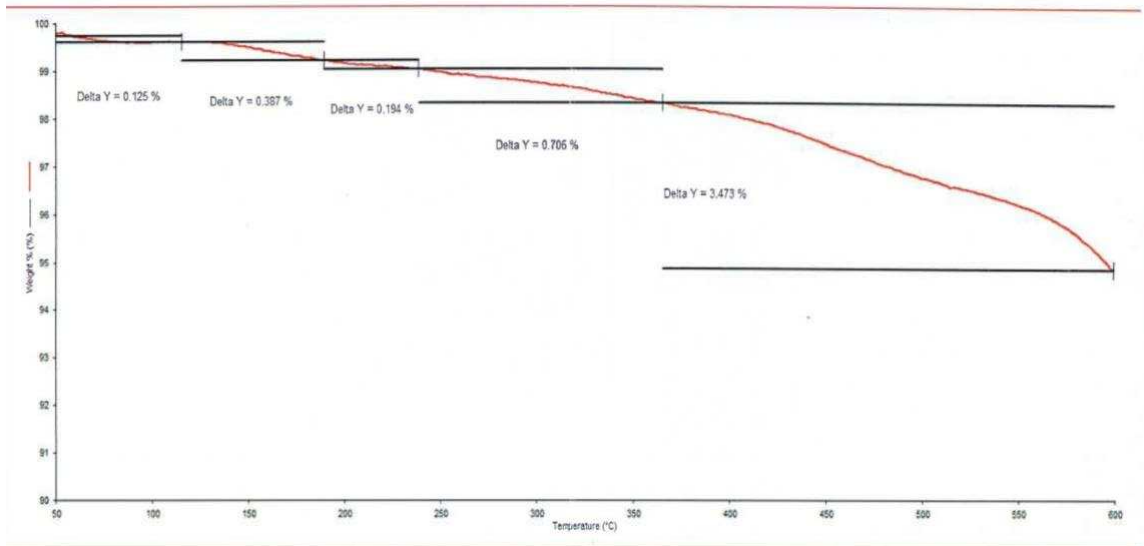


Fig. A 1 TGA curve of the HMWCNTs

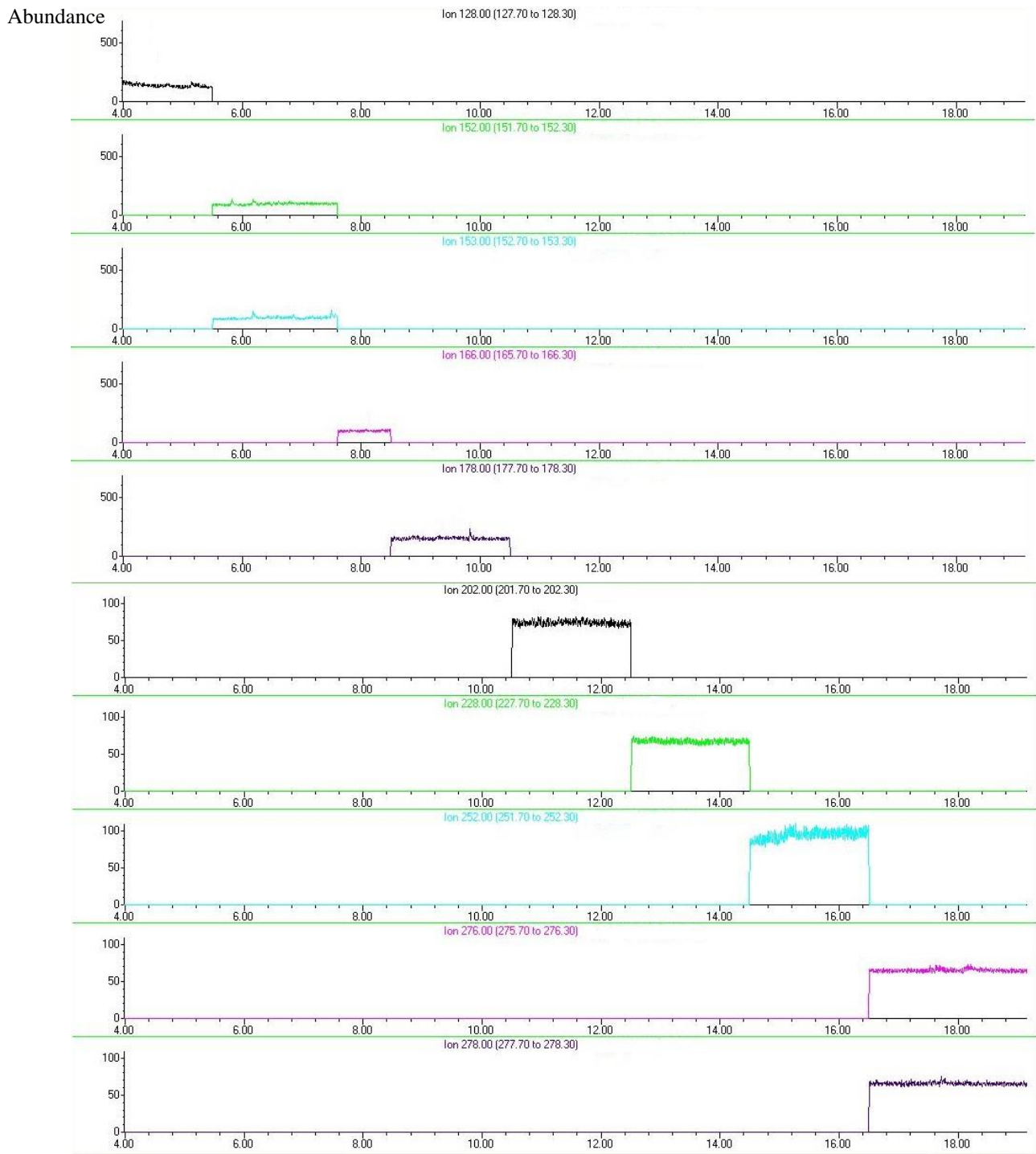


Fig. A 2 MEPS-SPME-GC-(SIM)-MS chromatogram of blank matrix extract.

Table A 1 The ζ -potential values of the acidic, basic and pristine COOH-MWCNTs

MWCNTs	COOH Concentrations (mmol/g)	ζ (mV)
MWCNT-HNO ₃	1.45	-31.1
MWCNT-H ₂ O ₂	0.94	-12.5
COOH-MWCNTs	0.34	-7.9

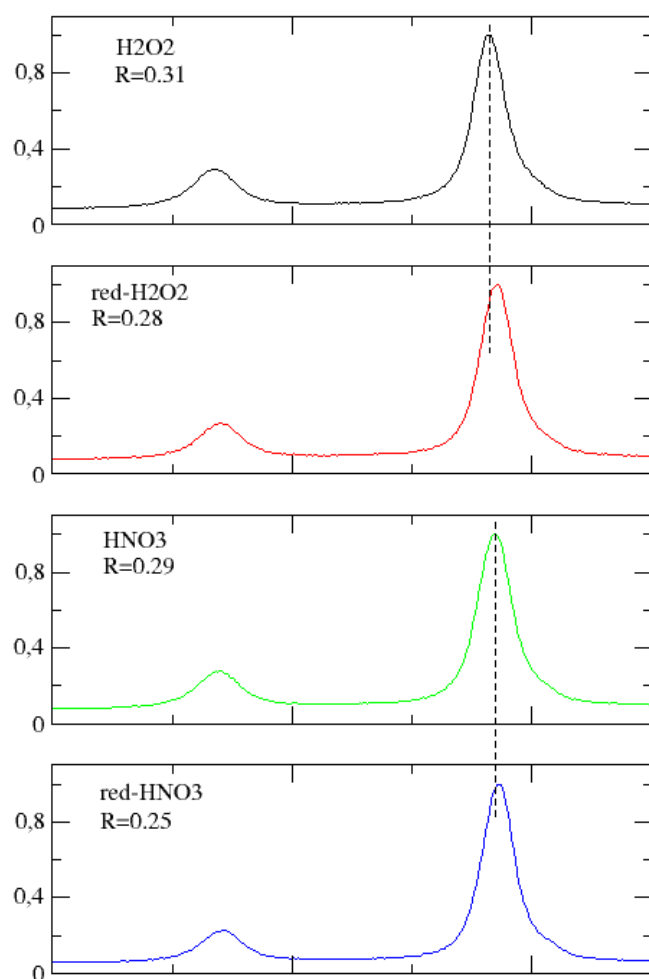
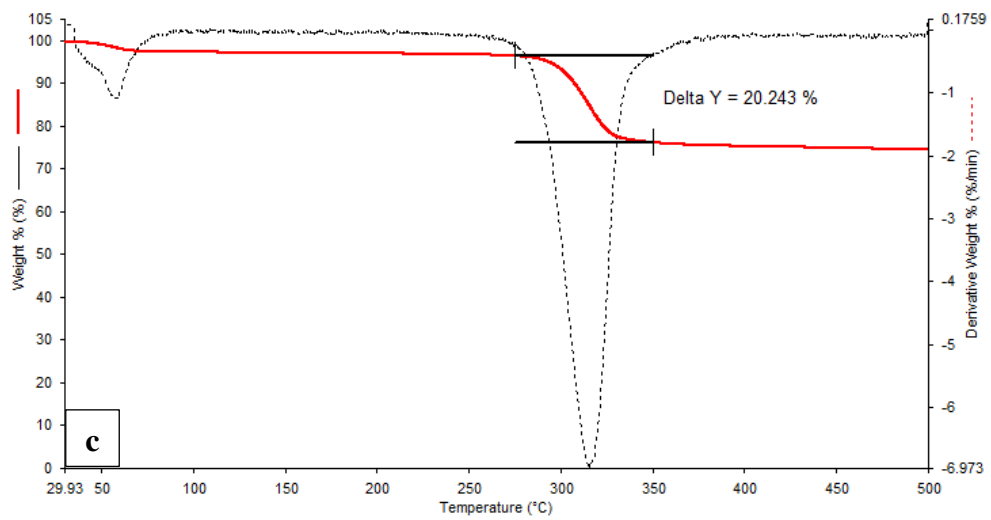
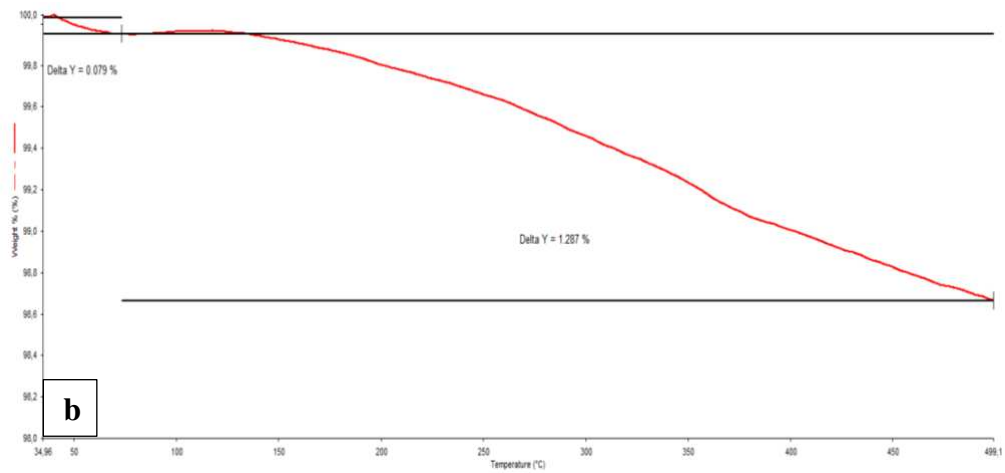
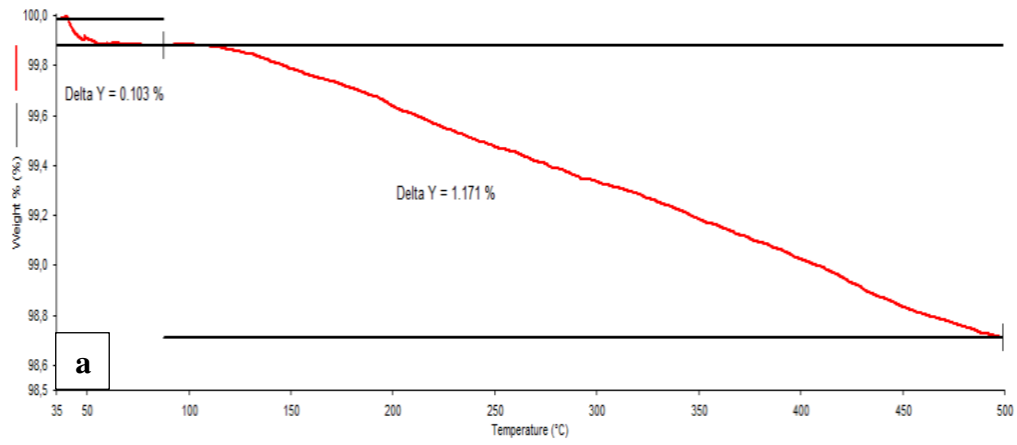
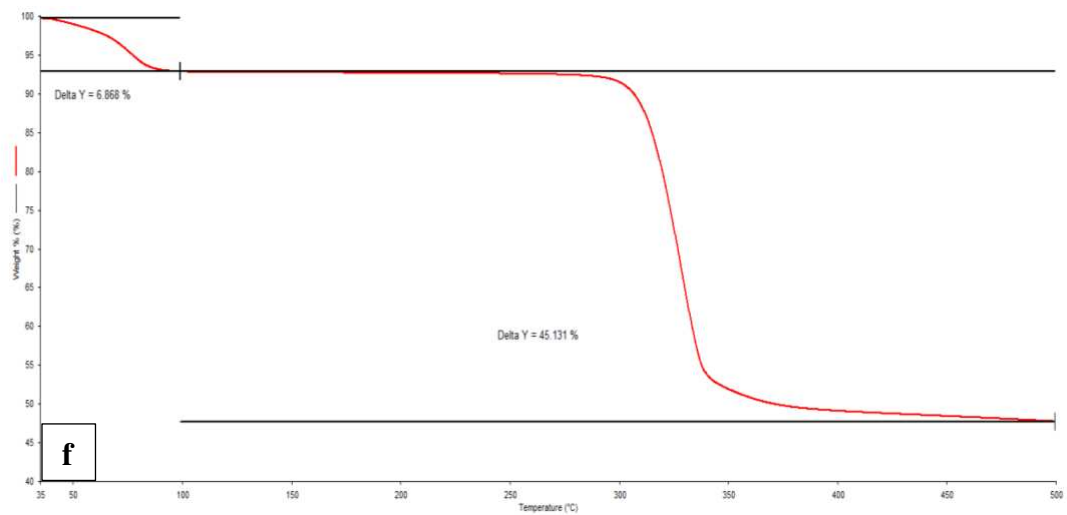
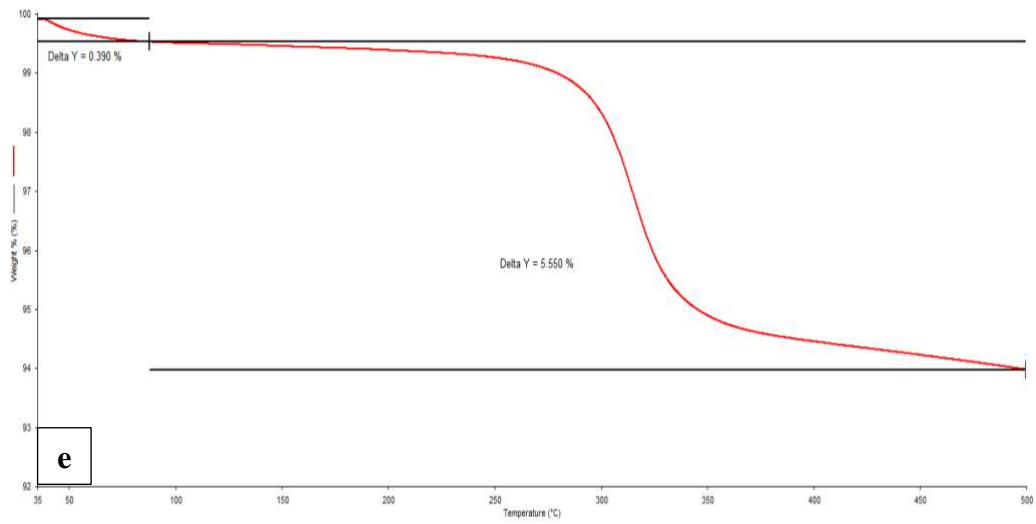
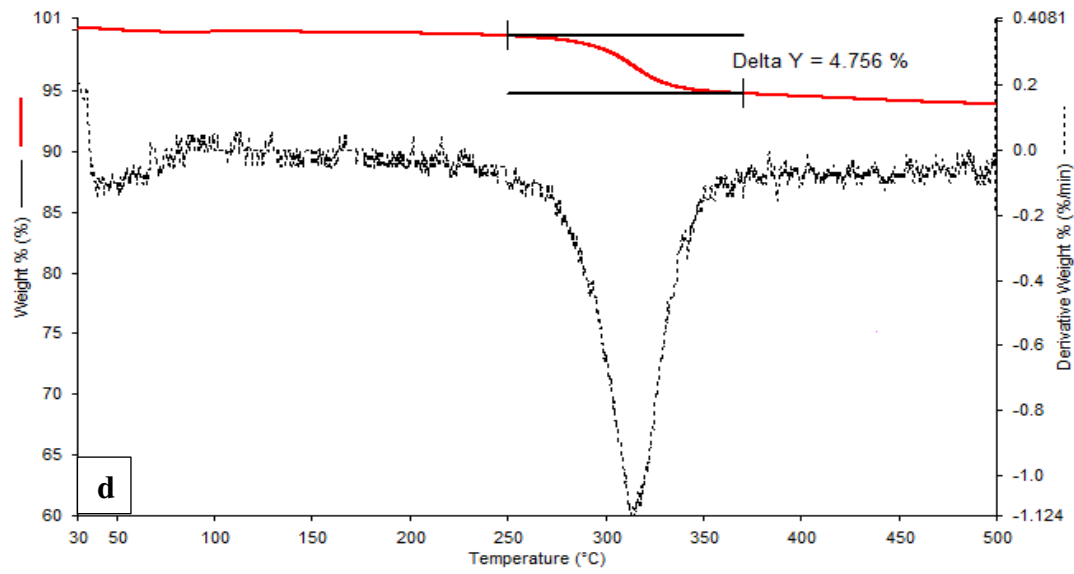


Fig. A 3 Raman spectra of the two systems that were pretreated with reduction by hydrazine hydrate (red-MWCNT-HNO₃ and red-MWCNT-H₂O₂) and their untreated counterparts (MWCNT-HNO₃ and MWCNT-H₂O₂). *R* value (ratio between the bands) gives an indication of the disorder of the MWCNTs. Reduced systems have slightly lower *R* values.





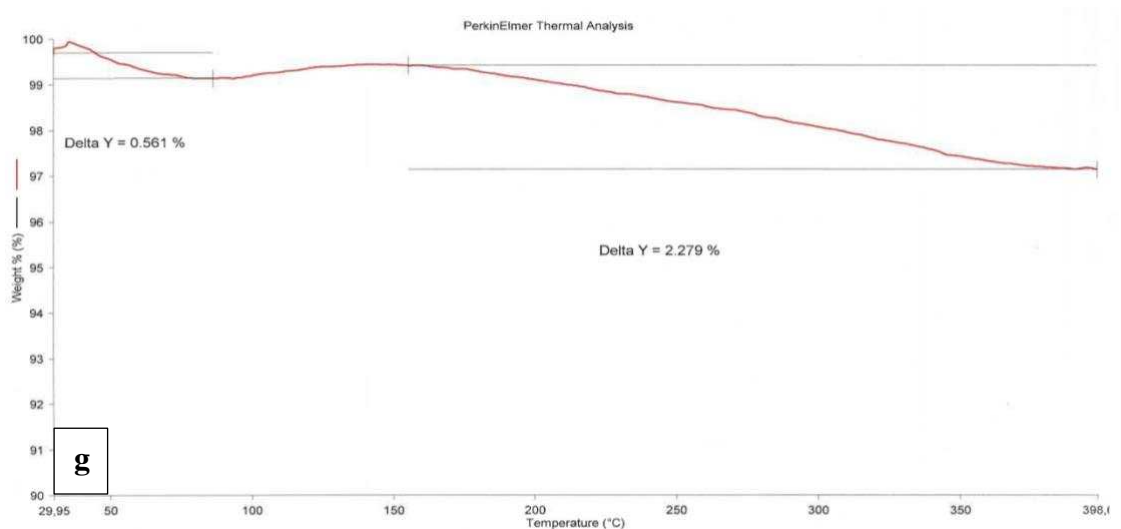
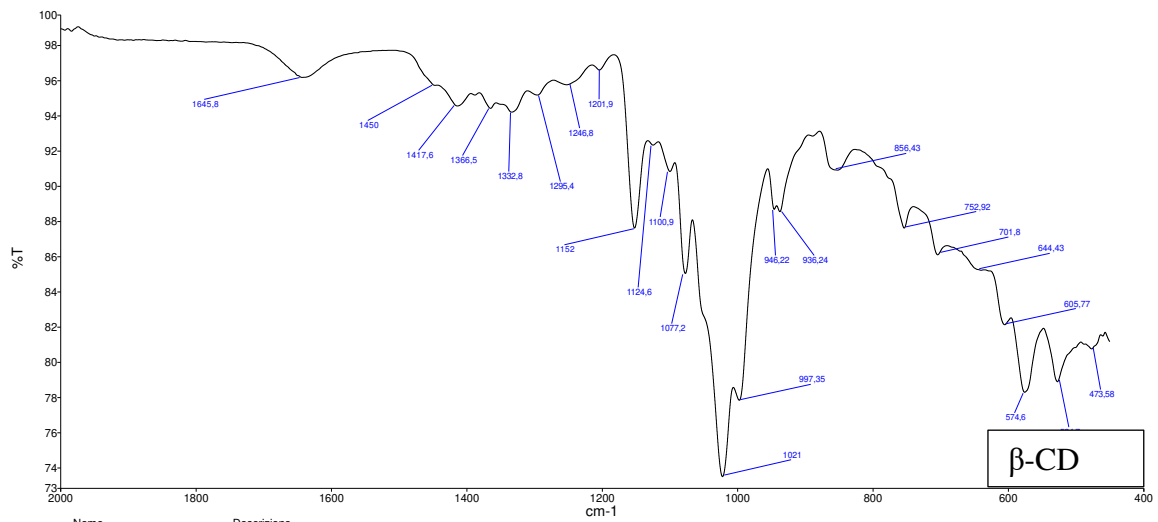
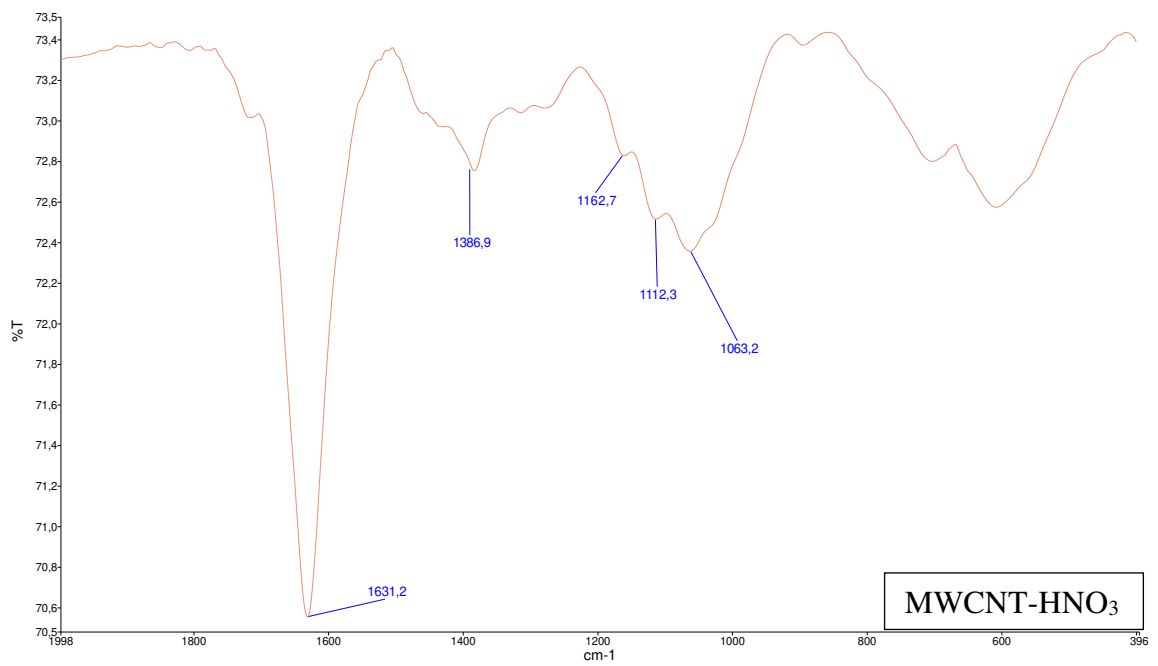
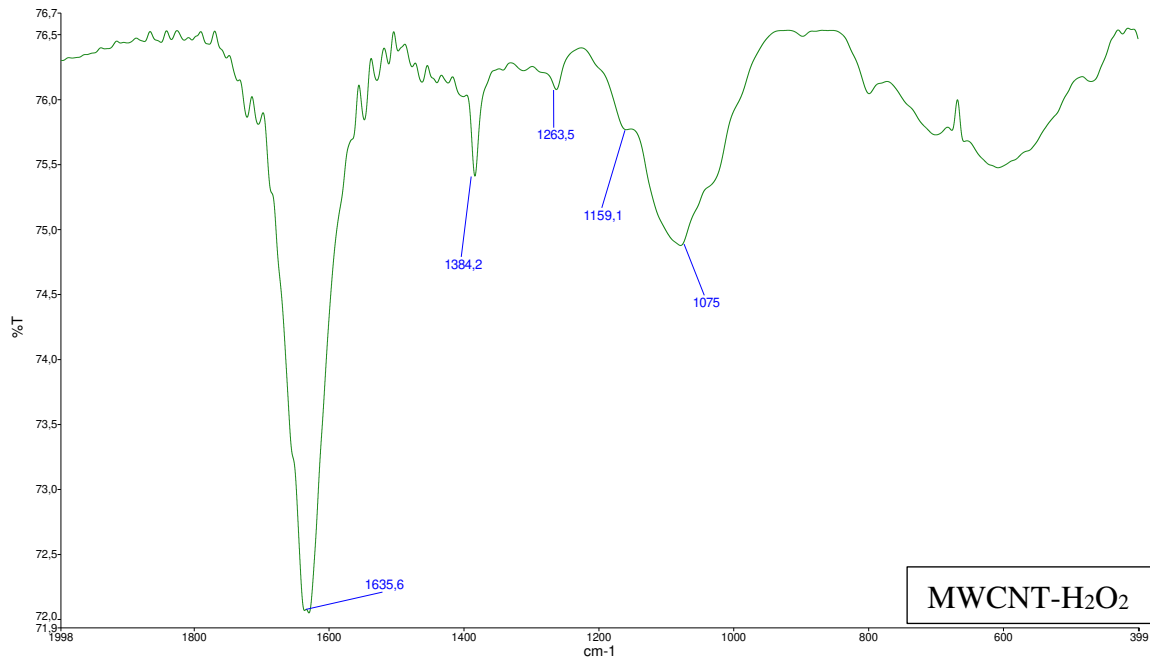
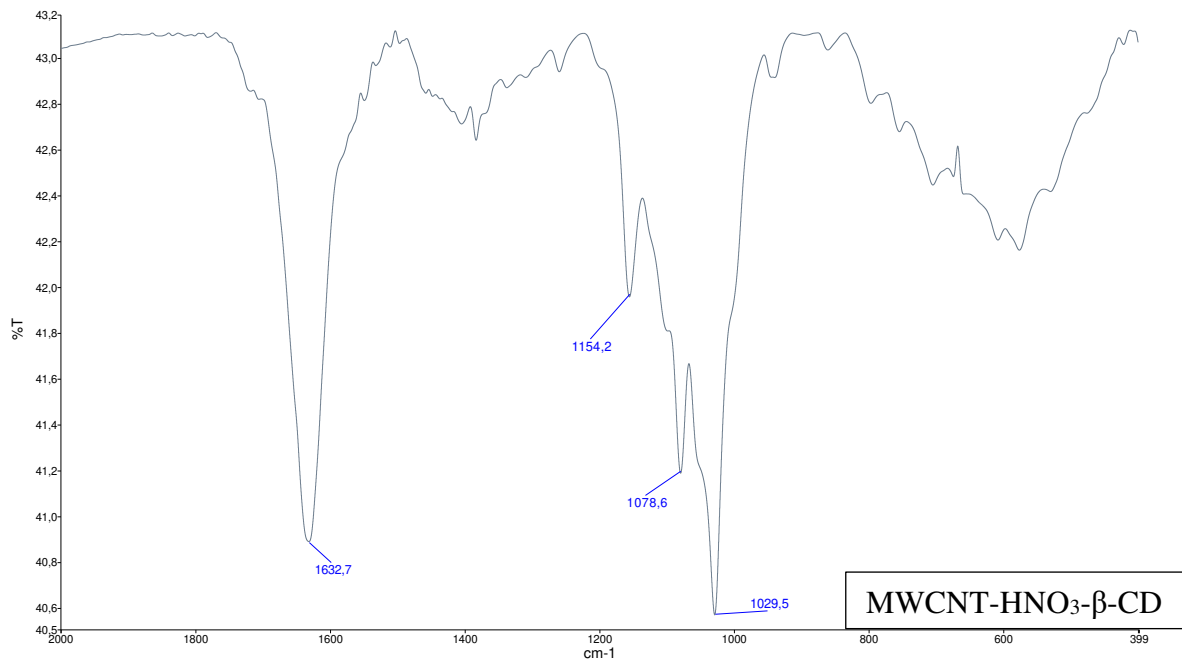


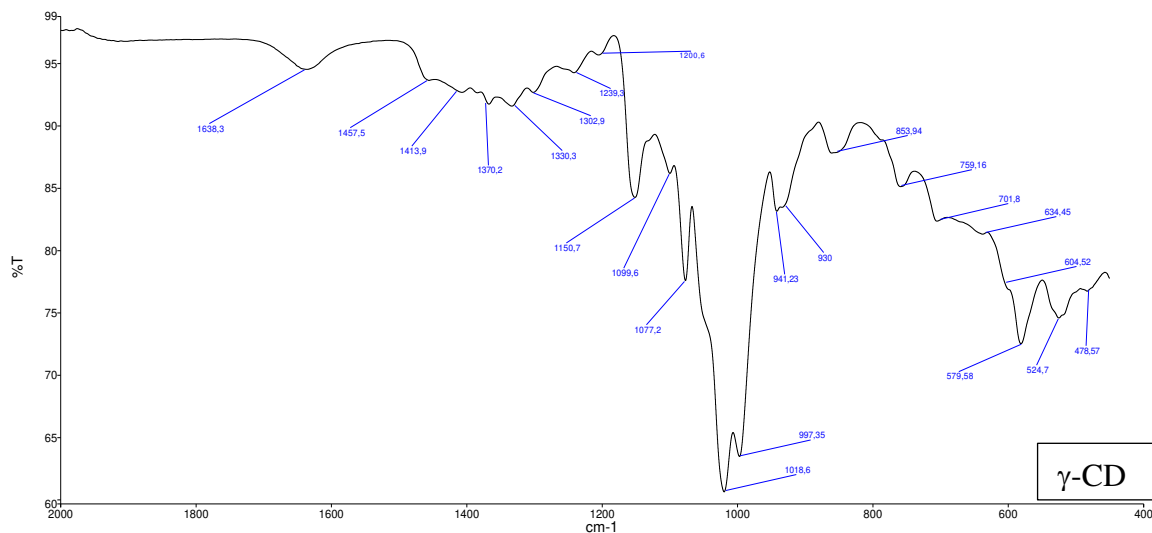
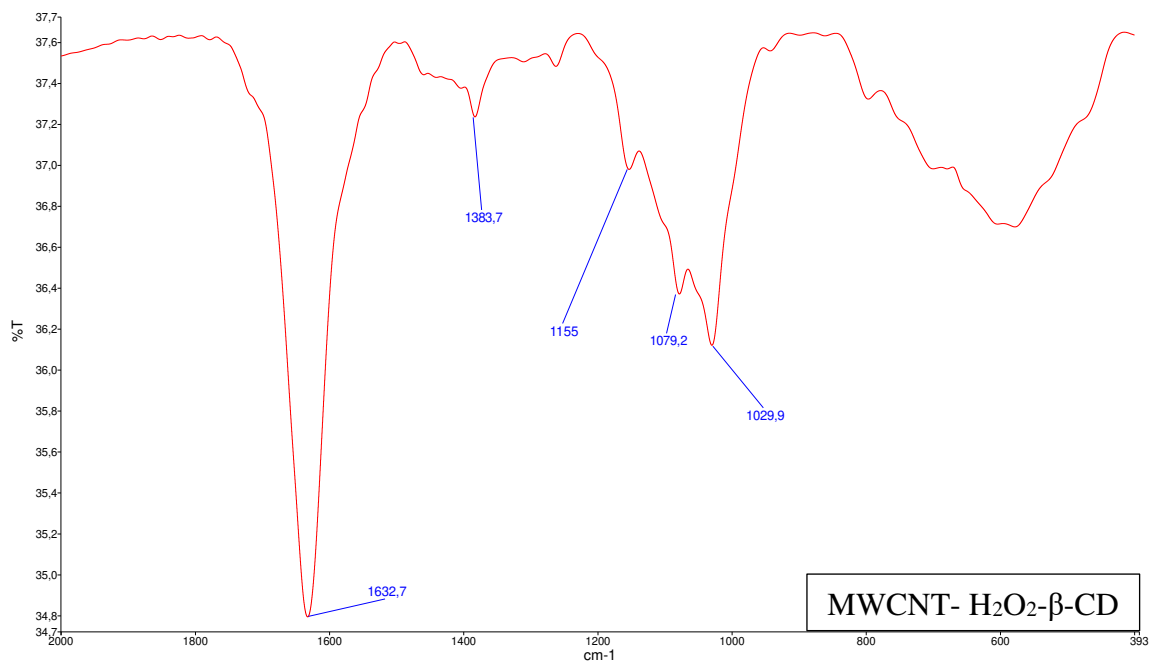
Fig. A 4 TGA curves obtained with (a) red-MWCNT-HNO₃, (b) red-MWCNT-H₂O₂, (c) MWCNT-HNO₃-β-CD, (d) MWCNT-HNO₃-γ-CD, (e) MWCNT-H₂O₂-β-CD, (f) MWCNT-H₂O₂-γ-CD and (g) pristine COOH-MWCNTs. Greater weight losses are observed for nanocomposites containing β-CDs compared to γ-CDs, highlighting a greater thermal stability of the latter.



Nome: Beta CD
 Descrizione: Sample 011 By Biscoglie Date giovedì, febbraio 18 2021







Nome gammaCD
 Descrizione Sample 017 By Bisceglie Date martedì, aprile 20 2021

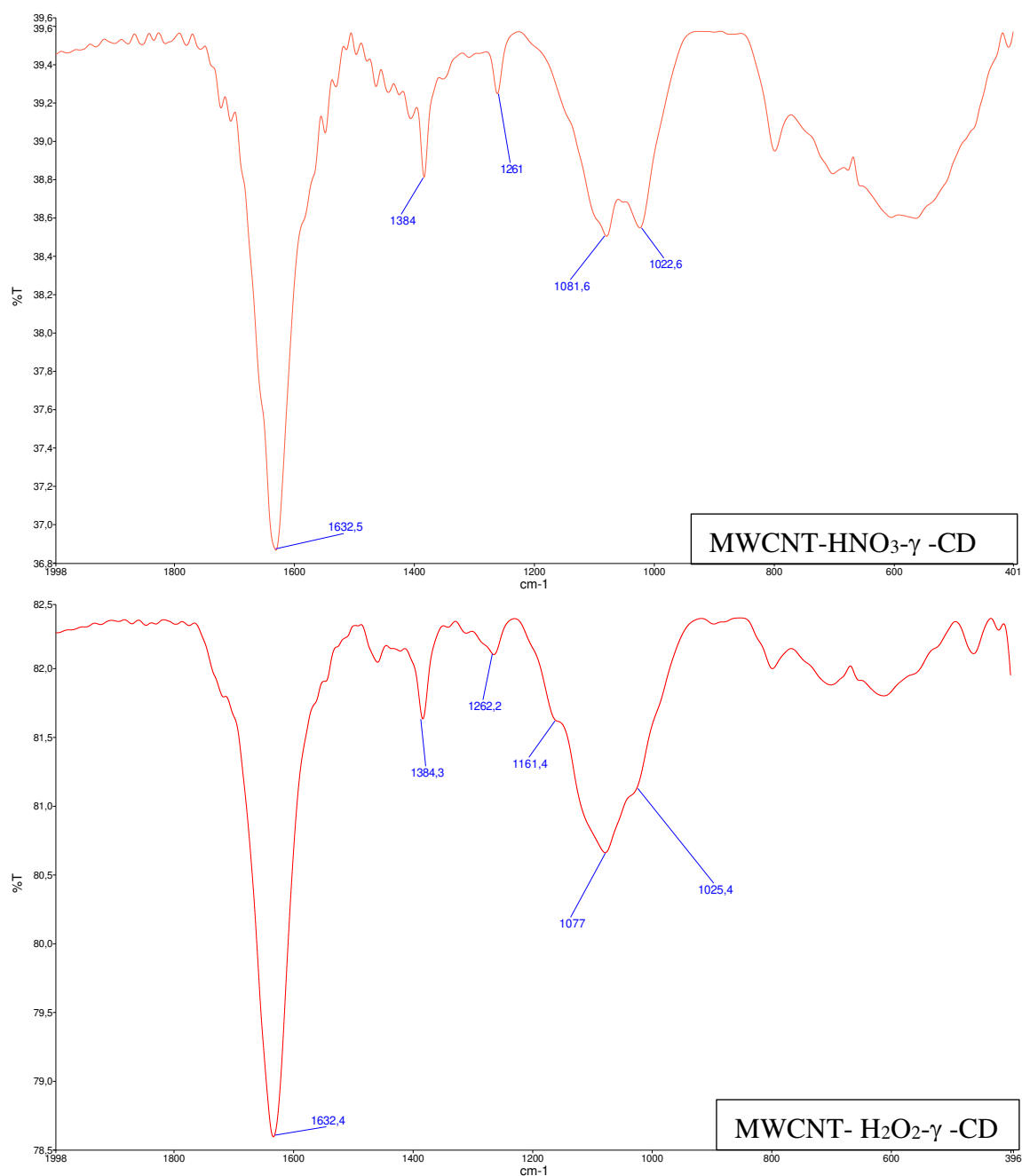


Fig. A 5 FTIR spectra showing pristine β - and γ -CD, MWCNT-HNO₃ and MWCNT-H₂O₂ reduced with hydrazine hydrate, and the four nanocomposites evaluated in this study. The presence of CDs on the MWCNTs was proved by presence of characteristics peaks of CDs in the spectra of the nanocomposites. However, no conclusions regarding the nature of the links between CDs and MWCNTs can be stated.

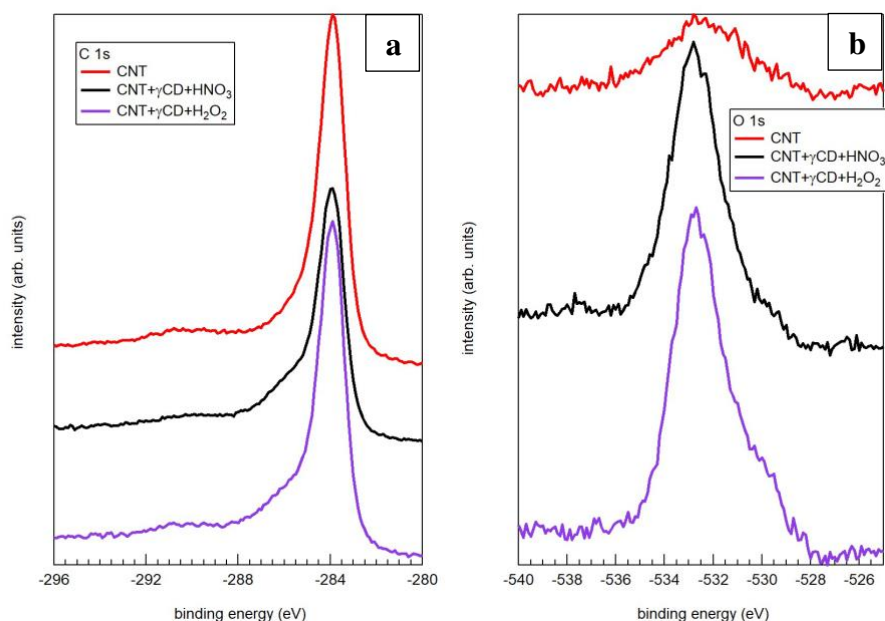


Fig. A 6 The figures show the XPS spectra relating to C 1s and O 1s of the 3 analyzed samples.

A higher intensity of the peak of the structures with high binding energies is observed in the samples containing CDs compared to the reference MWCNT sample.

- (a) In all the samples we observe a main peak of C at about 284 eV due to C-C bonds, and a series of structures with higher binding energies (292-285 eV) due to C-O and C-N bond.
- (b) The figure shows an increase in the intensity of the O 1s signal in samples containing CD compared to the pristine COOH-MWCNT. The O 1s line is asymmetrical with a main peak around 533 eV, due to carboxyl and hydroxyl groups, and a shoulder at lower bond energies (about 530 eV), due to physisorbed oxygen and/or carbonates.

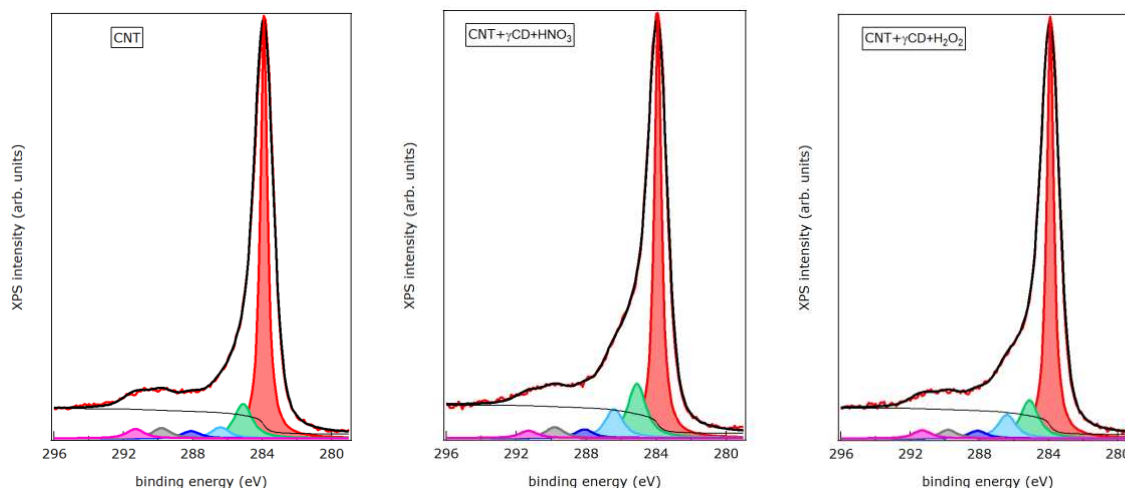


Fig A 7 The figure shows the fits of the XPS spectra of C 1s made with 6 components, according to the work reported by Datsyuk et al. [90].

Peak 1 283.9 eV → C-C

Peak 2 285.1 eV → defect C-OH

Peak 3 286.4 eV → C-O, C-N

Peak 4 288.1 eV → -O-C=O, C-OOH, N-C=O

Peak 5 289.8 eV → carbonates

Peak 6 291.3 eV → π - π transitions

The C atoms bonded to nitrogen (C-N) have a binding energy between 286 and 287 eV [130] and therefore are likely to overlap with the peak 3. The C atoms with N-C=O bonds have binding energy around 288 eV and overlap the peak 4 [131]. The interactions between CDs and can be ascribed to π - π , or H-bonding involving the surface of the CNTs.